# Design Analysis and Assist-As-Needed Control of a Stephenson III Six-Bar Linkage-based Robotic Gait Rehabilitation Orthosis

**Akim Kapsalyamov**

Supervisor: Assoc. Prof. Shahid Hussain
Co-Supervisor: Prof. Roland Goecke

Advisors: Prof. Nick Brown
Assoc. Prof. Prashant Jamwal

A thesis submitted for the degree of Doctor of Philosophy at the University of Canberra.

August 2023

# Abstract

Repetitive and task-oriented movements can strengthen muscles and improve walking capabilities among patients experiencing gait impairments due to neurological disorders. The demand for effective rehabilitation is high, given the large number of patients suffering from gait impairments. The traditional physiotherapy is laborious, may not provide the desired cadence and gait patterns, and requires constant presence of physiotherapists. This often leads to delayed treatment for many patients due to the high demand and a shortage of physiotherapists. Early phase post-stroke gait rehabilitation is crucial, as the ability to recuperate lost muscular abilities reduces over time.

Lower limb wearable rehabilitation robots have shown promise in improving the locomotor capabilities of patients experiencing gait impairments and reducing the burden on physiotherapists. However, the high cost of commercially available robots makes this technology inaccessible to many hospitals and rehabilitation centers. To address this issue, ongoing research is focusing on improving existing rehabilitation robots in terms of ease of use, innovative design, and cost reduction. Closed-loop linkage mechanisms have recently drawn attention in the development of gait rehabilitation robots due to their ability to address the drawbacks of commercially available robot orthoses. These mechanisms are affordable and capable of providing suitable trajectories for gait training therapy.

One of the challenging aspects in designing linkage-based robots is determining and calculating linkage parameters that will produce the required gait trajectories. This thesis presents an innovative approach to synthesizing the linkage dimensions to provide natural gait trajectories. Additionally, it introduces a novel and affordable robotic orthosis based on Stephenson III's six-bar linkage. The developed gait rehabilitation orthosis is a bilateral system powered by a single actuator on each side of the leg, capable of providing naturalistic knee and ankle joint motions relative to the hip joint, which are required during therapeutic gait training. This orthosis can be used in clinical settings and is actuated using only a single motor, yet it is capable of providing complex lower limb trajectory motions at its end-effector.

The initial design optimization was carried out using a genetic algorithm (GA), and a deep generative neural network model was developed for the linkage synthesis problem. This model represents an advancement in current kinematic synthesis methods, enabling it to generate dimensions of the links that satisfy various required target human lower limb trajectories during

walking in a short period. It will assist designers in determining optimal linkage dimensions to generate the required end-effector trajectories within a single mechanism.

To enhance the mechanism's velocity regulation control scheme and address fluctuations that may occur during operation due to external disturbances such as fixed patient's leg and inertia in closed loop linkage mechanisms, a Deep Reinforcement Learning control scheme was proposed to regulate the speed of the input crank to reach satisfactory performance needed for gait rehabilitation training. Experimental evaluations with healthy human subjects were conducted to demonstrate that the mechanism is capable of directing lower limbs on naturalistic gait trajectories with a required walking speed.

Furthermore, given the varied disability levels among neurologically impaired patients, the orthosis incorporates a patient cooperative control strategy. This is achieved through the application of impedance learning control, operating on an "assist-as-needed" principle. This innovative approach enables the robot to modify the assistive force it provides during gait cycle aligning with the patient's disability level and contributing towards active participation during the gait rehabilitation training. The proposed control scheme was evaluated in two distinct gait training modes while being worn by a human subject. In the "passive" mode subjects refrained from moving their legs, allowing the robot to guide their movements. While during the second 'active' mode, the subject engaged in normal walking activity while wearing the robot. Experimental results with healthy human subjects indicated reduced robot torques consequent to an increase in human torque. These results substantiate that customized robotic assistance based on the individual needs of patients can enhance their participation, which is essential to improve the treatment outcomes.

The concept of this research lies in the development of a novel, affordable, and adaptable robotic orthosis based on Stephenson III's six-bar linkage mechanism, capable of delivering naturalistic individualized lower limb motion. It advances the fields of dimensional synthesis of closed loop linkage mechanisms rehabilitation robotics with the use of deep generative neural network and a Deep Reinforcement Learning control scheme for enhanced velocity regulation. Moreover, the application of impedance learning control encourages active patient participation in gait rehabilitation training by customizing assistive force based on the patient's disability level. With these advancements, the research contributes significantly to the development of more cost-effective, adaptable, and efficient robotic gait rehabilitation systems, presenting a

promising solution for improving therapeutic outcomes for patients with gait impairments due to neurological disorders.

# Acknowledgments

I would like to express my profound gratitude and appreciation to my mentor and supervisor Assoc. Prof. Shahid Hussain. His consistent guidance, patience, and expertise in the field were vital to my doctoral journey. His diligent feedback consistently challenged me to refine my thought process and helping me grow both as a researcher and as a person.

My thanks go to my co-supervisor, Prof. Roland Goecke. His constructive observations and feedback, coupled with his knack for posing challenging questions, were instrumental in expanding my proficiency in presenting my work.

I owe a debt of gratitude to Prof. Nicholas Brown. His proficiency in physical biomechanics contributed significantly to the multi-disciplinary nature of my research. I would also like express my profound gratitude to Prof. Sunil Agrawal at Columbia University, USA for providing his valuable constructive feedback and guidance on shaping and improving final part of this research.

Special acknowledgement must go to Assoc. Prof. Prashant Jamwal. His technical advice and innovative thought processes were instrumental in shaping the trajectory of my research. His zeal, expertise, and precision were not only inspiring but also kept my work focused and grounded.

I would like to put my thanks to laboratory technician Jamie Plowman, for his constant technical support and inputs during prototype construction. The University of Canberra needs to be acknowledged for providing me with the Research Training Program scholarship to support my studies and stay in Canberra. My friends at the University of Canberra for sparing time for constructive discussions during my research. Also, my life friends Tasbolat Taunyazov, Anuar Abilgaziyev and Dias Bakhtiyarov also deserve acknowledgement.

On a more personal note, my heartfelt appreciation goes to my dear family, constant source of motivation and driving force in this research journey. My parents, Bauyrzhan and Zaidagul, for their endless support and love; my sisters, Zhanna and Dana, my niece and nephews Alimkhan, Sara, Iligai and Ibrai for their unwavering faith in me; my devoted wife, Adina, for her persistent encouragement and love, for her endless patience and generosity to allow me work on my thesis during extended working hours and my son Alkey, who is a ceaseless source of inspiration.

# Table of Contents

# List of Figures

# List of Tables

# List of Acronyms, Abbreviations, and Mathematical Notations

**Acronyms and Abbreviations**

| | |
|---|---|
| Active leg exoskeleton | ALEX |
| Ambulation-assisting robotic tool for human rehabilitation | ARTHUR |
| Artificial Neural Network | ANN |
| Body weight support | BWS |
| Center of mass | COM |
| Computer aided design | CAD |
| Conditional Generative Adversarial Networks | C-GAN |
| Cooperative double particle swarm optimization | CDPSO |
| Deep Deterministic Policy Gradient | DDPG |
| Degree of Freedom | DOF |
| Deep reinforcement learning | DRL |
| Differential evolution | DE |
| Direct current | DC |
| Electromyography | EMG |
| Evolutionary Algorithm | EA |
| Fully connected neural network | FCNN |
| Gait Trainer | GT |
| Generative Adversarial Networks | GAN |
| Genetic algorithm | GA |
| Gravity balancing orthosis | GBO |
| Hybrid assistive limb | HAL |
| Hybrid teaching-learning-particle swarm optimization | HTLPSO |
| Linkage design gait trainer | LGT |
| Lower extremity powered exoskeleton | LOPES |
| Long Short-Term Memory | LSTM |
| Machine learning | ML |
| Machine of gait training and rehabilitation | MGTR |
| Mean Squared Error | MSE |
| Mobile lower limb robotic exoskeleton | MLLRE |
| National Heart, Lung, and Blood Institute | NHLBI |
| Open Neural Network Exchange | ONNX |

| | |
|---|---|
| Proportional, Integral and Derivative | PID |
| Rectified Linear Unit | ReLU |
| Reinforcement learning | RL |
| Series elastic actuation | SEA |
| Sequential quadratic programming | SQP |
| Spinal cord injury | SCI |
| Three dimensional | 3D |

**Mathematical Notations**

| | |
|---|---|
| $a_t$ | Action |
| $a_{ix}, a_{iy}$ | Acceleration of the link $i$ along x and y axes at center of COM |
| $\alpha$ | Angular acceleration |
| $\theta_2, \theta_3, \theta_4, \theta_5, \theta_6, \theta_7, \theta_8, \theta_9, \gamma,$ $\alpha_0, \beta, \alpha_1, \beta_1, \alpha_2, \beta_2, \alpha_3, \beta_3$ | Assumed angles |
| $b$ | Bias vector |
| $A, B, C, D, E, G, H, K$ | Indication of position of the mechanism's joints |
| $\dot{\theta}_{curr}$ | Current angular velocity of the crank |
| $K_D$ | Derivative error |
| $\dot{\theta}_{des}$ | Desired angular velocity of the crank |
| $\Delta$ | Difference or change in the succeeding term |
| $\gamma$ | Discount factor |
| $o_t$ | Environment observation |
| g | Gravitational acceleration |
| $L_i$ | Indication of length of the mechanism's links |
| $\theta$ | Input angle at the crank |
| $K_I$ | Integral error |
| $K$ | Kinetic energy |
| $\mathcal{L}$ | Lagrangian |
| N | Linkage curve pairs |
| $m_i$ | Mass of the given link $i$ |
| $I_{1G}, I_{2G}, I_{5G}, I_{6G}$ | Mass moment of inertia about an axis passing through the center of mass for links 1, 2, 5, and 6, respectively |
| Cn | Number of input curves |
| $R_{ijx}, R_{ijy}$ | Position vector |

| | |
|---|---|
| $P$ | Potential energy |
| $\hat{\tau}_h$ | Predicted human torque |
| $K_P$ | Proportional error |
| LL | Random samples |
| $F_{jx}$ , $F_{jy}$ | Reaction forces along x and y axes for point $j$ |
| $\lambda$ | Regularizer weight |
| $T_r$ | Resultant torque |
| r | Reward |
| $T_{rob}$ | Robot torque |
| $F_{sh}$ | Shank interaction force |
| $F_{th}$ | Thigh interaction force |
| t | Time |
| $W$ | Weight matrix |

# Chapter 1. Introduction

There is a growing trend in the application of robotics technology in the healthcare sector, due to its numerous benefits, such as accuracy, precision, and the ability to continuously operate according to programmed instructions. One crucial area where this technology is being applied is in the gait rehabilitation of stroke patients [1, 2]. Lower limb rehabilitation aims to restore limb function and enable patients to regain the ability to walk normally. Studies have shown that high-frequency performance of specific repetitive training exercises can improve walking ability after a stroke [3, 4]. Wearable gait rehabilitation robots have emerged as a promising tool for gait rehabilitation training. These robots can guide patients' limbs along specific predefined trajectories and assist in performing iterative training exercises [5]. As a result, extensive research is being conducted to develop gait rehabilitation robots that can aid in gait training therapies while considering safety, control, and affordability.

This research aims to develop an innovative, cost-effective treadmill-based gait rehabilitation robot that is capable of providing naturalistic lower limb joint trajectories suitable for gait rehabilitation purposes. This chapter begins with an overview of the causes of gait impairments, followed by basic information on the anatomy of lower limbs and their movements. The conventional gait rehabilitation process is also described. The research goals and objectives, and the structure of the thesis are specified at the end of this chapter.

## 1.1 Stroke as a Cause of Gait Impairment

Stroke is recognized by the National Heart, Lung, and Blood Institute (NHLBI) in the USA as a prevalent neurological disorder worldwide. It occurs when blood flow to the brain is reduced or blocked, resulting in oxygen shortage and, in severe cases, the death of brain cells [6, 7]. The extent of brain damage determines the level of lesion for a stroke patient. While some patients may fully recover without severe consequences, the majority experience mortality or varying degrees of disability. Stroke survivors might have partial or complete limb paralysis, paired with language disabilities, memory loss and others. Stroke is considered a leading cause of disability globally [8, 9]. In Australia alone, approximately 56,000 people suffer from a stroke attack each year, and it is one of the country's major health concerns, significantly affecting mobility and walking capabilities [10]. The number of individuals living with the effects of stroke is predicted to reach up to 1 million by the year 2050 [11]. The financial burden of stroke in Australia amounts to an estimated $5 billion annually [12].

The disability of the locomotor is one of the side effects caused by stroke [13]. Over 80% of stroke survivors experience gait impairments [14, 15]. Abnormalities in gait performance include shorter stance phases, longer swing phases of the limb, asymmetry in gait phase time, shorter step length, cadence, and other spatiotemporal parameters [16-18]. These impairments, combined with muscle weakness and decreased walking speed, increase the risk of falls [19, 20]. The inability to perform normal walking hampers mobility and daily life activities for stroke patients.

To address this, rehabilitation therapies are crucial, and one of the primary goals is to re-establish patients' ability to walk and increase their mobility and movement independence [21-23]. While some individuals may quickly recover their walking abilities, still many patients experience abnormalities in their gait performance. In a study by Paolucci *et al.*, it was found that approximately 45% of patients leave rehabilitation centers in wheelchairs, and only around 14.41% can walk indoors, with less than 30% using crutches or other walking aids [24]. The effectiveness of rehabilitation therapy is highest during the early period after stroke, where about 50% of basic functions can be regained in the first three months, but this percentage decreases to 20-30% in the following three months [25]. Therefore, it is crucial to provide the rehabilitation as early as possible to regain much of the lost functional abilities.

## 1.2 Lower Limb Biomechanics

The human lower limb consists of the hip, knee, and ankle joints. There are around 30 bones that constitute the lower limb, the major ones are presented in Figure 1-1.

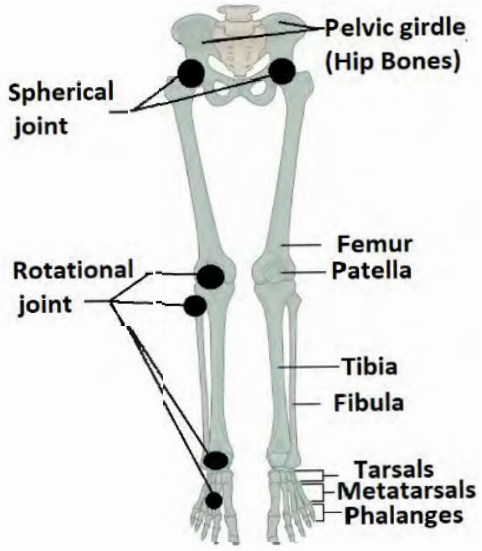


Figure 1-1. The major bones of the lower limb [26].

The hip joint has three Degrees of Freedom (DOFs) and can perform flexion/extension, abduction/adduction, and internal/external rotational motions through a spherical joint. The knee joint has one DOF, allowing only flexion and extension movements. The ankle joint also has three DOFs, with a rotational joint. Figure 1-2 describes the ankle motion during walking in four phases [27].

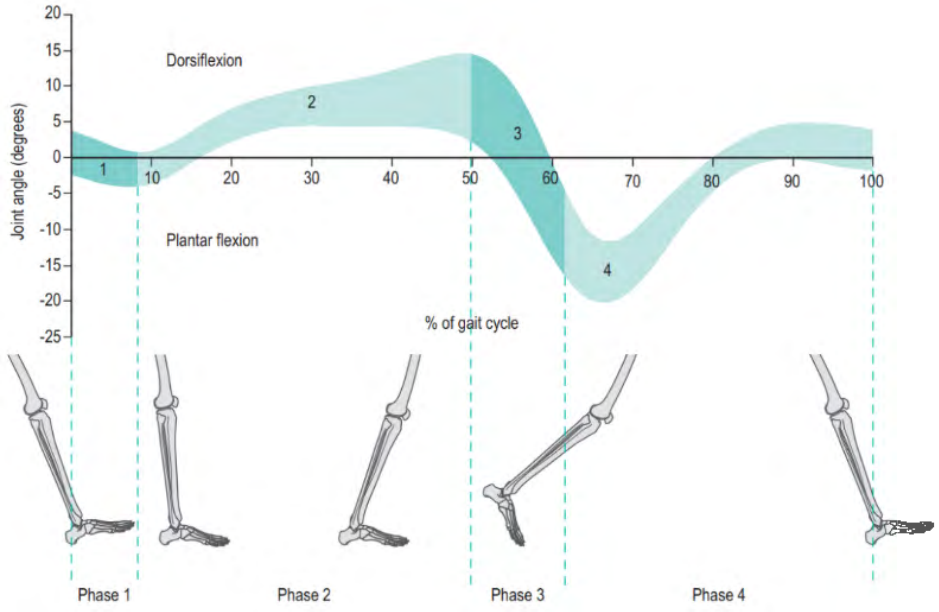


Figure 1-2. The movement of the ankle joint during a single gait cycle [27].

In the phase 1, the initial contact with the ground or heel strike occurs. At this stage, the plantar flexes around $3^0$ to $5^0$ until full contact with the ground is reached [27]. In phase 2, the tibia part starts to move over the ankle, and the maximum angle of dorsiflexion reaches around $10^0$. During the phase 3, when both feet are in contact with the ground, the heel starts elevating, causing the ankle to flex. The foot is pushed into plantar flexion, directing the body forward. In the phase 4, there is a fast dorsiflexion of the ankle occurs, which acts concentrically to allow foot clearance from the walking surface.

Although the movements of knee joints occur in all three planes (sagittal, coronal, and transverse), most of the motions during the gait cycle occur in the sagittal plane, when the knee joint flexes or extends. The range of motion for flexion/extension movements alters between $0^0$ and $70^0$ [27]. The movement of the knee joint can be described in five phases, as shown in Figure 1-3.

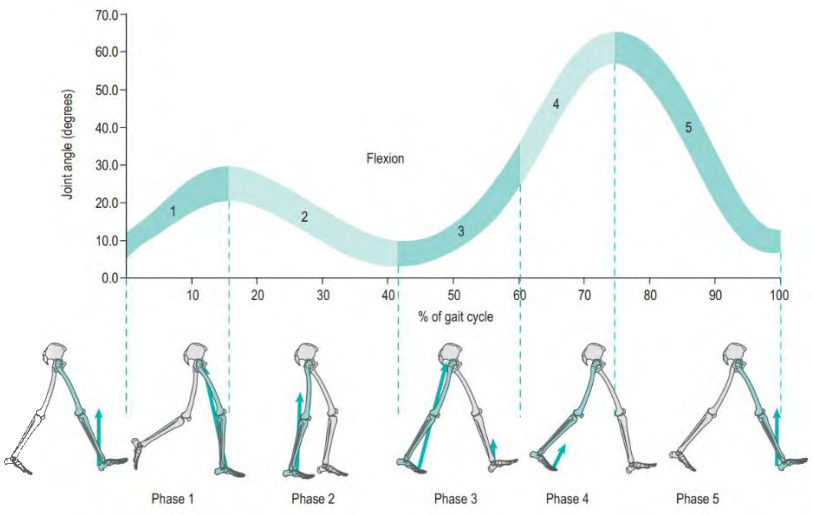


Figure 1-3. The movements of the knee joint during a single gait cycle [27].

During the first phase following the initial contact, the knee joint undergoes a bending motion, flexing to approximately $20^0$ when the knee is bent while bearing maximum weight. This flexion allows the knee joint to absorb the load at a rapid rate of $150^0$ - $200^0$ per second. Concurrently, the ankle joint undergoes plantar flexion, resulting in a combined effect that functions as a shock absorber during the lower limb's loading. Throughout this process, the knee extensors engage in eccentric contractions. In the next phase after the initial peak of knee flexion, the knee joint undergoes extension at a speed of $80^0$ - $100^0$ per second until it reaches near full extension. This extension is crucial for facilitating a seamless movement of the body over the supporting limb during the stance phase. After the initial phase of knee flexion, which aligns with the moment when the heel lifts off the ground, the lower limb enters the propulsive phase of the gait cycle. During this phase, the knee undergoes further flexion in preparation for the upcoming swing phase, commonly known as pre-swing. When the knee reaches a flexion of approximately $40^0$, toe-off occurs. At this point, the knee flexes rapidly, at a speed of $300^0$-$350^0$ per second. This flexion, along with ankle dorsiflexion, allows the toe to lift off the ground. As the swing phase progresses from the initial stage to the middle, the knee continues to flex further, reaching a maximum angle of $65^0$-$70^0$. During the swing phase, the knee rapidly extends to prepare for the next heel strike. In the late swing phase, the knee undergoes a swift extension, at a rate of $350^0$ - $400^0$ per second, in preparation for the subsequent heel strike [27].

The hip joint flexes as the leg moves forward to initiate a step and subsequently extends until the push-off phase. Figure 1-4 shows the movement of the hip joint during a single gait cycle.

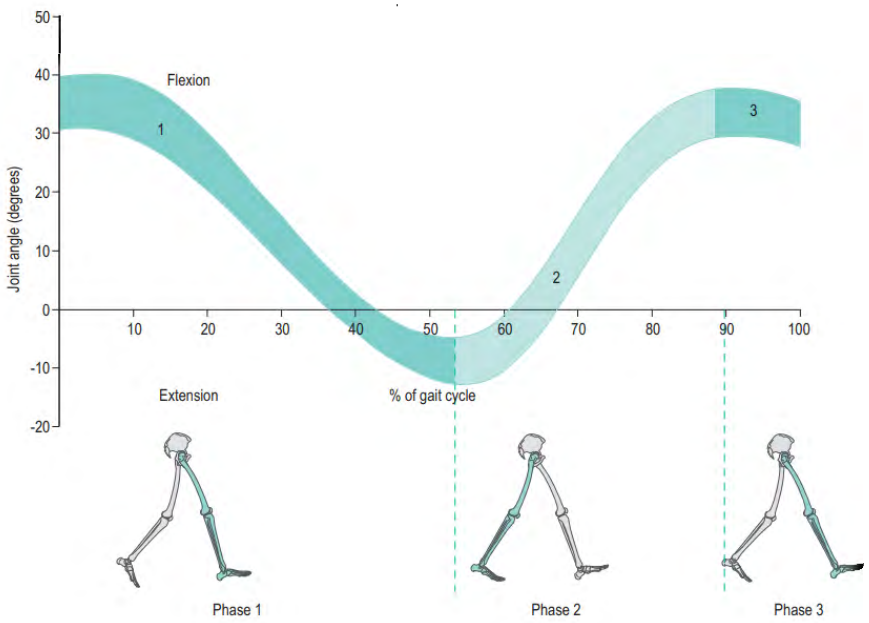


Figure 1-4. The movements of the hip joint during a single gait cycle [27].

The maximum flexion of the hip occurs during swing phase 3. After the initial contact in phase 1, the hip extends, and the maximum hip extension occurs right after the opposite foot strike in phase 2, at which point weight is transferred to the forward limb and the trailing limb begins to flex at the hip, marking the pre-swing period. At around 60% of the gait cycle, the toe lifts off the ground, and the hip rapidly flexes at a rate of $200^0$ per second.

## 1.3 Conventional Gait Rehabilitation

One of the primary goals of stroke rehabilitation is to restore lost gait capabilities. The traditional approach involves the manual gait training. Training with a Body Weight Support (BWS) system has been used extensively for the past two decades [28]. Preliminary research findings have demonstrated that repetitive and task-oriented training of patients with gait impairments can help in restoring walking capabilities [29-33]. The BWS system is used to unload the weight of patients who cannot walk or stand by themselves. It has been shown that the manual gait rehabilitation process involving the BWS system has had positive outcomes on the improvement of step length and cadence of neurologically impaired patients [34-37]. Conventional therapies require the constant presence of nurses and therapists during the procedure who help to direct the limbs in a predefined gait trajectory as shown in Figure 1-5.

Figure 1-5. Manual gait training using the BWS system [28].

During the training on a treadmill, the legs of a patient should be directed along a physiological trajectory in a repetitive and reproducible manner [38]. Therefore, the whole rehabilitation process depends on the skills of a physiotherapist, which may vary. The patient's treatment and progress are evaluated intuitively. Moreover, given the physical fatigue and common complaints of back pain from physiotherapists, it may reduce the patients' training time and prolong the recovery period.

## 1.4 Research Outline

### 1.4.1 Problem Definition

Although multi-DOF gait rehabilitation robots have shown promising results in rehabilitating the impaired gait of patients suffering from neurological conditions, they are still unaffordable to many hospitals and rehabilitation centers due to their high prices. For instance, the cost of the commercially available gait rehabilitation robots varies in the range between $60,000 and $300,000 [39]. And since the majority of human walking occurs in the sagittal plane the usage of multiple actuators can be redundant. Therefore, single-DOF linkage-based mechanisms can be sufficient to train and rehabilitate the walking ability among stroke patients. However, currently, there is no linkage-based mechanism available for gait rehabilitation purposes that has been synthesized based on knee and ankle joint trajectories, thus a naturalistic gait pattern has not been fully achieved. These trajectories should be generated relative to the hip joint. The existing mechanisms cannot be adjusted to accommodate people with different leg lengths. There is no optimal synthesis method capable of predicting linkage dimensions given two lower limb trajectories without solving higher-order polynomial equations. Proper control of

mechanisms has not been explored. The velocity of linkage-based mechanisms can vary due to the inertia and disturbances caused by a human subject; thus, the training efficiency can be affected. A patient cooperative control strategy, which considers the efforts and disability level of patients, has not been explored on single DOF gait rehabilitation robots. Chapter 2 presents the literature review on the existing single and multi-DOF gait rehabilitation robots and illustrates the given drawbacks.

### 1.4.2 Research Objectives and Scope

The overall goal of this research is to develop an affordable gait rehabilitation orthosis that can produce more naturalistic lower limb movements for patients who have gait impairments due to neurological disorders. The aim of this research can be further explained using the following research objectives:

#### 1.4.2.1 Synthesis of the mechanism dimensions given two objective functions as knee and ankle joint trajectories and proof-of-concept

The dimensional synthesis of the mechanism should be carried out by considering two human gait trajectories simultaneously for ankle and knee joints using existing optimization techniques. The Euclidean distances between the generated trajectories at coupler points and the target human trajectories should be minimized. Dynamic requirements in terms of velocity, acceleration, and force/torque should be satisfied. The provision of naturalistic lower limb walking trajectories can eliminate many issues related to joint self-alignment and enhance the overall effectiveness of rehabilitation training.

#### 1.4.2.2 Development of a machine learning tool for automatic dimension calculation based on knee and ankle joint trajectories

An automated framework tool based on a machine learning technique should be developed, capable of automatically generating the optimal linkage parameters given two trajectory curves. Once trained, the model should be able to generate new dimensions given new inputs. The tool should address the drawbacks of the current synthesis methods approach and serve as an assistive tool for linkage designers.

#### 1.4.2.3 Development of the robotic gait training orthosis

The linkage with synthesized dimensions should be further upgraded to resemble a fully operational wearable gait rehabilitation orthosis for treadmill training. It should provide naturalistic trajectory motions for the hip, knee, and ankle joints. Sensors should be installed to receive feedback on position and the interaction forces between the orthosis and the human. The developed orthosis should be wearable, lightweight, and safe for any user. Muscle weakness in the ankle joint resulting in foot drop condition should be also managed, as stroke patients cannot dorsiflex/plantarflex their feet.

#### 1.4.2.4 Velocity regulation control using machine learning tools

As for the initial step in controlling the prototype, a proper velocity regulation control scheme should be designed. Particularly, deep reinforcement learning-based control should be designed and employed to reduce the fluctuation occurring in the mechanism due to external disturbances, the inertia of unbalanced mechanisms, and forces (human subjects in the case of gait rehabilitation).

#### 1.4.2.5 Patient cooperative control strategy via impedance learning control

Design an impedance learning control strategy that takes into account human participation during gait training and operates in ‘assist-as-needed’ principle. The robot should be capable of increasing or decreasing the assistive torque supplied at the crank depending on the force supplied by the human joints during walking. This control scheme should be able to assist the patients depending on their demands.

One of the significant research questions is to check the effectiveness of the developed rehabilitation robot orthosis with the implemented control scheme. This question is a clinical question that can be addressed with extensive long-term therapeutic gait training with patients with neurological disorders. While this is accurate, it is beyond the scope of this thesis. The effectiveness of the proposed robot orthosis and the implemented control scheme will be tested with healthy human subjects. However, the robot orthosis will be able to provide repetitive and task-oriented gait training by assisting the legs in moving along natural human gait trajectories, where the role of physiotherapists will be only to supervise.

## 1.5 Thesis Organization

This thesis demonstrates the work implemented to meet the above-mentioned research objectives. Chapter 2 provides the literature review, discusses the drawbacks of currently employed multi-DOF gait rehabilitation orthoses, explores the current stage in the employment of single DOF mechanisms in the gait rehabilitation field and identifies its drawbacks. Chapter 3 provides the initial design description, justification on the selected mechanism, and presents the forward kinematics analysis together with the dynamic force analysis for the proof-of-concept prototype. Chapter 4 describes the developed machine learning tool for predicting the linkage dimensions of the mechanism, capable of generating various required lower limb walking trajectories needed for gait rehabilitation. Chapter 5 covers the initial control schemes implemented on the robot for velocity regulation. Chapter 6 describes the implemented patient cooperative control strategy based on the impedance learning control scheme to assist the human only when needed. Finally, chapter 7 provides the conclusion of this research.

## 1.6 Chapter Summary

This chapter provides an overview of stroke definition and the biomechanics of the lower limbs during walking. It also discusses the manual gait rehabilitation therapy with the use of a BWS system and treadmill. The chapter highlights the drawbacks and challenges associated with manual gait training. Furthermore, it outlines the aims and objectives of the study.

# Chapter 2. Literature Review

## 2.1 Robot-Assisted Gait Rehabilitation

Gait rehabilitation training can be achieved through the application of wearable robots. It is possible to recover from impaired gait due to neurological disorders using gait rehabilitation robotic orthoses [40-42]. These robots guide patients' limbs along specific predefined trajectories and assist in performing iterative training motions with higher accuracy and reliability [43, 44]. Compared to conventional approaches, robot-based gait rehabilitation offers several benefits, including reduced burden on healthcare workers. Doctors and physiotherapists can focus on analysing the progress made in the gait performance, leading to more effective treatment solutions [45-48]. By quantifying the recovery process through measuring interaction forces and limb movement ability, subjectivity in conventional gait training can be eliminated. Currently, there are two types of gait rehabilitation robots available - one based on treadmill training and the other assisting walking over the ground [49]. However, the latter type has limitations such as battery dependency and the need for crutches to support balance and avoid falling.

### 2.1.1 Existing Multi-DOF Gait Rehabilitation Robots

This subsection presents a selection of commercially available gait rehabilitation robots, as well as pioneering models that have demonstrated promising results with human subjects. The robots discussed in this section all possess multiple DOFs.

#### 2.1.1.1 LOKOMAT

Hocoma (Zurich, Switzerland) developed one of the most popular exoskeletons for rehabilitating patients with mobility impairments, known as Lokomat shown in Figure 2-1 [50]. It is a wearable robotic orthosis capable of assisting hip and knee joint movements in the sagittal plane. The robot utilizes direct current (DC) motors for actuation, and foot dorsiflexion motion is achieved using passive elastic bands. Lokomat's operation assumes perfect alignment with the human lower limb joints. Force/torque sensors installed in series with DC motors measure the interaction force. Lokomat has proven its effectiveness in rehabilitating post-stroke patients [51]. The overall system consists of the BWS, which suspends the subject over the treadmill.

There are two versions available - LokomatPro and LokomatNanos, which can be reconstructed or modified based on customer requirements [52]. The exoskeleton provides

movements in the knee and hip joints with its four DOFs. A linear type of actuation is applied in the system. Visual and audio signal feedback from the interface motivates the subject's participation. Moreover, the system employs the method that can adapt the speed of the treadmill depending on the disability level of the patients [53].

Figure 2-1. Lokomat (Hocoma, Switzerland) [49].

#### 2.1.1.2 ReoAmbulator

Motorika developed ReoAmbulator, shown in Figure 2-2, another treadmill-based rehabilitation exoskeleton designed for people with various disorders such as multiple sclerosis, cerebral vascular disease, sports injuries, and others [54]. It also uses a BWS system to suspend the person. It incorporates an adaptive strategy that analyzes the user's progress and adapts the training accordingly. ReoAmbulator has undergone clinical trials and experiments in rehabilitation centers worldwide.

Figure 2-2. ReoAmbulator (Motorika) [54].

#### 2.1.1.3 LokoHelp

LokoHelp, as shown in Figure 2-3, is another commercially available robotic gait rehabilitation system aimed at improving the overall training process and symmetry of legs during walking. Freivogel *et al*. evaluated its application on patients, showing progress in patients' walking performance after using the LokoHelp gait trainer.[55].

Figure 2-3. LokoHelp [55].

#### 2.1.1.4 ReWalk

ReWalk presented in Figure 2-4 is one of the oldest and well-known wearable robotic exoskeletons designed for individuals with spinal cord injuries (SCI) to train and rehabilitate hip and knee joints. It enables users to stand, walk, turn around, and go upstairs [56], [57]. Some clinical trials have been conducted with ReWalk [56-58], revealing some difficulties in controlling the system due to its complexity.

Figure 2-4. ReWalk [56].

#### 2.1.1.5 Hybrid Assistive Limb (HAL)

A Japanese company introduced Hybrid Assistive Limb (HAL), shown in Figure 2-5, a robotic exoskeleton intended for post-stroke patients and individuals with gait disorders Figure 2-5. The training with the HAL *[63]*. The device has been certified as a medical device and has undergone several steps and studies [59-63]. While promising results have been achieved, the HAL device remains expensive, limiting its accessibility to many rehabilitation centers and hospitals.

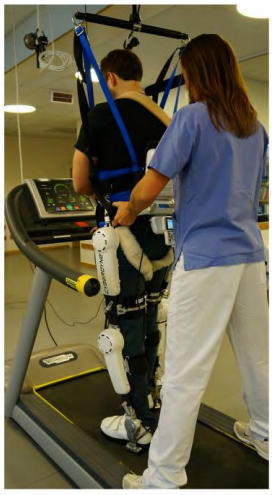

Figure 2-5. The training with the HAL [63].

#### 2.1.1.6 LOPES I and LOPES II

The Lower Extremity Powered Exoskeleton (LOPES) is an interactive treadmill-based device designed for gait rehabilitation shown in Figure 2-6 (a) [64]. It can operate in two modes: "patient-in-charge" and robot-in-charge", where the patient can move their legs without being constrained by the exoskeleton in the first mode and the robot guides the patient in the latter. Bowden cables, also known as Series Elastic Actuation (SEA) have been used in pairs with electric motors to actuate the system. The usage of cables allows for the placement of the motor at a distance, reducing the weight of the exoskeleton. Linear potentiometers have been used to measure the displacement in the springs, enabling the estimation of forces. The exoskeleton features eight impedance controlled DOFs to support pelvis, hip, and knee motions. However, the ankle joint is not actuated, as it has been reported that the sensors cannot accurately capture the readings needed for inverse dynamic modelling [64]. This may result in inefficient control of the exoskeleton due to inaccurate joint torque measurements. Additionally, the presence of joint friction in the exoskeleton makes measuring the sprint displacement not the best approach

for quantifying joint torques [65]. Upgraded LOPES II version, shown in Figure 2-6 (b), employs an admittance controller and was tested on stroke patients. [66].

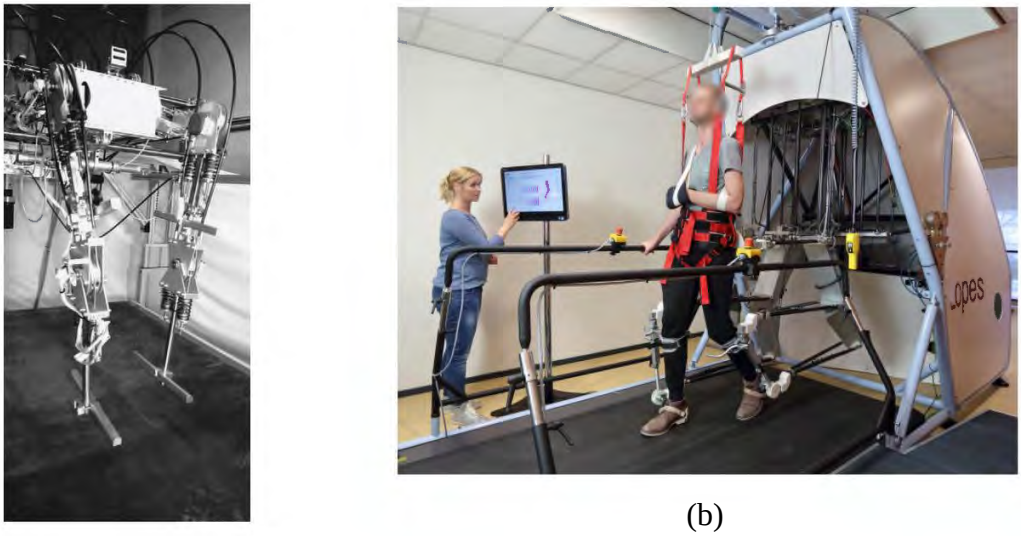


(a) (b)

Figure 2-6. (a) LOPES I [64], (b) LOPES II [66].

#### 2.1.1.7 ALEX

The Active leg exoskeleton (ALEX) shown in Figure 2-7 [67] was developed at the University of Delaware for gait rehabilitation. It is based on gravity balancing orthosis (GBO), which does not have any mechanical actuation and utilizes a parallelogram mechanism to determine the center of mass (COM). The exoskeleton is attached to a walker via a parallelogram mechanism that supports its weight. During the swing phase for foot clearance, the ankle joint is not actuated. Instead, it relies on force field control to ensure proper clearance of the foot. The hip and knee joints in the sagittal plane are actuated using linear actuators, while the remaining DOFs are passively managed using the springs.

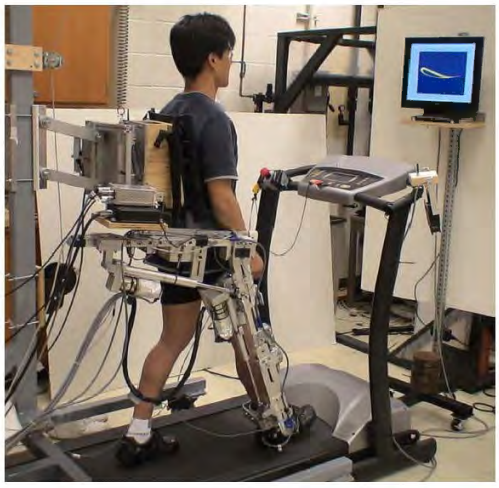

Figure 2-7. ALEX [67].

#### 2.1.1.8 Mobile lower limb robotic exoskeleton (MLLRE)

Another new mobile lower limb robotic exoskeleton (MLLRE) has been designed for rehabilitating the legs of patients with neurological impairments, as shown in Figure 2-8 [68]. The robot operates in a sagittal plane, supporting movements for knee flexion/extension of hip and knee joints. The ankle dorsiflexion movement is passive and has been achieved using springs. The BWS system is used to unload the subject while training on the treadmill.

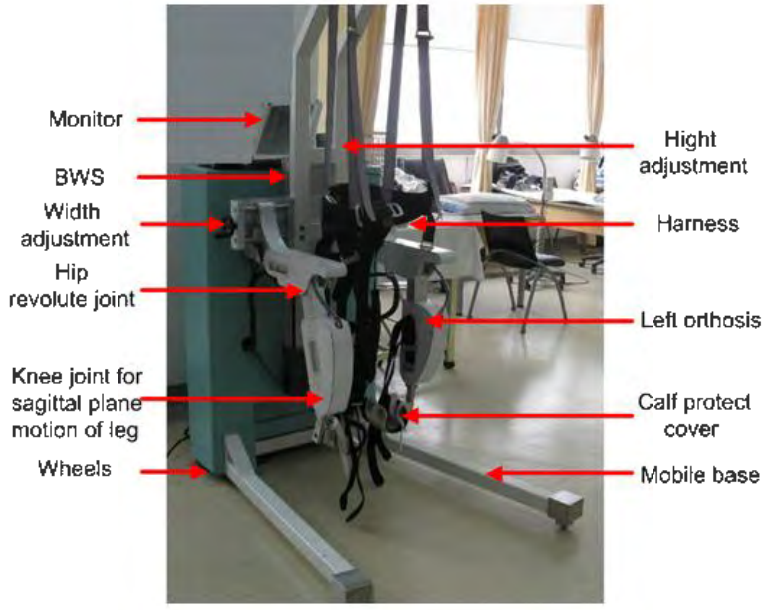


Figure 2-8. MLLRE and its main components labelled [68].

#### 2.1.1.9 Ambulation-assisting robotic tool for human rehabilitation

Ambulation-assisting robotic tool for human rehabilitation (ARTHUR) is a device designed to assist and manipulate human stepping [69]. It can control the position and force, providing motions in the sagittal plane for knee and ankle joints. The robot is said to be lightweight and generate the required forces for the gait rehabilitation process. However, it does not consider the motions of the pelvis during walking or the hip joint motions.

### 2.1.2 Single DOF Mechanisms for Gait Rehabilitation

The gait rehabilitation of patients can also be done via gait trainers, which have recently gained much attention among researchers [70]. The efficacy of such trainers has been presented in [71-74]. The walking capability of subacute stroke patients has improved after using a robot-assisted gait trainer in [75]. It typically comprises a mechanism that directs the ankle joint along the walking trajectory and a gravity support system [76]. Subjects' feet are placed on the pedal

with the help of therapists, and guided movement is initiated to complete the walking during the training. Additionally, functional electrical stimulation can be attached during training with the gait trainer [77]. This subsection introduces some of the examples of proposed concepts of single DOF mechanisms and the optimization techniques used to determine the required linkage dimensions to match the natural lower limb trajectories.

#### 2.1.2.1 Gait Trainer I and II

Gait Trainer (GT I) and its upgraded version GT II are among the first examples of single DOF robots based on a double crank and rocker gear mechanism developed for training the gait among nonambulatory subjects, as shown in Figure 2-9 [78, 79]. The feet are placed on pedal-based foot platforms. Further, the robot provides ellipsoid-like shape movement of the foot-plate. However, the robot does not take into consideration the efforts exerted by the subject, leaving it without active human participation, which is one of the crucial factors that can speed up the recovery process of patients with impaired locomotor capabilities.

Figure 2-9. Electromechanical Gait Trainer [79].

#### 2.1.2.2 Four-bar linkage by Singh *et al.*

A conceptual design exoskeleton based on a four-bar linkage developed to track natural trajectories of gait has been proposed by Singh *et al*. [80]. The work is more focused on the synthesis process, which involves determining the linkage dimensions that match the natural trajectories of the hip and ankle joint trajectories. The conceptual design, which can potentially

be used in gait rehabilitation, is shown in Figure 2-10. Hybrid teaching-learning particle swarm optimization (HTLPSO) has been used to find the best design of the linkage. The optimization problem formulation does not take into account the knee joint trajectory as a target design variable, which may affect the quality of the produced trajectories. Moreover, the concept has not been produced and tested with human subjects, and how it can be attached and motorized has not been discussed, leaving the question of its applicability by the human user open.

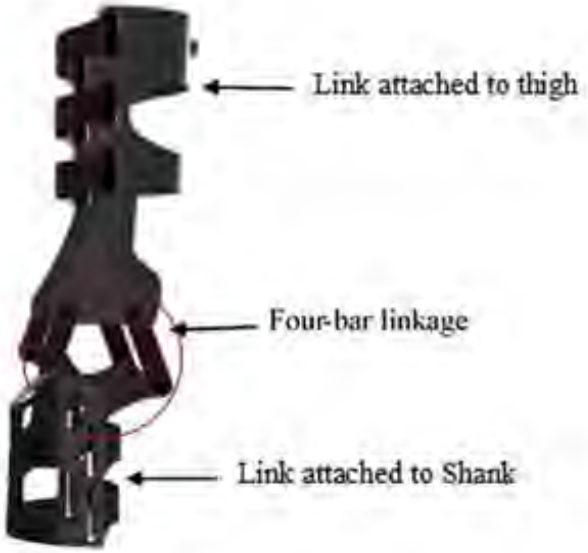


Figure 2-10. Four-bar linkage concept designed by Singh et.al. [80].

#### 2.1.2.3 Cam-driven parallelogram linkage controlled six-bar linkage

Homotopy-directed optimization has been used to determine the dimensions of six-bar linkages for natural ankle trajectory generation, as reported in [81, 82]. The work is mainly focused on the synthesis methods, which have produced a large set of solutions. However, among them, some solutions still had branch defects, which had to be sorted out. The branch defects among linkages mean that the generated mechanism is not able to operate at all due to the crashes of links during operation or the link rotation at some parts of the linkage is physically impossible. The proposed concept of the six-bar linkage is shown in Figure 2-11. It has been reported that the mechanism will be driven using cam parallelogram linkage. The mechanism has not been evaluated for its feasibility in a clinical study, and an actual prototype has not been constructed. It has not mentioned how it will be attached and strapped to human legs. Moreover, the natural trajectory of the knee joint has not been considered as a target design vector variable during linkage dimensions optimization, which may result in poor tracking of the knee joint trajectory points.

Figure 2-11. Six-bar linkage for ankle trajectory generation [81].

#### 2.1.2.4 The machine of gait training and rehabilitation

A five-bar linkage-based machine of gait training and rehabilitation (MGTR) has been designed for gait rehabilitation purposes, as shown in Figure 2-12 [83]. The device is an end-effector type, similar to the GT II device mentioned above. It has been tested on healthy subjects, and muscle activity has been measured using an electromyography (EMG) sensor. The results indicated that rectus femoris muscle activity during gait training was close to the normal gait. The drawback of this mechanism is that it does not provide naturalistic lower limb joints, which may not be suitable for different patients. Moreover, due to the different anthropometric parameters among people, the prototype is not adjustable for people with different leg lengths.

Figure 2-12. MGTR in use by human subjects [83].

#### 2.1.2.5 Seven bar and cam-linkage mechanism

A gait rehabilitation system based on seven-bar and cam-linkage mechanism has been developed in the work by Shao *et al*. [84]. GA is employed during the dimension synthesis part to enable the mechanism to follow the target path which is a widely used technique in synthesizing the dimensions of mechanisms [85]. The system employs a BWS system to unload the weight of the patient and is indicated to be operated using a single motor at a constant speed for both sides, which can simplify the control scheme of the mechanism. The 3D model of the proposed gait rehabilitation system is shown in Figure 2-13. The prototype has not been tested with human subjects, moreover adjustability to people with different leg lengths has not been considered in the design. The dynamic aspect has not been explored, questioning its usability and applicability on human subjects with impaired gait performance. In addition, the developed mechanism is bulky, which may cause some inconveniences to patients with impaired gait characteristics.

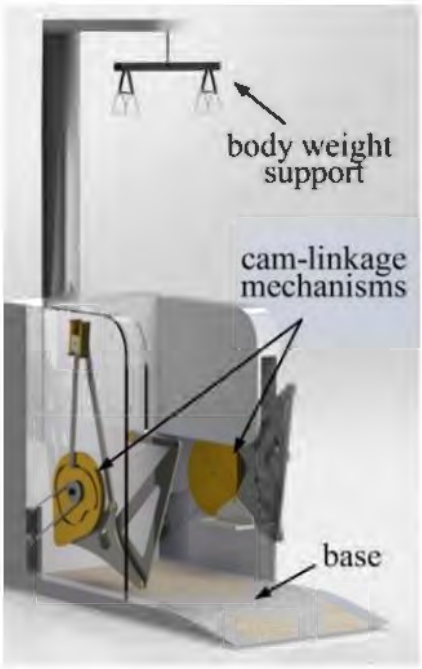


Figure 2-13. 3D model of the proposed gait rehabilitation robot [84].

#### 2.1.2.6 Watt I six-bar mechanism

Watt I six-bar linkage mechanism has been used to generate lower limb trajectories for gait rehabilitation [86]. A data-driven approach is implemented to predict the linkage dimensions based on body parameters. The prediction of trajectories from body parameters is implemented using a genetic algorithm optimized support vector machine approach. Further, the prototype

has been constructed to check its applicability in moving the lower limbs of human subjects, as shown in Figure 2-14. The prototype is actuated using a single motor and driven at a constant speed. The proposed robot has not achieved the natural trajectory of lower limbs. Moreover, the constructed prototype can be applied only to people with similar anthropometric parameters; the adjustability of the robot to match different leg lengths has not been considered in the design. Additionally, the proposed robot provides similar training as end-effector type robots, which produce elliptical gait trajectories. Since the robot does not consider the efforts exerted by human subjects, gait rehabilitation using the proposed prototype may not be efficient. The footplate is left free without any constraints and not controlled, which may cause problems for stroke patients who usually are not capable of dorsiflexing/plantarflexing their feet.

Figure 2-14. Watt I six-bar mechanism [86].

#### 2.1.2.7 Active gait trainer based on six-bar linkage

A six-bar linkage-based active gait trainer has been developed to support the gait movements of children with walking impairments, as shown in Figure 2-15 [87]. The system can operate in three modes: in the first mode, a child has an abnormality in walking, and the robot will respond to meet the load variances and disturbances exerted by a child. In the second mode, the robot follows the walking and assists only when required. The third mode is designed for children who can produce a normal gait trajectory but cannot walk long distances due to weakness in the muscles. The proposed prototype is not designed to follow a naturalistic gait pattern; instead, a basic mechanism has been designed to illustrate the robust control scheme.

Figure 2-15. Gait trainer based on six-bar linkage [87].

#### 2.1.2.8 Cam linkage for ankle joint

A cam-based mechanism has been implemented to realize a low-cost and lightweight exoskeleton that can trace and assist the ankle joint movement during walking [88]. The design was inspired by Chebyshev and Pantograph mechanisms. Solidworks and ADAMS software were used to design and do the numerical simulation of the proposed concept of the exoskeleton. The simulated exoskeleton with a human subject is shown in Figure 2-16.

Figure 2-16. A simulation of the exoskeleton with a human subject in ADAMS software [88].

#### 2.1.2.9 Jansen eight-link gait trainer

Jansen eight link mechanism has been used to generate ankle joint movements during walking for gait training purposes [89]. The concept is meant to be affordable for patients, and it uses a single motor to actuate the system. The interior point method has been used for the optimization of the linkage dimensions [90]. Two link adjustments allowed the robot to match the ankle trajectories for different canonical gait patterns. A unilateral wooden proof-of-concept prototype has been constructed, as shown in Figure 2-17. A simple velocity feedback controller has been implemented to control the mechanism. The device allows ground contact proprioception. However, foot clearance has not been considered in the design of the prototype. Stroke survivors usually do not have the ability to control the orientation of the foot, a non-controlled foot may be further injured during gait training with this device. Although the authors claim that the proposed robot can generate natural ankle trajectories, the knee joint trajectory has not been considered during the design stage. Proper movement of the knee joint during walking is an important aspect of gait training process. Although the prototype has been constructed, it has not been tested using human subjects, and only trajectory generation at the ankle joint has been analyzed.

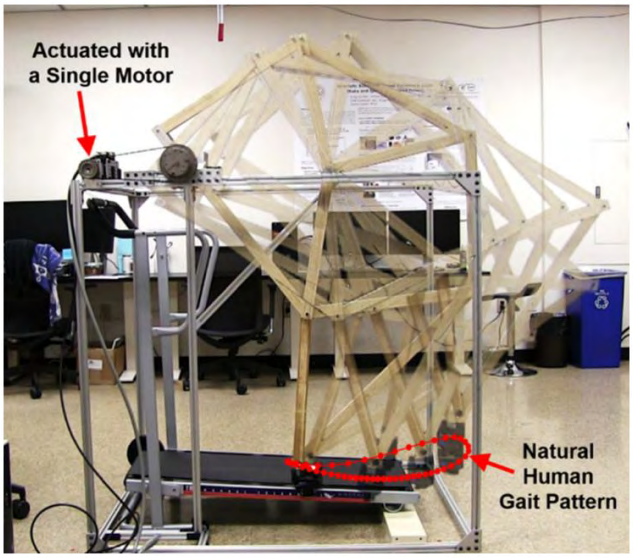


Figure 2-17. Wooden proof-of-concept prototype of the eight-link Jansen gait trainer [89].

#### 2.1.2.10 Linkage design gait trainer

The linkage design gait trainer (LGT) is based on a four-bar linkage and has been developed for generating walking trajectories required for gait rehabilitation [91]. The trust region-reflective algorithm has been used to optimize the link dimensions to reduce the errors between

target and generated ankle joint trajectories. It has been designed to operate over the ground. Acrylic plastic has been used to manufacture the prototype, allowing physiotherapists to monitor the walking pattern of the subject, as shown in Figure 2-18. The device is a single DOF mechanism. The walking frame has been constructed and tested on healthy human subjects. However, as the knee joint trajectory has not been considered in the optimization process, there were some deviations in the knee joint angles from the desired paths. Another limitation of the trainer is that the subject should match the initial walking phase to start using the device.

Figure 2-18. Linkage design gait trainer during operation [91].

#### 2.1.2.11 Mech-Walker

Mech-Walker is a low-cost gait rehabilitation device that can produce the ankle joint trajectory required for gait rehabilitation [92]. The mechanism is based on the eight-bar Jansen linkage, as shown in Figure 2-19.

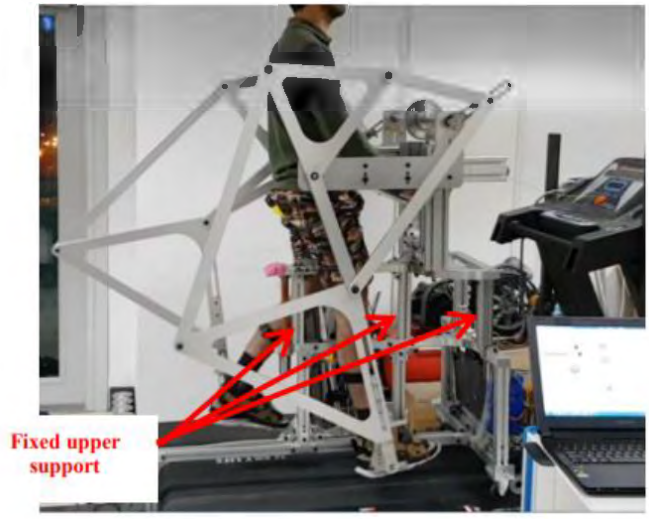


Figure 2-19. Mech-Walker with a healthy human subject [92].

The adjustability of links in the mechanism allows accommodating users with different leg lengths. The custom designed seat has been placed to support the weight of the subject. The dimensional synthesis has been done using the semi-global numerical optimization search as presented in [93]. The Mech-Walker robot is similar to the Jansen eight-bar linkage gait trainer presented in [89], and therefore they share the common limitations mentioned above.

#### 2.1.2.12 Six-bar linkage mechanism

A six-bar linkage has been designed for the purpose of rehabilitating human gait [94]. The mechanism can generate the ankle joint trajectory. The cooperative double particle swarm optimization (CDPSO) algorithm has been used to synthesize the dimensions of the links in the mechanism. The constant speed is reported to be sufficient to control the prototype. The 3D model of the gait rehabilitation system based on six-bar linkage is shown in Figure 2-20. Numerical simulations have been implemented to check their applicability to human subjects. However, as the limitation of the study, a physical prototype has not been constructed, and thus no experimental evaluation has been done on the feasibility of the proposed mechanism. Additionally, the knee joint trajectory has not been considered during the optimization process, resulting in poor lower limb trajectory generation.

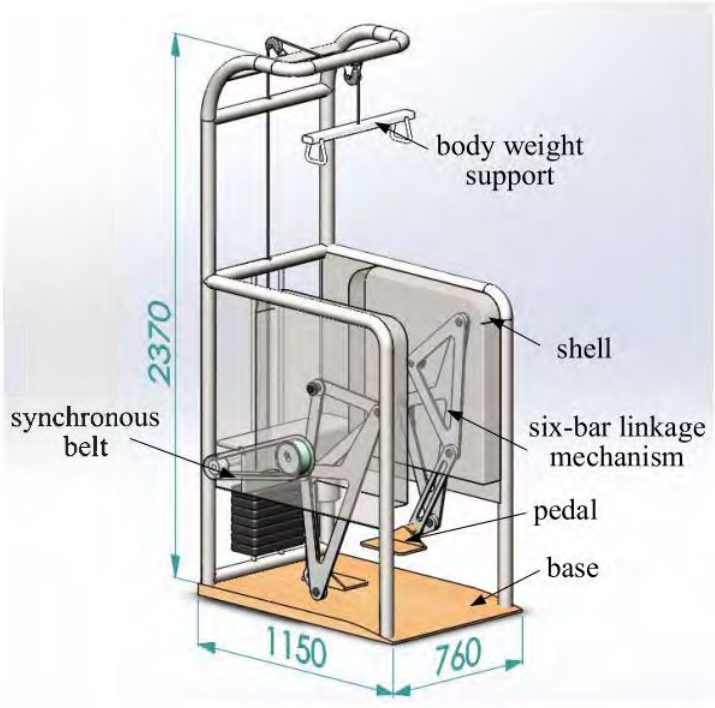


Figure 2-20. 3D model of the gait rehabilitation system based on six-bar linkage [94].

#### 2.1.2.13 Eight-bar linkage mechanism

An end-effector-based device for lower limb rehabilitation has been innovatively designed using an eight-bar linkage mechanism, as detailed in [95]. The design's most notable feature is its significantly reduced energy consumption; compared to traditional designs, this device consumes 52.13% less energy, leading to less control effort required by the user. The design methodology employed for this device is particularly unique as it concurrently incorporates kinematic synthesis, structure shape design, and dynamic performance. The device's design, as depicted in Figure 2-21, facilitates the training of the lower limbs in a seated position, which, while being a potential advantage in terms of accessibility and comfort, presents a potential limitation. As the user is seated during training, the device may not perfectly emulate the natural trajectory of the lower limb during walking. Thus, while it provides significant improvements in terms of energy efficiency and control effort, the exact replication of a naturalistic walking trajectory remains a challenge for this design approach.

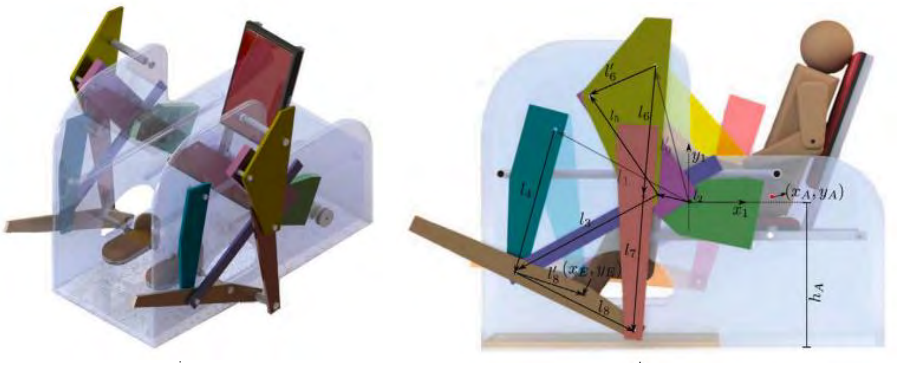

Figure 2-21. Eight-bar linkage based rehabilitation device [95].

#### 2.1.2.14 Four-bar linkage mechanism for children's gait rehabilitation

The rehabilitation system based on four-bar linkage has been designed for children with cerebral palsy or other psycho-motor impairment of two to twelve years old [96]. The system is reconfigurable and can adapt to different human's anthropometric parameters. It generates the drop type ankle trajectory. The synthesis of a four-bar mechanism has been done involving a Sequential Quadratic Programming (SQP), Differential Evolution (DE), mathematical programming method and an evolutive algorithm. The comparative analysis demonstrated that DE outperforms SQP due to the limited feasibility space derived from the problem constraints. The result obtained from DE has been simulated using computer aided design (CAD) software. The proposed system has not been manufactured and tested with children. Moreover, the

trajectories generated by the mechanism are not naturalistic as only ankle trajectory has been used during the design stage.

Figure 2-22. The proposed concept of the children's gait rehabilitation [96].

## 2.2 Chapter Summary

Despite the demonstrated efficacy of currently available multi-DOF gait rehabilitation robots in restoring the walking abilities of patients requiring training [97-99], the underlying aim of these devices is to provide necessary training to as many patients as possible. Regrettably, the high cost of these devices renders them unaffordable for a significant number of patients, resulting in an inability to access this form of rehabilitation. On the other hand, since the majority of previously developed multi-DOF gait rehabilitation robots tackle the motion produced in the sagittal plane, the utilization of multiple motors in current exoskeletons may not be entirely justified. As the major part of the range of motion of leg movement during walking is in the sagittal plane, it is possible to ignore coronal and transverse plane lower limb movements [100]. According to the rehabilitation outcomes from LOKOMAT, the sagittal plane motion was enough to rehabilitate impaired locomotor capabilities among patients suffering due to neurological disorders [51, 98]. One of the approaches addressing the issues of currently existing exoskeletons involves single DOF linkage-based mechanisms. Such mechanisms are lightweight and can reproduce human-like gait patterns in a sagittal plane [101]. Their actuation requires a smaller number of motors, which simplifies the control architecture and lowers the cost. Linkage-based mechanisms are closed-loop chains comprised of four or more links connected by rotary or sliding joints [102]. These mechanisms are usually presented in the form of four-bar, six-bar, eight-bar, and ten-bar arrangements. However, very

few research works have been done on the application of linkage-based mechanisms in the gait rehabilitation process. The following Table 2-1 provides the summary on the proposed linkage-based mechanisms for gait rehabilitation purposes.

Table 2-1. Summary on the Linkage-based Mechanisms Used for Gait Rehabilitation.

| **Mechanism** | **Linkage Type** | **Synthesis Method** | **Design target trajectory** | **Adjustability for different leg lengths** | **Experimental Validation** |
|---|---|---|---|---|---|
| Exoskeleton | Four-bar [80] | Hybrid teaching-learning-particle swarm optimization (HTLPSO) algorithm and Genetic Algorithm (GA) | Ankle | No | No |
| Exoskeleton | Six-bar [81] | Homotopy - directed optimization | Ankle | Yes | No |
| Exoskeleton | Six-bar [82] | Homotopy - directed optimization | Ankle | No | |
| End-effector gait trainer | Five-bar [83] | Missing | Ankle | No | Yes |
| End-effector gait trainer | Seven-bar [84] | Genetic Algorithm (GA) | Ankle | No | No |
| End-effector gait trainer | Watt I six-bar [103] | Data driven approach | Ankle | No | Yes |
| End-effector gait trainer for children | Six-bar [87] | Missing | Ankle | No | Yes |
| Exoskeleton | Cam-mechanism [88] | Missing | Ankle | Yes | No |

| | | | | | |
|---|---|---|---|---|---|
| Gait trainer | Jansen eight-bar [89] | Interior point method | Ankle | Yes | Yes |
| Gait trainer | Four-bar [91] | Trust region-reflective algorithm | Ankle | No | Yes |
| Walker | Jansen eight-bar [92] | Semi-global numerical optimization | Ankle | Yes | Yes |
| Gait trainer | Six-bar [94] | Cooperative double particle swarm optimization (CDPSO) algorithm | Ankle | No | No |
| End-effector gait trainer | Eight-bar [95] | Evolutionary Algorithm (EA) | Ankle | No | No |
| Gait-trainer for children | Four-bar [96] | Mathematical programming methods, evolutive algorithm, sequential quadratic programming (SQP) and differential evolution (DE) | Ankle | Yes | No |

Previously proposed concepts for linkage-based exoskeletons have typically focused solely on the movement of the ankle joint, without taking into consideration the critical role of the knee joint in the gait rehabilitation process. Furthermore, most of them are still in the theoretical stage, with their primary focus being on synthesis methods and simulation. The feasibility of the studies on human subjects has not been properly validated. Only a couple of walkers have tested the proof-of-concept prototypes on healthy subject. The dynamic aspect of the robots has not been studied or covered among them.

The end-effector of the linkages is called couplers, and the trajectories produced at those points are referred to as coupler curves. Dimensional synthesis, which involves determining optimal linkage dimensions that satisfy lower limb trajectories, is a challenging process that

may require solving higher-order polynomial equations in a standard approach or solving other constrained optimization problems. These methods demand higher computational resources, as even a small deviation in one of the link's lengths can significantly alter the output motion. Previous concepts based on linkage mechanisms have been used to synthesize four-bar [104-107], Stephenson II six-bar , Stephenson III six-bar [108], seven-bar [84], eight-bar [89, 92, 109], and ten-bar [110] for ankle trajectory generation. However, none of the proposed synthesis methods took into consideration the concurrent knee trajectory movement in the optimization task, even though knee joint motion is a crucial factor to consider during the gait training process. Moreover, linkages' synthesis has been traditionally done using synthesis methods that involve solving higher-order polynomial equations and performing iterative calculations, demanding high computational resources. Additionally, the continuity aspect of the input is often ignored, as the problem is formulated with a discrete position objective, which can result in various order or branch defects[111]. For instance, the mechanism may pass through all the required position points but not in the correct order.

An alternative and often underrated approach to synthesize linkage dimensions is through the application of modern machine learning techniques. However, there are only a few works that have employed a machine learning approach for the synthesis of linkage-based mechanisms, but not for rehabilitation purposes. For example, Khan *et al*. utilized an artificial neural network (ANN)-based approach to map Fourier coefficients describing the target curve and its corresponding linkage parameters. This approach showed the potential of deriving a four-bar linkage mechanism capable of tracing desired trajectories (coupler curves). Similarly, Deshpande *et al*. used auto-encoder neural networks to synthesize defect-free four-bar linkage solutions for motion generation problems [112]. The machine learning framework has proven effective in generating various sets of defect-free solutions for four-bar linkages.

In summary, the synthesis of linkage-based mechanisms to generate ankle trajectories for gait rehabilitation purposes has mainly been presented using conventional synthesis techniques, which can lead to branch or order defects during the design optimization stage. Moreover, different people have varying anthropometric features, such as different leg lengths, resulting in different shapes of gait trajectories. This poses a challenge in recalculating linkage dimensions to fit individuals with different leg lengths, requiring more computational resources during iterative calculations. Since, knee joint trajectory has not been considered in proposed linkage-based rehabilitation mechanisms, it may cause misalignments between human joints

and the robot, negatively affecting the overall gait training process. To overcome defects during the mechanism design stage, machine learning-based synthesis techniques have demonstrated their effectiveness, but they have been implemented primarily on non-rehabilitation four-bar mechanisms, targeting only a single trajectory. Furthermore, fully functional gait rehabilitation robots have not been constructed, and their engineering feasibility has not been adequately validated with human subjects. Moreover, patient cooperative control strategies have not been developed for single DOF mechanisms.

In summary, this chapter presented a detailed review of the current state-of-the-art in the field of gait rehabilitation robots. It identified key gaps in the literature, notably:

1) The absence of consideration for knee joint trajectory in the synthesis of linkage-based mechanisms.
2) The issues faced in adapting linkage dimensions to different leg lengths due to the high computational resources required in iterative calculations.
3) The limited utilization of machine learning techniques in the synthesis of linkage-based mechanisms for gait rehabilitation purposes.
4) The lack of validation of the engineering feasibility of gait rehabilitation robots with human subjects.
5) The nonexistence of patient cooperative control strategies for single DOF mechanisms.

Addressing these gaps forms the core of this research and the basis of the upcoming chapters. Chapter 3 presents the design evolution of the robot, addressing the first gap by considering both the ankle and knee joint trajectory in generating naturalistic lower limb motions. Chapter 4 moves forward by employing machine learning techniques to synthesize the dimensions of the mechanisms, addressing the second and third gaps identified. This new approach is expected to ease the estimation of linkage dimensions compared to traditional synthesis approaches. Chapter 5 will then tackle the fourth gap by addressing velocity regulation in linkage-based mechanisms. The developed machine learning framework will regulate velocity, ensuring consistency and stability, considering the inertia of the human leg attached to the robot. Finally, in chapter 6, we address the last gap by developing a novel patient cooperative control strategy. This ensures active participation from human subjects, contributing significantly to gait rehabilitation. By aligning the findings of this review with the subsequent chapters, this research aims to provide comprehensive solutions to the identified gaps in the field of gait rehabilitation

robots, fostering the development of cost-effective and efficient rehabilitation systems.

# Chapter 3. Wearable Robot Orthosis Design Evolution and Analysis

This chapter outlines the systematic development of an initial proof-of-concept for a single DOF linkage-based gait rehabilitation prototype. It justifies the choice of linkage type and then conducts position analysis to determine the location of the end-effectors in relation to the input angle of the crank. After the position analysis, force analysis is carried out to evaluate the inherent torques and forces acting within the mechanism. These evaluations are crucial in identifying appropriate motor characteristics that align with the system requirements.

Subsequently, the chapter focuses on optimizing the dimensions of the linkage. This involves a thorough perturbation analysis, which aids in identifying elements that have a significant impact on the trajectory curve at the coupler points or end-effectors. The chapter concludes with a description of the initial control scheme implemented in the robot, presenting a proof-of-concept prototype made from acrylic plastic. This prototype not only validates the theoretical framework but also facilitates a hands-on evaluation of the system's functionality. By proceeding methodically, this chapter provides a detailed insight into the step-by-step evolutionary design process of a linkage-based robotic system designed for gait rehabilitation. The content of chapter 3 is published in [113].

## 3.1 Design Evolution and Mechanism Description

As previously mentioned, linkage-based mechanisms can be comprised of four or more bars. Studies have shown that four-bar mechanisms are not capable of providing the prescribed timing for complex trajectory motions of the ankle joint [114]. Eight-bar and ten-bar mechanisms, synthesized to generate ankle trajectory for gait rehabilitation, tend to be bulky due to the high number of links. As a result, they might not be the most suitable candidates for gait rehabilitation. Conversely, six-bar mechanisms, such as the Stephenson III, strike a balance between the benefits of four-bar mechanisms and those of eight or ten-bar linkages. They are compact, yet they can produce the naturalistic lower limb trajectories needed for gait rehabilitation [108, 115-117].

Given these findings, this study adopts the Stephenson III six-bar linkage as the foundational principle of our proposed orthosis design. This single DOF planar mechanism consists of two four-bar linkages, where one linkage actuates the other, as shown in Figure 3-1. The motor rotates the crank $\overline{A_{st}D_{st}}$, and the desired motions are produced at joints $E_{st}$ and $G_{st}$, which are referred to as coupler points. The mechanism has three fixed joints $A_{st}$, $B_{st}$, and $C_{st}$.

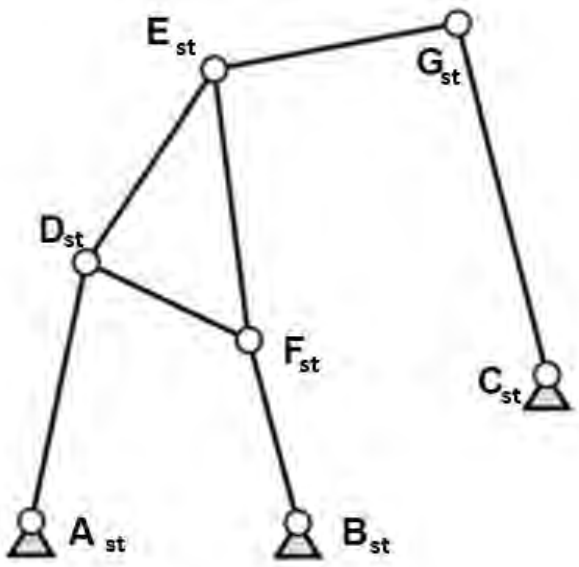


Figure 3-1. The standard shape of the Stephenson III six-bar linkage.

One primary design requirement for the orthosis is to position both fixed and moving joints above the ground while ensuring the link proportions align with human lower limb anatomy. It's also essential to maintain the functional aspect of continuous motion, meaning the trajectory points must be followed sequentially by the planar linkage's coupler. Aligning the linkage parameters with the anatomy of the human lower limbs is crucial to guarantee synchronized movement between the human limbs and the exoskeleton during gait training. Drawing inspiration from the earlier work by Tsuge *et al*. [108], we introduced modifications to the Stephenson III six-bar linkage. This resulted in the configuration shown in Figure 3-2, where the fixed joints A (origin), B, and $G$ are elevated above the ground, and the joints $G, E, K$ are designed to align with the human hip, knee, and ankle joints, respectively.

The proposed mechanism employs a single motor located at joint A. This motor rotates continuously in a single direction in an anticlockwise direction for the left leg and clockwise for the right leg. Structurally, same as the standard shape mentioned previously, the modified mechanism integrates two four-bar linkages, together forming the six-bar linkage. One of these four-bar linkages functions as the driver for the other.

Link $\overline{BC}$ is the mechanism's rocker arm. Consequently, the link $\overline{\text{AD}}$ of length L9 acts as a crank to the whole linkage system. The input angle provided to the actuator is denoted by $\theta$. The length between joints $A$, B, and $G$ are specified via Euclidean distances. All the links within the mechanism connect through rotary joints. The design includes two ternary links ($\overline{CDE}, \overline{HEK}$) and four binary links ($\overline{AB}, \overline{GH}, \overline{BC}, \overline{AD}$) as illustrated in Figure 3-2. The link $\overline{CDE}$

is the coupler link on which the first coupler point $E$ is being placed. The first four-bar linkage $\overline{ABCD}$ with coupler point at joint $E$ acts as a crank part for the second four-bar mechanism, where the link $\overline{GH}$ is the second rocker arm. Joint $H$ is the second coupler point of the mechanism. GIM® software was utilized to heuristically locate the fixed joints $A$ and $B$ relative to the hip joint $G$ and set the initial dimensions of the linkage.

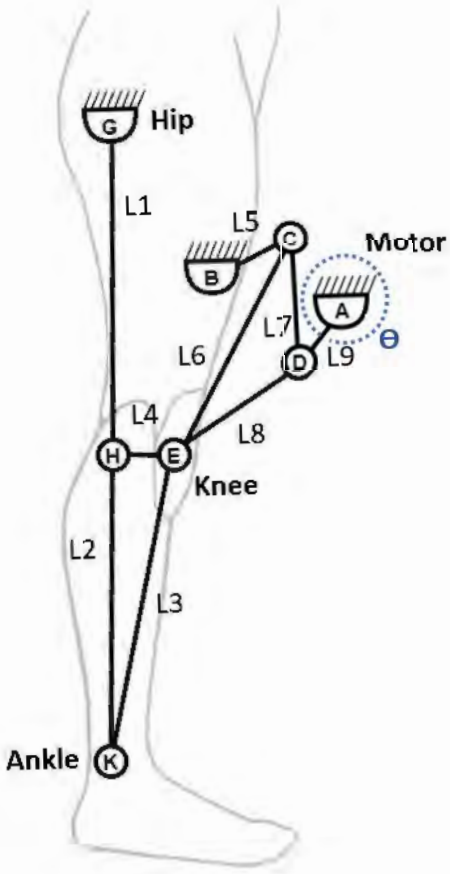


Figure 3-2. The mechanism of the gait rehabilitation robotic orthosis matching the lower limb joints.

## 3.2 Mechanism Analysis

### 3.2.1 Forward Kinematics Analysis

Using analytical geometry, the position coordinates of each joint corresponding to the input angle $\theta$ about fixed joint $A$ in the mechanism were derived. The derivations of the coordinate positions of each joint are summarized below. The notations and configurations defined for analyzing the mechanism analysis are shown in Figure 3-3. The lengths between the joints are defined to be $Li$.

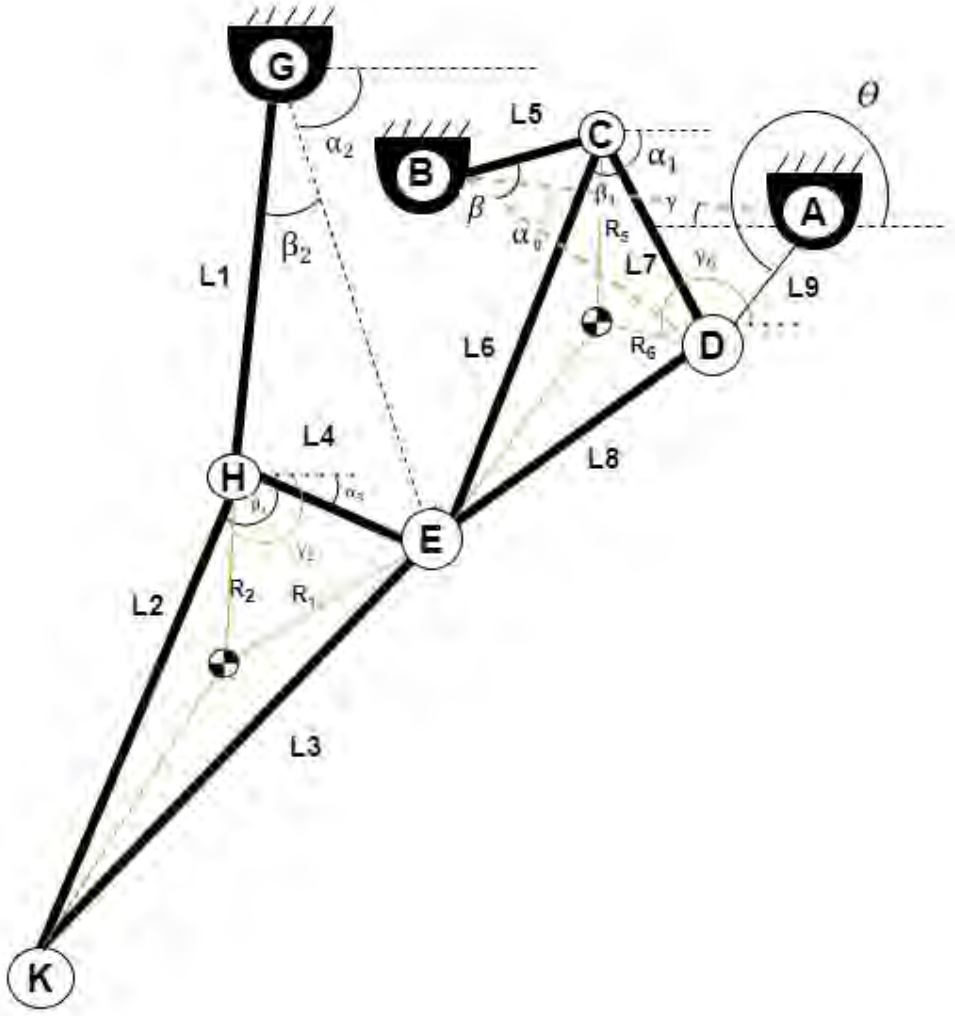


Figure 3-3. Scheme of Stephenson III six-bar linkage for motion evaluation.

Point $A$ is considered to be the origin of the reference frame. The distances between points $A$ and $B, B$ and $D$ are specified by their Euclidean distances. Angles $\gamma$, $\alpha_0$, $\beta$, $\alpha_1$, $\beta_1$, $\alpha_2$, $\beta_2$, $\alpha_3$, and $\beta_3$ from Figure 3-3 are determined using laws of sines and cosines as follows:

$$\begin{cases} \gamma = \tan^{-1}\left(\frac{A_y+B_y}{A_x-B_x}\right) \\ \alpha_0 = \sin^{-1}(L9 * \sin(\Pi - \theta - \gamma)/\overline{BD}) \\ \beta = \cos^{-1}\left(\frac{\overline{BD^2}+\overline{BC^2}-\overline{CD^2}}{2*\overline{BD}*\overline{BC}}\right) \end{cases} \tag{3.1}$$

$$\begin{cases} \alpha_1 = \tan^{-1}\left(\frac{D_y-C_y}{C_x-D_x}\right) \\ \beta_1 = \cos^{-1}\left(\frac{L6^2+L7^2-L8^2}{2*L6*L7}\right) \end{cases} \tag{3.2}$$

$$\begin{cases} \alpha_2 = \tan^{-1}\left(\frac{E_y-G_y}{G_x-E_x}\right) \\ \beta_2 = \cos^{-1}\left(\frac{L1^2+\overline{EG}^2-\overline{HE}^2}{2*L1*EG}\right) \end{cases} \tag{3.3}$$

where $\overline{EG}$ is the Euclidean distance between joints $E$ and $G$. The expressions for angles $\alpha_3$ and $\beta_3$ are as follows:

$$\begin{cases} \alpha_3 = \tan^{-1}\left(\frac{G_y - E_y}{G_x - E_x}\right) \\ \beta_3 = \cos^{-1}\left(\frac{\overline{HE}^2 + \overline{HK}^2 - \overline{EK}^2}{2 * \overline{HE}^2 * \overline{HK}^2}\right) \end{cases} \tag{3.4}$$

To reduce the complexity of the linkage dimensional synthesis problem, the coordinate positions for the fixed joints $A$, $B$, and $G$ were initialized as shown in Table 3-1. All joints' coordinates estimation based on the input angle $\theta$ are illustrated in Table 3-1.

Table 3-1. Coordinate Positions of Joints (mm).

| Joint | X coordinate | Y coordinate |
|---|---|---|
| **A** | 0 | 0 |
| **B** | $-133.2$ | 50.6 |
| **G** | $-170.7$ | 203.4 |
| **D** | $A_x + L9 * cos(\theta)$ | $A_y + L9 * sin(\theta)$ |
| **C** | $B_x + L5 * cos(\alpha_0 + \beta - \gamma)$ | $B_y + L5 * sin\ (\alpha_0\ + \beta - \gamma)$ |
| **E** | $C_x\ +\ L6 * cos\ (\alpha_1 +\ \beta_1)$ | $C_y - L6 * sin(\alpha_1 + \beta_1)$ |
| **H** | $G_x +\ L1 * cos(\alpha_2 +\ \beta_2)$ | $G_y - L1 * sin(\alpha_2 +\ \beta_2)$ |
| **K** | $G_x\ +\ L2 * cos\ (-\alpha_3 +\ \beta_3)$ | $G_y\ -\ L2 * sin\ (-\alpha_3 +\ \beta_3)$ |

## 3.3 Dynamic Force Analysis

Dynamic force analysis for the proposed mechanism can be performed using classical mechanics [118]. Joint reaction forces and the joint torques at the joints of the mechanism in the sagittal plane were found using Equations (3.5-3.7).

$$\sum F_x = ma_x \tag{3.5}$$

$$\sum F_y = ma_y \tag{3.6}$$

$$\sum T_r = I_g \alpha \tag{3.7}$$

Here, $F_x$ and $F_y$ are the reaction forces directed along the x and y axes respectively, $m$ is the mass of the given link, $a_x$ and $a_y$ are accelerations along the x and y axes respectively, $T_r$ is the resultant torque, $I_g$ is the mass moment of inertia about an axis passing through the center of mass, and $\alpha$ is angular acceleration. The centers of mass are located at the mid-point of each rigid linkage, and all joints are assumed to be revolute and frictionless. Figure 3-4 shows the free-body diagrams of each of the moving links in the mechanism.

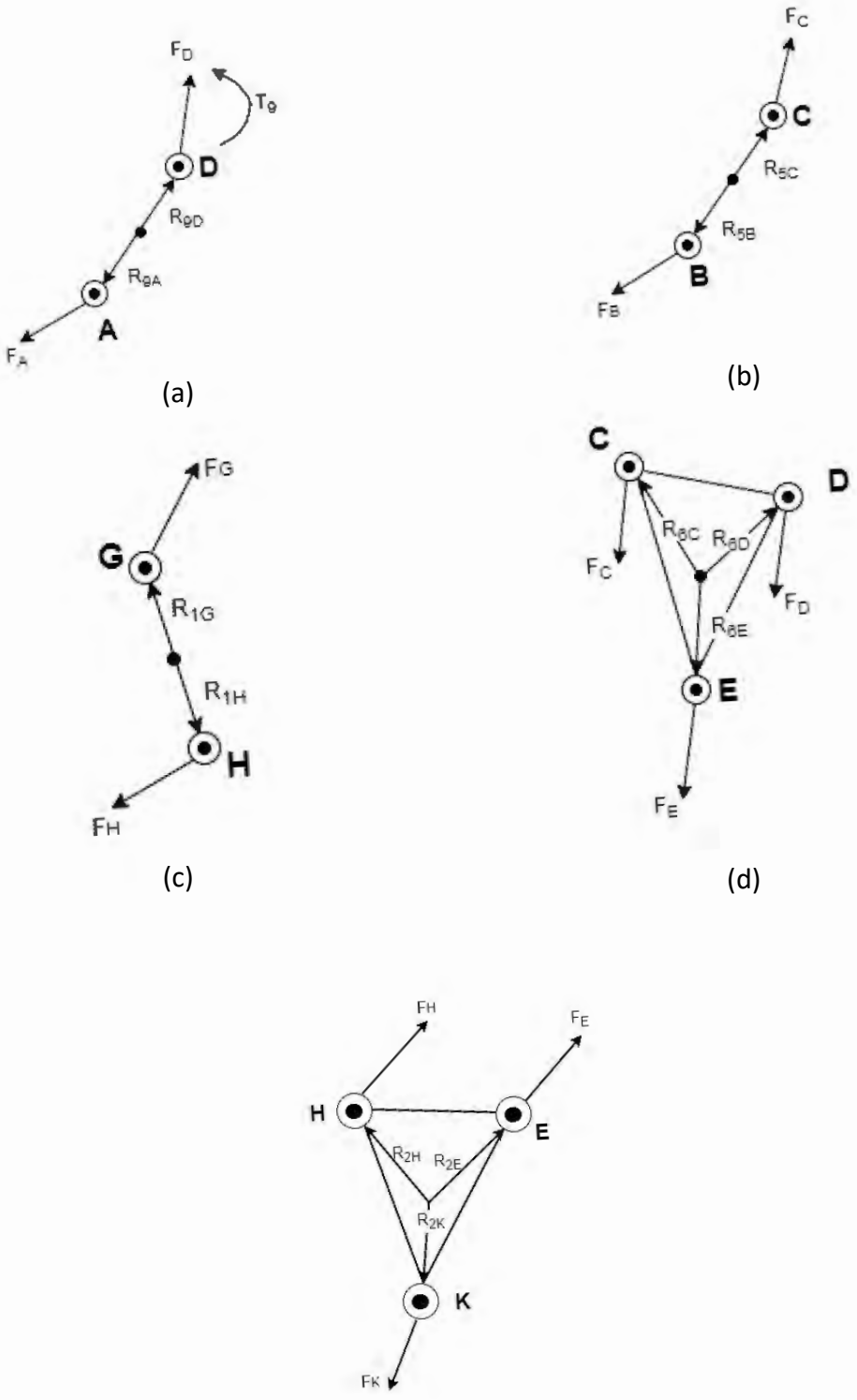


Figure 3-4. The free-body diagram of forces in the mechanism.

The corresponding Newtonian equations derived for the moving link in Figure 3-4(a) are presented below:

$$\begin{cases} F_{Ax} + F_{Dx} = m_9 a_{9gx} \\ F_{Ay} + F_{Dy} = m_9 a_{9gy} \\ T_9 + (R_{9Ax}F_{Ax} - R_{9Ay}F_{Ay}) + \left(R_{9Dx}F_{9Dx} - R_{9Dy}F_{Dy}\right) = 0 \end{cases} \tag{3.8}$$

where $F_{Ax}$ and $F_{Ay}$ are the reaction forces at point $A$ along the x and y axes, respectively, $m_9$ is the mass of link $\overline{AD}$, $a_{9gx}$ and $a_{9gy}$ are the accelerations of the point at center of mass gravity of the link $\overline{AD}$ along the x and y axes, respectively. The points where the forces act are described by the position vectors $R$. For instance, $R_{9Ax}$ is the position vector indicating at which point the force $F_{Ax}$ in link $\overline{AD}$ acts. $T_9$ is the torque acting on the link $\overline{AD}$ by the motor. Continuing the derivation in the same way for the remaining moving parts in Figure 3-4 (b-e), we obtain the following set of Newtonian Equations (3.9-3.12):

$$\begin{cases} F_{Bx} + F_{Cx} = m_5 a_{5gx} \\ F_{By} + F_{Cy} = m_5 a_{5gy} \\ (R_{5Bx}F_{Bx} - R_{5By}F_{By}) + (R_{5Cx}F_{Cx} - R_{5Cy}F_{Cy}) = I_{5g}\alpha_5 \end{cases} \tag{3.9}$$

The Newtonian equations for the moving part in Fig. 3-4 (c) are specified in the below set of Equations (3.10).

$$\begin{cases} F_{Gx} + F_{Hx} = m_1 a_{1gx} \\ F_{Gy} + F_{Hy} = m_1 a_{1gy} \\ (R_{1Gx}F_{Gx} - R_{1Gy}F_{Gy}) + (R_{1Hx}F_{Hx} - R_{1Hy}F_{Hy}) = I_{1g}\alpha_1 \end{cases} \tag{3.10}$$

From Fig. 3-4 (d) Newtonian equations are as follows.

$$\begin{cases} F_{Ex} - F_{Cx} - F_{Dx} = m_6 a_{6gx} \\ F_{Ey} - F_{Cy} - F_{Dy} = m_6 a_{6gy} \\ (R_{6Ex}F_{Ex} - R_{6Ey}F_{Ey}) - (R_{6Cx}F_{Cx} - R_{6Cy}F_{Cy}) - (R_{6Dx}F_{Dx} - R_{6Dy}F_{Dy}) = I_{6g}\alpha_6 \end{cases} \tag{3.11}$$

The Newtonian equations for the moving part in Figure 3-4 (e) are as follows.

$$\begin{cases} F_{Kx} - F_{Ex} - F_{Hx} = m_2 a_{2gx} \\ F_{Ky} - F_{Ey} - F_{Hy} = m_2 a_{2gy} \\ (R_{2Kx}F_{Kx} - R_{2Ky}F_{Ky}) - (R_{2Ex}F_{Ex} - R_{2Ey}F_{Ey}) - (R_{2Hx}F_{Hx} - R_{2Hy}F_{Hy}) = I_{2g}\alpha_2 \end{cases} \tag{3.12}$$

Here, $I_{1g}, I_{2g}, I_{5g}, I_{6G}$ are the mass moment of inertia about an axis passing through the center of mass for links 1, 2, 5 and 6, respectively. The equations (3.8-3.12) can be put in the form of a matrix with unknown variables coefficients creating the $M$ matrix (contains geometric details), $Q$ vector with unknown forces and torques, and constant terms in $P$ vector, which contains dynamic details of the system:

$$M \times Q = P \tag{3.13}$$

Where matrix $M$ is defined as below:

| | | | | | | | | | | | | | | |
|---|---|---|---|---|---|---|---|---|---|---|---|---|---|---|
| 1 | 0 | 0 | 0 | 0 | 0 | 1 | 0 | 0 | 0 | 0 | 0 | 0 | 0 | 0 |
| 0 | 1 | 0 | 0 | 0 | 0 | 0 | 1 | 0 | 0 | 0 | 0 | 0 | 0 | 0 |
| $R_{9Ax}$ | $-R_{9Ay}$ | 0 | 0 | 0 | 0 | $R_{9Dx}$ | $-R_{9Dy}$ | 0 | 0 | 0 | 0 | 0 | 0 | 1 |
| 0 | 0 | 1 | 0 | 1 | 0 | 0 | 0 | 0 | 0 | 0 | 0 | 0 | 0 | 0 |
| 0 | 0 | 0 | 1 | 0 | 1 | 0 | 0 | 0 | 0 | 0 | 0 | 0 | 0 | 0 |
| 0 | 0 | $R_{5Bx}$ | $-R_{5By}$ | $R_{5Cx}$ | $-R_{5Cy}$ | 0 | 0 | 0 | 0 | 0 | 0 | 0 | 0 | 0 |
| 0 | 0 | 0 | 0 | -1 | 0 | -1 | 0 | 1 | 0 | 0 | 0 | 0 | 0 | 0 |
| 0 | 0 | 0 | 0 | 0 | -1 | 0 | -1 | 0 | 1 | 0 | 0 | 0 | 0 | 0 |
| 0 | 0 | 0 | 0 | $-R_{6Cx}$ | $R_{6Cy}$ | $-R_{6Dx}$ | $R_{6Dy}$ | $R_{6Ex}$ | $-R_{6Ey}$ | 0 | 0 | 0 | 0 | 0 |
| 0 | 0 | 0 | 0 | 0 | 0 | 0 | 0 | 0 | 0 | 1 | 0 | 1 | 0 | 0 |
| 0 | 0 | 0 | 0 | 0 | 0 | 0 | 0 | 0 | 0 | 0 | 1 | 0 | 1 | 0 |
| 0 | 0 | 0 | 0 | 0 | 0 | 0 | 0 | 0 | 0 | $R_{1Gx}$ | $-R_{1Gy}$ | $R_{1Hx}$ | $-R_{1Hy}$ | 0 |
| 0 | 0 | 0 | 0 | 0 | 0 | 0 | 0 | -1 | 0 | 0 | 0 | -1 | 0 | 0 |
| 0 | 0 | 0 | 0 | 0 | 0 | 0 | 0 | 0 | -1 | 0 | 0 | 0 | -1 | 0 |
| 0 | 0 | 0 | 0 | 0 | 0 | 0 | 0 | $-R_{2Ex}$ | $R_{2Ey}$ | 0 | 0 | $-R_{2Hx}$ | $R_{2Hy}$ | 0 |

Matrices *Q* and *P* are presented further.

$$Q = \begin{pmatrix} F_{Ax} \\ F_{Ay} \\ F_{Bx} \\ F_{By} \\ F_{Cx} \\ F_{Cy} \\ F_{Dx} \\ F_{Dy} \\ F_{Ex} \\ F_{Ey} \\ F_{Gx} \\ F_{Gy} \\ F_{Kx} \\ F_{Ky} \\ T_9 \end{pmatrix}; \quad P = \begin{pmatrix} m_9 a_{9x} \\ m_9 a_{9y} \\ 0 \\ m_5 a_{5x} \\ m_5 a_{5y} \\ \frac{I_5 \sqrt{C_{ax}^2 + C_{ay}^2}}{L5} \\ m_6 a_{6x} \\ m_6 a_{6y} \\ \frac{I_6 \, \Delta\omega_6}{\Delta t} \\ m_1 a_{1x} \\ m_1 a_{1y} \\ \frac{I_1 \sqrt{G_{ax}^2 + G_{ay}^2}}{L1} \\ m_2 a_{2x} - F_{Kx} \\ m_2 a_{2y} - F_{Ky} \\ I_2 \alpha_2 - (R_{2Kx} F_{Kx} - R_{2Ky} F_{Ky}) \end{pmatrix}$$

Where $\omega_6$ is the angular velocity which is the difference of angle $\alpha_1$ with respect to time t, and $\Delta$ indicates the difference or change in the succeeding term. Then, the column vector $Q$ with 15 unknowns is calculated by multiplying the inverse of matrix $M$ on both sides of Equation (3.13).

## 3.4 Design Optimization

While the position analysis from the available set of linkage dimensions can be carried out as described in the previous subsection 3.2.1, finding the required linkage dimensions to achieve target positions of points $E$ and $K$ is non-trivial. This analysis is termed inverse kinematics and can result in either no solution, a unique solution, or a multitude of solutions. Achieving the target knee and ankle joint trajectories encounters these three outcomes for the required linkage dimensions. In other words, when designing the orthosis, it is necessary to find a unique set of linkage dimensions that will provide the desired trajectories at joints $E$ and $K$. In previous research, this problem has been resolved by imposing additional constraints [119-121], which may not always work in the absence of feasible constraints. Therefore, in the present research, it is proposed to resolve this issue through optimization.

In fact, the linkage dimension synthesis problem for the proposed orthosis is a multi-objective optimization task. The two objectives for the linkage dimension synthesis are the minimization of error functions representing the differences (in the form of Euclidean distances) between the

desired knee and ankle trajectory points and the corresponding generated coupler points from the mechanism as shown in Equations (3.14-3.15). These two objectives were combined into one objective by summing with unity weights (Equation 3.16). There are two major constraints drawn from the Grashof's condition, and one of these dictates that the sum of the shortest and longest link in the $\overline{ABCD}$ linkage should be less than the sum of the other links, as denoted in Equation (3.17). Another constraint is that the link between points $A$ and $D$, which acts as a crank, should be the shortest one among $L7$, $L5$ and $\overline{AB}$ as denoted in Equation (3.18). The input angle $\theta^i$ at joint $A$ should be either in ascending or in descending order in Equation (3.19), and the number of input positions corresponds to the number of desired trajectory points. Therefore, the objective functions are as follows:

$$f_1(V) = \sum_{i=1}^{N}[(P_{x,i} - E_{x,i})^2 + (P_{y,i} - E_{y,i})^2] \tag{3.14}$$

$$f_2(V) = \sum_{i=1}^{N}[\left(R_{x,i} - K_{x,i}\right)^2 + \left(R_{y,i} - K_{y,i}\right)^2] \tag{3.15}$$

$$Minimize\ F(V) = (f_1(V) + f_2(V)) \tag{3.16}$$

$$\text{Subjected to } L9 + L7 < L5 + AB, \tag{3.17}$$

$$L9 < (L7, L5, \overline{AB}), \tag{3.18}$$

$$\theta^i < \theta^{i+1} < \cdots < \theta^N, \quad i = 1, \tag{3.19}$$

$$V_{lower} < V < V_{upper} \tag{3.20}$$

$$|\overline{HK} - \overline{EK}| < \overline{HE} < \overline{HK} + EK \tag{3.21}$$

$$|L2 - L3| < L4 < L2 + L3 \tag{3.22}$$

Where $(P_{x,i}, P_{y,i})$ and $(R_{x,i}, R_{y,i})$ are the sets of desired trajectory points for the knee and ankle coupler curves, respectively. $\overline{AB}$ is the Euclidean distance between joints $A$ and $B$. $\theta^i$ are the input link angles at joint $A$. $V = (L1,\ L2,\ L3,\ L4,\ L5,\ L6,\ L7,\ L8,\ L9)^T$ is the design variable vector for the mechanism that should be between the lower bound $V_{lower}$ and upper bound $V_{upper}$ in Equation (3.20), $N$ is the total number of targeted points, and $(E_{x,i}, E_{y,i})$ and $(K_{x,i}, K_{y,i})$ are the generated parametric trajectory points by the mechanism for the knee and ankle coupler curves respectively. The desired trajectory points are human biomechanical trajectories adapted from Winter [122]. The triangle inequality theorem must be satisfied to confirm that the group of links $L2, L3, L4$ and $L6, L7, L8$ can form triangles and, therefore,

satisfy inequalities (3.21) and (3.22). To solve the given minimization problem, a GA was implemented in the Matlab® environment. The desired trajectory points come from the standard biomechanical knee and ankle joint center trajectories adopted from [122].

To select the vital dimensions of the mechanism that qualify as the set of design variables, a perturbation analysis is carried out. It is designed to converge to a smaller set of important design variables to save computational time during the optimization. Therefore, the sensitive mechanism dimensions, which affect the coupler point K position error more than other dimensions, need to be identified. A sensitivity analysis of the mechanism's coupler point K position error in relation to the desired trajectory points R vis-à-vis changes in the link lengths was carried out. Specifically, 2000 perturbations were applied for each link length in the range of ±10% of the intuitively selected initial dimensions.

### 3.4.1 Perturbation Analysis:

The results of the perturbation analysis are presented in Table 3-2 and the distribution of errors related to the position of the coupler point *H* shown in (Figure 3-5(a) to 3-5(i)), where the x-axis represents the distribution error in mm.

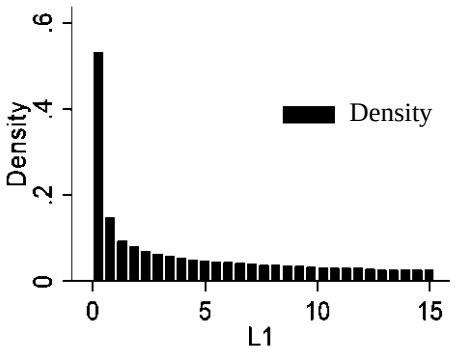


(a) Error distribution by varying L1

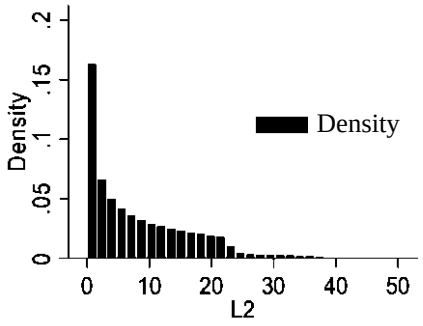


(b) Error distribution by varying L2

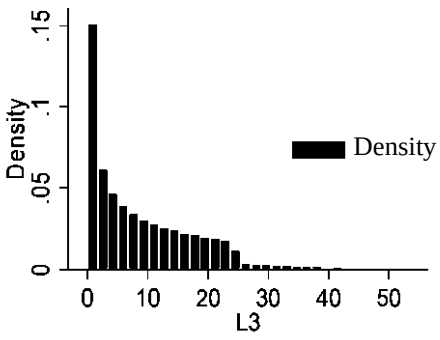


(c) Error distribution by varying L3

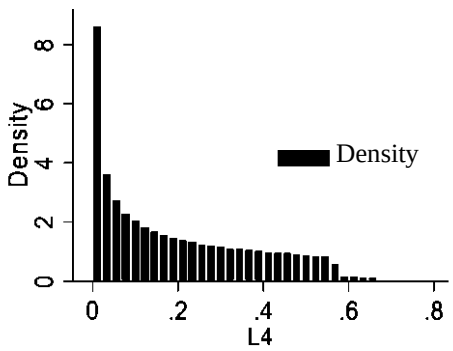


(d) Error distribution by varying L4

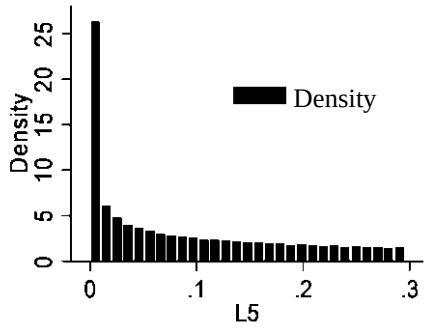


(e) Error distribution by varying L5

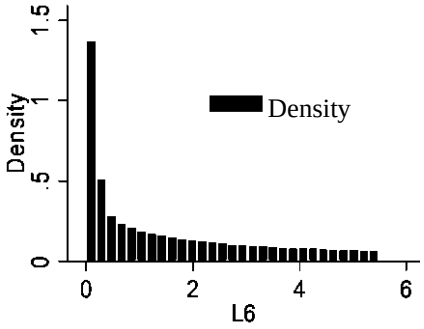


(f) Error distribution by varying L6

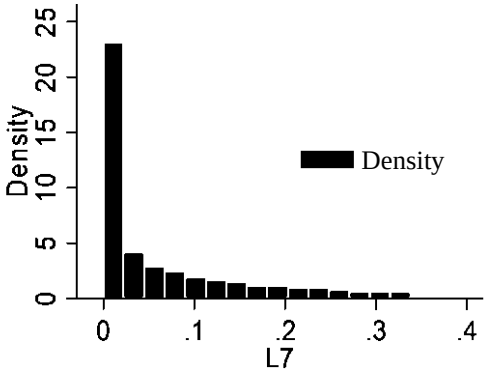


(g) Error distribution by varying L7

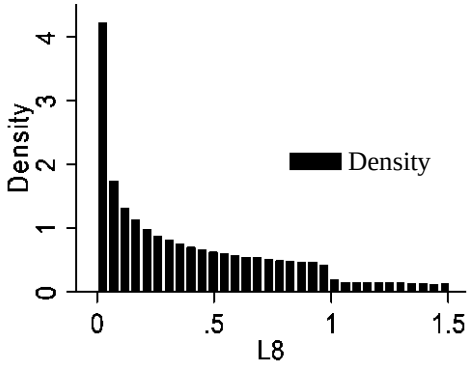


(h) Error distribution by varying L8

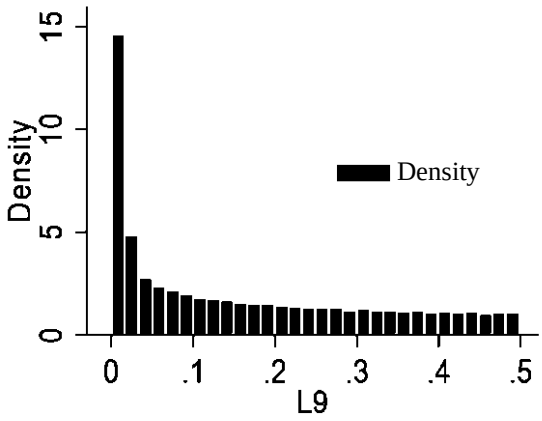


(i) Error distribution by varying L9

Figure 3-5. Histogram of coupler point H position error in relation to the change of each linkages lengths to demonstrate +10% and -10% perturbation.

Although the number of perturbations was set to 2000 in the range of ±10% of the initial dimensions, some of the given linkage dimensions could not converge in reaching the position of coupler point *K* and were thus neglected, since some varied combinations of linkage dimensions cannot form a linkage. As can be noted from Table 3-2, the larger the standard deviation, the higher is the spread of errors around the corresponding mean, and hence the higher is the

uncertainty. The largest mean values and standard deviations were observed for links $L1, L2$, and $L3$. The initial linkage dimensions used are presented in Table 3-3.

Table 3-2. Summary Statistics of the Coupler Point H Position Error (mm) due to Deviation of Linkage Dimensions.

| Variable | Obs. | Mean | Std. Dev. | Min | Max |
|---|---|---|---|---|---|
| L1 | 865 | 4.39 | 4.51 | 0.00 | 15.22 |
| L2 | 1,892 | 8.81 | 9.02 | 0.00 | 50.89 |
| L3 | 1,995 | 9.49 | 9.57 | 0.00 | 54.15 |
| L4 | 1,233 | 0.20 | 0.18 | 0.00 | 0.67 |
| L5 | 994 | 0.09 | 0.09 | 0.00 | 0.30 |
| L6 | 929 | 1.54 | 1.58 | 0.00 | 5.48 |
| L7 | 234 | 0.06 | 0.08 | 0.00 | 0.34 |
| L8 | 1,696 | 0.41 | 0.38 | 0.00 | 1.51 |
| L9 | 1,001 | 0.16 | 0.15 | 0.00 | 0.50 |

The mean and standard deviation for $L6$ are moderate, while the lowest mean and standard deviation are found for links L4, L5, $L7, L8$, and $L9$. These results show that, overall, the size of the errors between coupler point K and desired trajectory points R increase when we vary the length of links $L1, L2$, and $L3$, while the size of errors does not vary much for links $L5, L7, L8$, and $L9$. Lengths of links $L1$, $L2$, and $L3$ were taken as the design variables for the linkage optimization using the GA. Results from the optimization are discussed in the following section.

Table 3-3. Initial Linkage Dimensions

| Linkage | Initial Lengths (mm) | Linkage | Initial Lengths (mm) |
|---|---|---|---|
| L1 | 330 | L6 | 277 |
| L2 | 570 | L7 | 150 |
| L3 | 620 | L8 | 169 |
| L4 | 93 | L9 | 78 |
| L5 | 87 | | |

### 3.5 Preliminary Control

To allow real-time interaction, the robot was controlled using Simulink Realtime, Matlab® 2022, and dSPACE MicroLabBox. To achieve the desired cadence of 0.33 Hz one human stride (left foot contact to left foot contact) the mechanism's velocity was adjusted to 2.1 rad/s which is used as an input at joint A. The following velocity feedback controller input was used:

$$u = Gain \cdot (\dot{\theta}_{des} - \dot{\theta}_{curr}) \tag{4.23}$$

Where u is the control input, $\dot{\theta}_{des}$ is the desired velocity at the input joint $A$, and $\dot{\theta}_{curr}$ is the actual velocity calculated from the encoder, as shown in Figure 3-6. The walking speed can also be adjusted to a different value depending on the requirements of each individual.

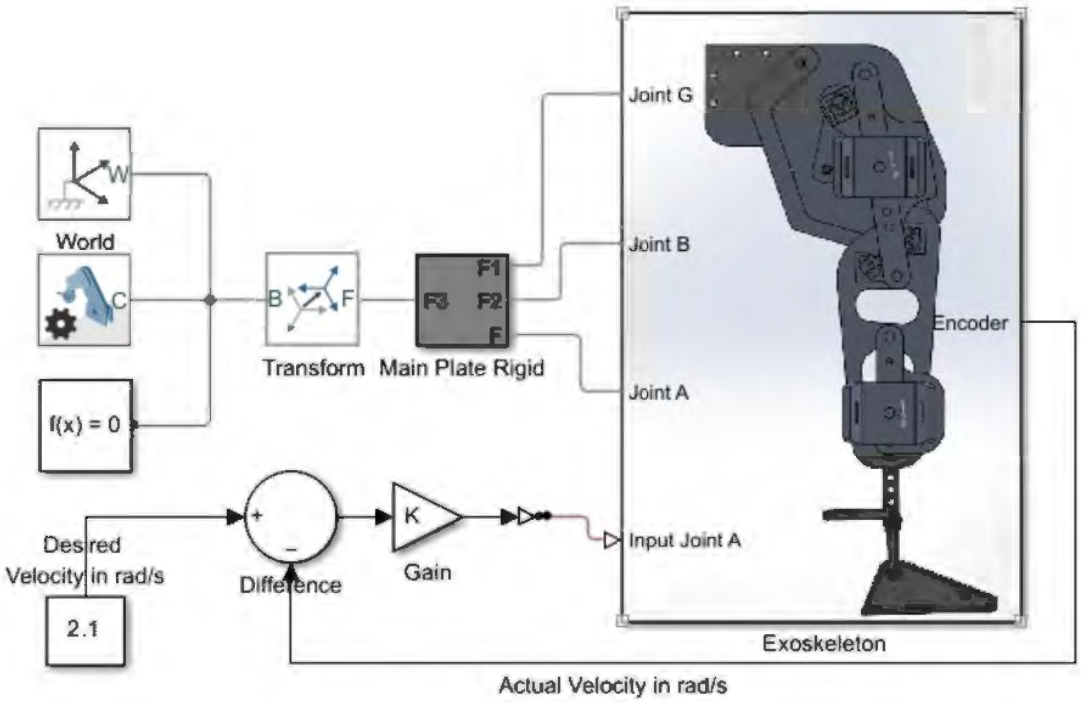


Figure 3-6. The velocity feedback controller implemented via Matlab Simulink.

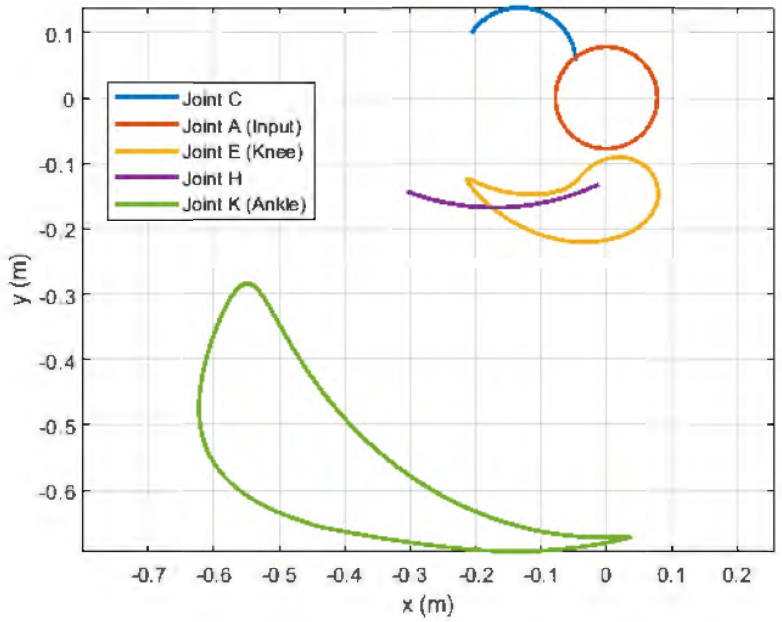


Figure 3-7. Trajectory generated by each joint of the underactuated gait rehabilitation robot.

### 3.6 Results and Discussion

In order to allow full circular motion to the crank $L9$ fixed at point $A$, the mechanism should satisfy the Grashof's criterion specified in Equation (3.17). Substituting the values from Table 3-3 in (17), we obtain the values of $(L9 + L7)$ as 228 mm and $(L5 + \overline{AB})$ as 229 mm, which indicates that the Grashof's criterion is satisfied. The coordinate positions of each joint derived from analytical geometry have been verified by analysing the position encoder values in Matlab®. The trajectories generated at each joint of the mechanism (using the final linkage dimensions) are illustrated in Figure 3-7.

The position trajectories for joint $E$ and joint $K$ represent the trajectories generated by the knee and ankle joints of a healthy human relative to the hip joint. Further, the positions have been differentiated over time to find out the velocity for knee and ankle joints in m/s when the input speed at joint $A$ was kept at 2.1 rad/s. The velocity graph for the input speed of 2.1 rad/sec is shown in Figure 3-8.

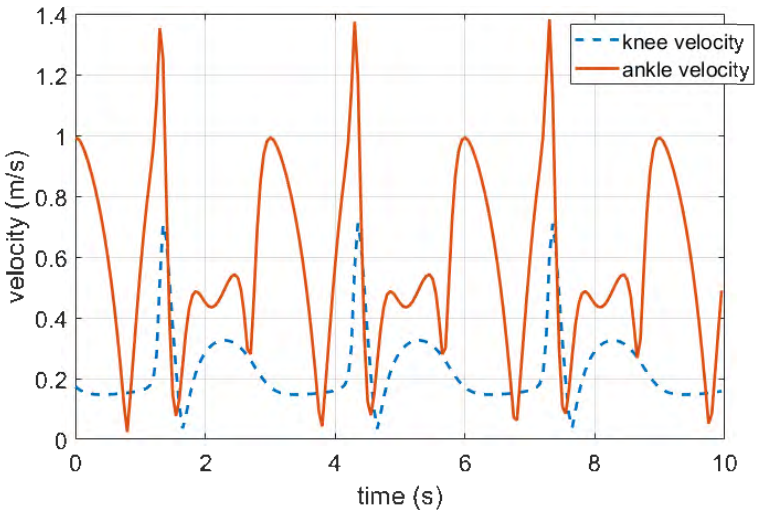


Figure 3-8. Velocities of ankle and knee joints over a given period for the motor input of 2.1 radians per second.

As can be seen from the graph the knee joint velocity exceeds the ankle joint velocity for some periods of time. Next, the linear acceleration for the ankle and knee joints has also been graphed as shown in Figure 3-9.

In order to obtain the initial set of linkage dimensions that will satisfy the target trajectories of the knee and the ankle joints, a forward kinematic analysis was carried out and the dimensions were verified using the GIM® software [123].

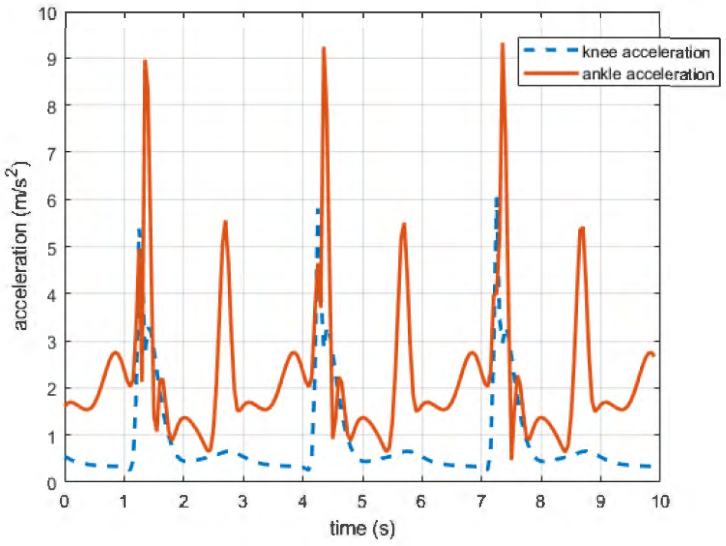


Figure 3-9. Acceleration of ankle and knee joints over a given period for the motor input of 2.1 radians per second.

The initial linkage dimensions obtained subsequent to the kinematic analysis before optimization are listed in Table 3-3. Subsequent to the optimization, which was carried out using the GA toolbox in Matlab®, the optimal set of linkage dimensions (that result in the minimum error in the ankle and knee trajectories) obtained for links $L1, L2, L3$ are 371.0134 mm, 529.4524 mm, and 580.7254 mm, respectively. The linkage lengths of $L4$ to $L9$ remained the same to initial ones. The linkage dimensions from Table 3-3 were used as the initial population of solutions while using the GA toolbox in Matlab®. The human target and actual trajectories produced by the robot at the knee and the ankle joints are illustrated in Figure 3-10.

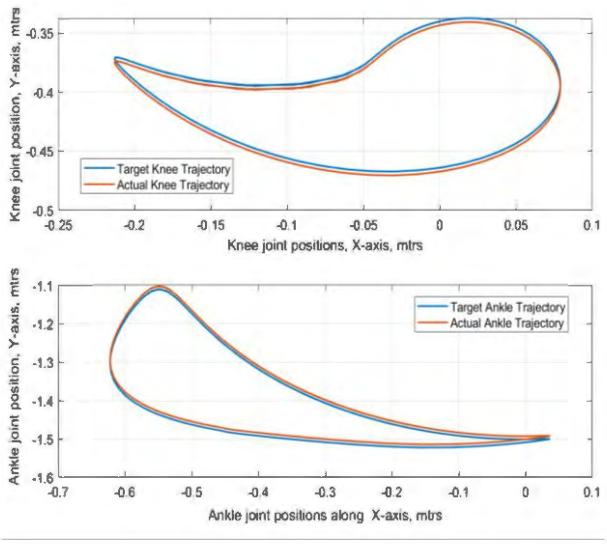


Figure 3-10. Ankle and Knee joint trajectories from optimal linkage dimensions vis-à-vis target trajectories.

It is evident from this illustration that the orthosis design with optimized linkage dimensions was able to achieve the targeted human joint trajectories. The reaction force and the torque generated at the knee joint during the gait cycle were calculated using the dynamic force analysis. The reaction force at the knee joint and the required torque at the input joint *A* are shown in Figures 3-12 and 3-13, respectively. As can be seen from Figure 3-12, the force sometimes exceeds 1100 N, and this is one of the reasons that we need sensor feedback to the actuator to avoid stalling. This also confirms the mechanical advantage of such type of mechanisms. The errors between generated and target trajectories for knee and ankle joints for the given period of time are illustrated in Figure 3-11 (a, b). The errors between human target and robot-produced trajectories are small, implying that the robot is capable of providing naturalistic lower limb joint motions required during walking.

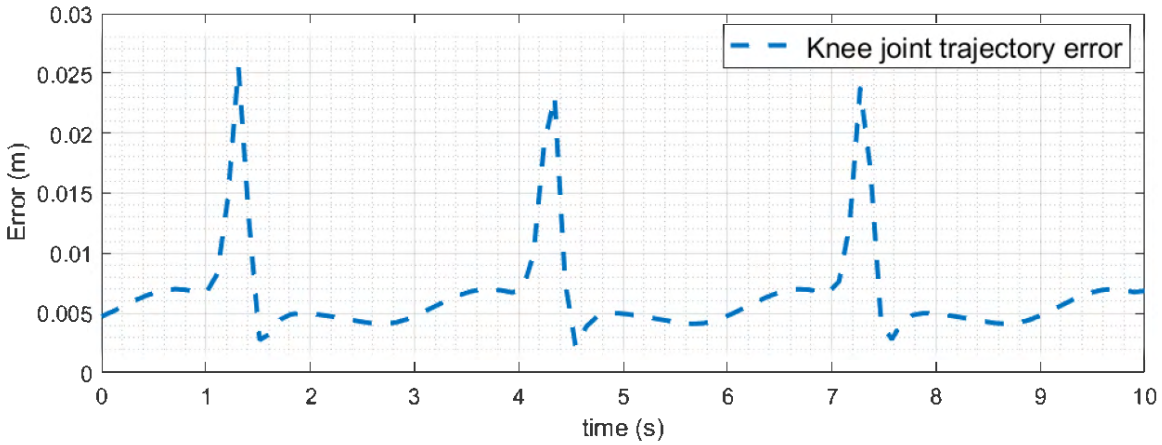


(a)

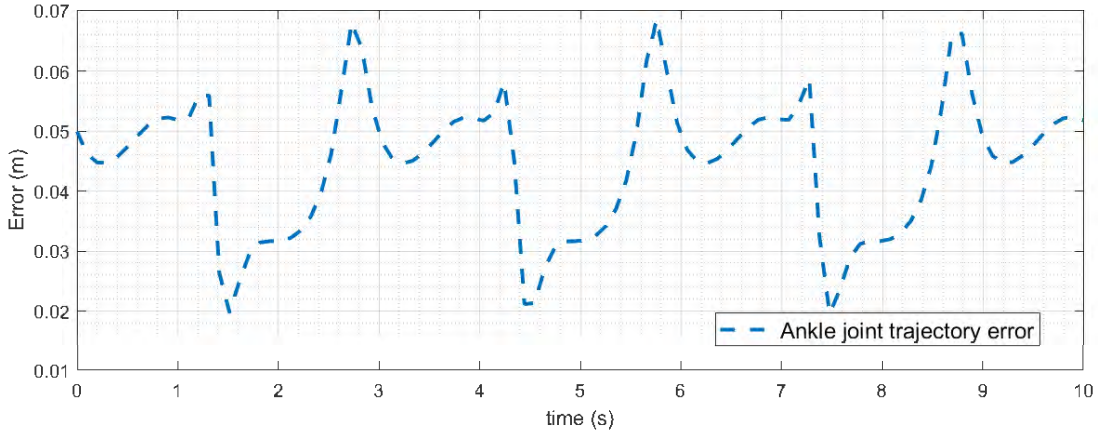


(b)

Figure 3-11. The errors between target and generated (a) knee joint trajectories and (b) ankle joint trajectories over time.

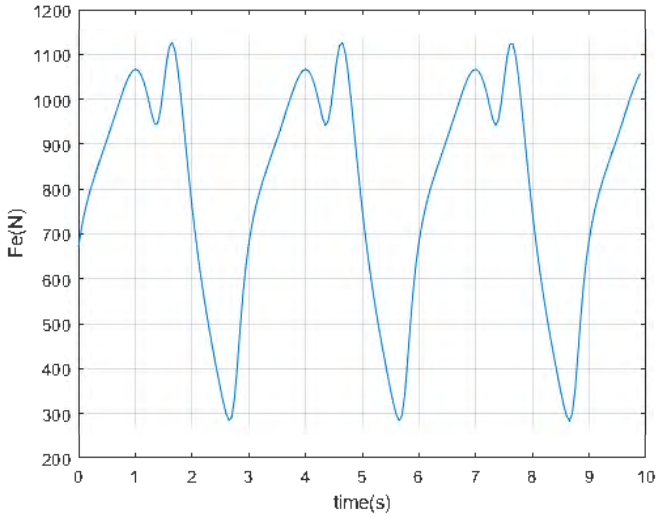


Figure 3-12. Force generated at the hip joint over a period.

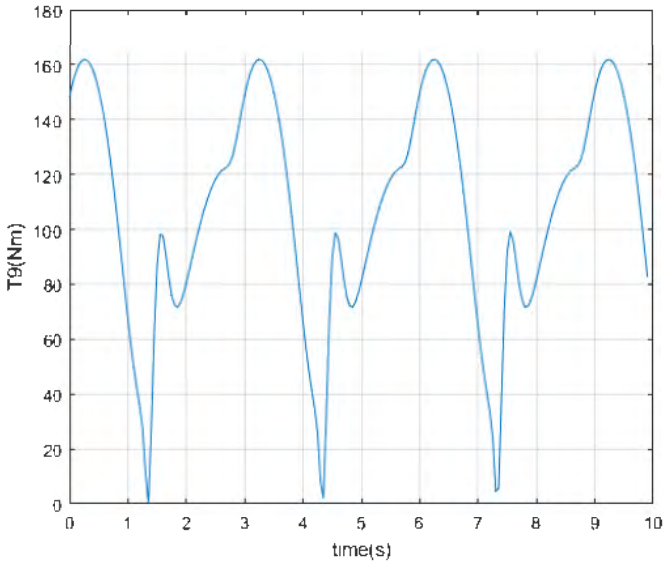


Figure 3-13. The torque required for the motor at the input joint A at crank link L9 over a period.

For the calculations of the reaction force, the material of the orthosis was considered to be aluminum, and the mass of the load on it was chosen to be 16 kg, representing the average mass of a leg taken from a person weighing around 90 kg. Since the subject will be supported by the BWS, the mass load on the orthosis would be the mass of the human leg. The torque required at the input joint varies substantially, as shown in Figure 3-13. At some period of time, the torque at the crank comes close to zero; this is due to the inertia occurring during the operation of the robot.

The final dimensions of the system were also verified with the use of the GIM® software [123]. Figure 3-14 (a) displays the simulated mechanism design and its generated trajectories

for the knee and ankle joints. The initially manufactured prototype of the proposed mechanism, made from acrylic plastic, is shown in Figure 3-14 (b). This material was chosen for the first laboratory prototype to validate its robustness and ability to work. The results of joint rotations measured during the experiment trial over a period are presented in Figure 3-15.

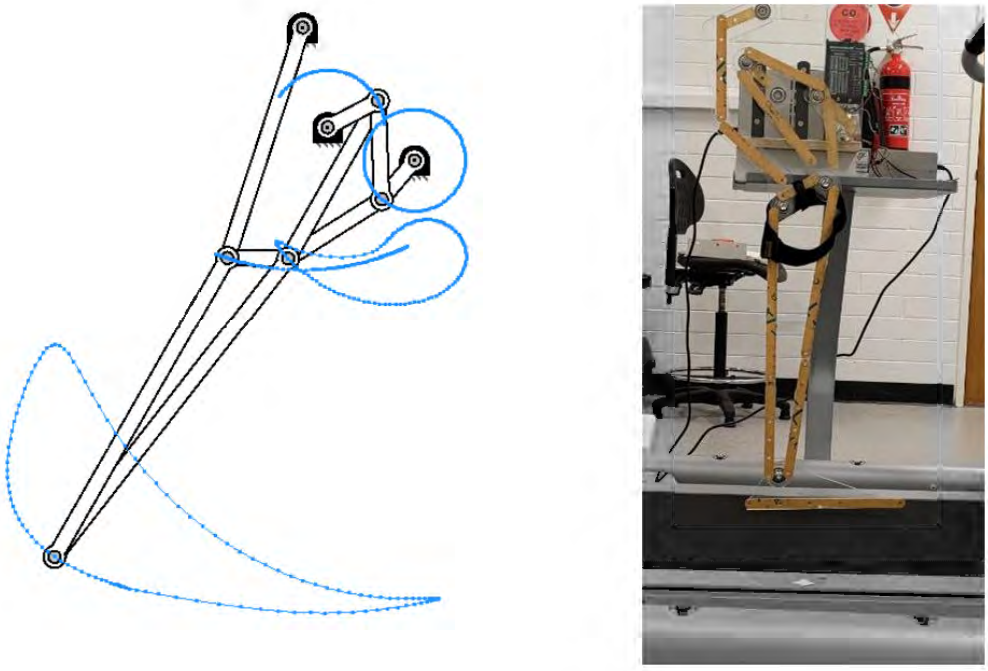

(a) (b)

Figure 3-14. (a) Synthesized linkage with trajectories generated at each rotary joint. (b) A fabricated prototype of the underactuated mechanism using acrylic plastic during operation.

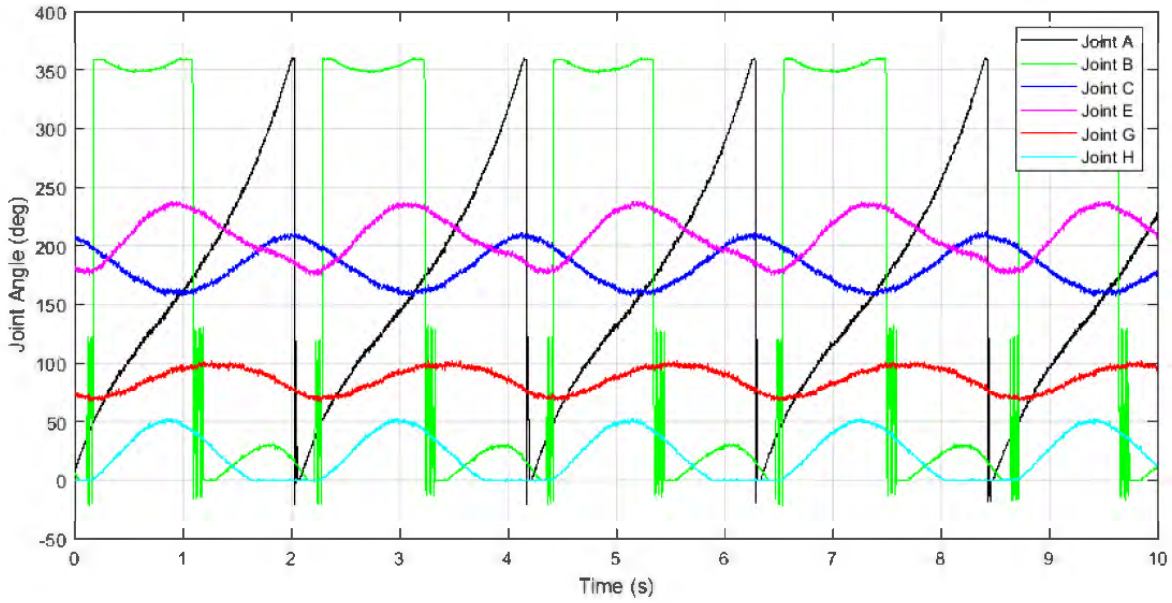


Figure 3-15. Each rotary joint positions measured with the encoders over a period.

## 3.7 Chapter Summary

This chapter describes the mechanism of a proof-of-concept prototype initially fabricated using acrylic plastic to assess the feasibility of the proposed linkage. The mechanism is a lightweight and uses a simple control scheme with a single actuator, which implies low energy consumption. It provides naturalistic ankle and knee joint trajectories suitable for gait rehabilitation purposes. The lightweight design and provision of naturalistic lower limb motions during walking, as demonstrated by the deviation error in Figure 3-11, allow individuals to expend less metabolic energy. To optimize the orthosis's design, a genetic algorithm was employed to obtain an optimal set of linkage dimensions. The position analysis for the underactuated mechanism, concerning generated coupler curves for joints $E$ and $K$, was also conducted. Joint $E$ and $K$ represent the knee and ankle joint centers, respectively. By differentiating the position over time, we could obtain the velocity generated at different coupler points for the 2.1 rad/s input velocity at the crank. Further differentiation of velocity over time enabled obtaining acceleration results, confirming that the mechanism can achieve the necessary walking pace required for gait training. Additionally, a dynamic force analysis was performed, indicating that the proposed system can generate the required torques for guiding patients' lower limbs during rehabilitation. We determined the necessary torque profile for the motor, which assisted in selecting an appropriate actuator capable of running the system.

The proposed underactuated mechanism demonstrates the possibility of generating naturalistic motions for ankle and knee joint center trajectories using a reduced number of actuators. In summary, synthesizing the dimensions of a six-bar linkage that can simultaneously track multiple desired trajectories is a challenging task, as even slight variations in linkage dimensions can significantly affect the final end-effector trajectory, as evidenced by the conducted perturbation analysis. Such a concept has the potential to significantly reduce the workload on physiotherapists, and due to its low-cost nature, many patients will be able to access high-quality rehabilitation training.

In this chapter, a validation of the Stephenson III six-bar linkage-based gait rehabilitation orthosis was conducted, encompassing both kinematic and dynamic analyses. The dimensions of the linkage were optimized for desired walking trajectories using a genetic algorithm. While the optimization results were satisfactory and allowed the mechanism to closely follow the target trajectories, recalculating these dimensions to accommodate varying leg lengths among individuals proved to be a lengthy and intricate process. Given these challenges highlighted in

this chapter, there's a strong need to develop a machine learning framework that will automatically predict the dimensions of the linkage given two target trajectory points. Machine learning tools can potentially provide an optimal solution to the dimensional synthesis problem, optimizing all dimensions concurrently rather than focusing solely on the critical ones. Thus, this sets the groundwork for the subsequent work in chapter 4.

# Chapter 4. Synthesis of a Six-Bar Mechanism for Generating Knee and Ankle Motion Trajectories using Deep Generative Neural Network

## 4.1 Introduction

As mentioned in section 2.2, linkage-based mechanisms can come in the form of four-bar arrangements or more complex configurations. The value of the length of each link is critical since it determines the shape of the produced trajectories at the coupler points. The design of linkage-based mechanisms involves determining the precise dimensions of the links and the position of fixed joints of the mechanism to reproduce the target trajectory motions (coupler curves). This is a challenging task since even a small deviation in one of the link's lengths can largely alter the output motion. However, as revealed in chapter 2 none of the previously proposed synthesis methods used in developing gait rehabilitation robots took into consideration the concurrent knee trajectory movement in the optimization task, although knee joint motion is an important factor to consider during the gait training process. Moreover, determining required linkage parameters has been done using traditional synthesis methods. Such approach is a complex process, which involves solving higher-order polynomial equations and subsequently performing iterative calculations, demanding high computational resources. In addition, the continuity aspect of the input is usually ignored due to formulating the problem by a discrete position objective, which can lead to various order or branch defects [111]. For instance, where the mechanism has passed through all the required position points, but not in the correct order.

Another underrated approach that can be used to synthesize linkage dimensions is through the application of modern machine learning techniques. There are only a few works that employed a machine learning approach for the synthesis of linkage-based mechanisms, but not for rehabilitation purposes. For instance, Khan *et al*. have used an artificial neural network (ANN) based approach to map the Fourier coefficients, which describe the target curve together with its corresponding linkage parameters [124]. The application of ANN and local optimizers has demonstrated the possibility of deriving a four-bar linkage mechanism that can trace desired trajectories (coupler curves). A set of defect-free four-bar linkage solutions has been synthesized using auto-encoder neural networks for the motion generation problems by Deshpande *et al.* [112]. The motion planning of lower limbs has been studied for achieving better efficiency in gait rehabilitation in multi-DOF robots. For instance, recurrent neural networks have been used for individualized gait generation in [125]. The prediction of

individual gait patterns has been presented by Luu *et al*. in [126]. Lower limb joint trajectories has been modelled in [127, 128] using hybrid automata. The application of machine learning methods has demonstrated effectiveness in multi-DOF gait rehabilitation robots and in addition, it can generate various sets of defect-free solutions for industrial four-bar linkages. Therefore, applying such techniques in designing linkage-based gait rehabilitation devices is promising.

To sum up, the synthesis of linkage-based mechanisms to generate ankle trajectory for the gait rehabilitation has been presented using conventional synthesis techniques, which can lead to branch or order defects during the design optimization stage. Moreover, individuals have different anthropometric features, like different leg lengths, causing different shapes of gait trajectories. Thus, recalculation of linkage dimensions to fit people with different leg lengths is a challenging process that may require more time and computational resources during iterative calculations. Furthermore, knee joint trajectory has not been considered among proposed linkage-based rehabilitation mechanisms, which may cause human joint and robot misalignments and negatively affect the overall gait training process. To avoid defects during the mechanism design stage, machine learning-based synthesis techniques have demonstrated effectiveness, but were only implemented on non-rehabilitation four-bar mechanisms, targeting only a single trajectory. Considering traditional approach on determining optimal dimensions of the linkage, which was presented in previous chapter 3, the method presented in this chapter advances the work in dimensional synthesis area. It aims not only to determine optimal dimensions but also to find out the ideal positions of the fixed joints. This tool can be useful to designers of closed loop linkage mechanisms to quickly determine optimal parameters of the linkage.

This chapter presents the implementation of a novel form of a new deep generative neural network framework that can be used in the synthesis of optimal linkage dimensions of the Stephenson III six-bar linkage for the purpose of gait rehabilitation. Since the linkage should generate two paths within a single mechanism corresponding to the human knee and ankle joint trajectories for gait rehabilitation, the problem becomes complex for solving with conventional techniques. The presented model in this chapter can generate the linkage solutions within an acceptable dimensions range, such that it can fit people with different anthropometric parameters and provide their respective gait trajectories. The content of chapter 4 is published in [129].

The chapter is organized as follows. Section 4.2 presents the methodology, providing a brief description of the fundamental deep-learning-based generative tool used to construct the final framework. Section 4.3 provides a detailed description of the developed conditional generative deep learning framework used to solve the problem set in this study. The obtained results from the deep generative neural network framework and their further discussions are provided in Section 4.4. Conclusions drawn from the proposed research are provided in Section 4.5.

## 4.2 Methodology

The derived expressions in the previous chapter for the corresponding Cartesian coordinate positions of the mechanism's moving joints, as indicated in Table 3-1, as a function of the input angle $\theta$ to the motor and linkage length dimensions, are extracted and presented in the following form:

$$\begin{cases} D_x = A_x + L9 * cos(\theta) \\ D_y = A_y + L9 * sin(\theta) \end{cases} \tag{4.1}$$

$$\begin{cases} C_x = B_x + L5 * cos(\alpha + \beta - \gamma) \\ C_y = B_y + L5 * sin\ (\alpha\ + \beta - \gamma) \end{cases} \tag{4.2}$$

$$\begin{cases} E_x = C_x + \ L6 * cos\ (\alpha_1 + \ \beta_1) \\ \ E_y = C_y - L6 * sin(\alpha_1 + \beta_1) \end{cases} \tag{4.3}$$

$$\begin{cases} H_{\mathrm{x}} = G_x + \ L1 * cos(\alpha_2 + \ \beta_2) \\ \mathrm{H_y} = \ G_y - L1 * sin(\alpha_2 + \ \beta_2) \end{cases} \tag{4.4}$$

$$\begin{cases} K_x = G_x \ + \ L2 * cos\ (-\alpha_3 + \ \beta_3) \\ K_y = \ G_y - \ L2 * sin\ (-\alpha_3 + \ \beta_3) \end{cases} \tag{4.5}$$

Joints $E$ and $K$ in the mechanism correspond to the knee and ankle joints, respectively. Therefore, we target the mechanism to generate desired trajectories at joints $E$ and $K$.

### 4.2.1 Generative Adversarial Networks (GANs) and Conditional-GANs

Proper linkage dimensions and parameters can be determined by learning the conditional distribution from the six-bar linkages and their corresponding coupler curves simulated within acceptable dimensions range and constraints. Since the synthesis of a six-bar linkage is a non-convex optimization problem [108], we employ a deep generative neural network framework, which will synthesize new samples of linkage dimensions.

A popular machine learning algorithm developed for the task of unseen sample generation is known as Generative Adversarial Networks (GANs), first introduced by Goodfellow *et al*. in [130]. The algorithm has confirmed its efficacy in various complex distribution modelling tasks such as the synthesis of high-fidelity realistic images of human faces and natural scenes, image-to-image translation, speech and language generation, and text-to-image synthesis. The model consists of two major parts, generator G and discriminator D. Generator G is trained to learn a mapping from the vector of random noise $z \epsilon N(0,1)$, with lower dimensions to the sample from the training distribution $x \epsilon X$, while the discriminator D is trained to learn to assign correct labels to the original samples $x \sim p_{data}(x)$ and samples coming from the generator module $z \sim p_z(z)$.

The training aims to maximize the probability of the correct labelling for D and at the same time minimize $\log(1 - G(z))$ to optimize the generator G. The minimax objective function of GANs is given by the following equation:

$$\min_G \max_D V(D,G) = E_{x \sim p_{data}(x)}[log\, D(x)] + E_{z \sim p_z(z)}[log(1 - D(G(z)))] \quad (4.6)$$

The overall architecture of GANs is shown in Figure 4-1.

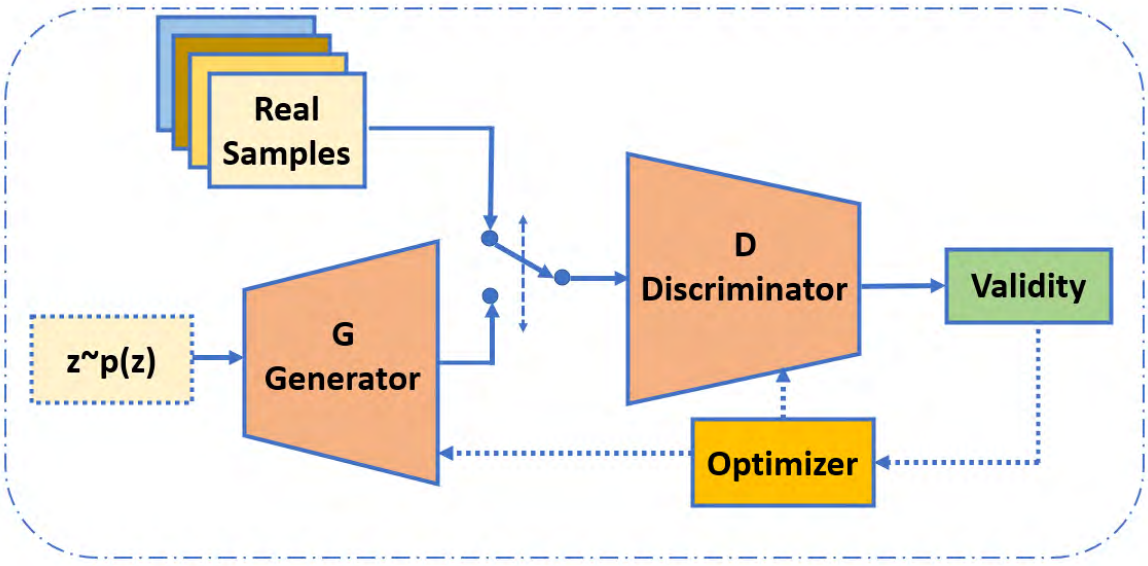


Figure 4-1. The architecture of Generative Adversarial Networks (GANs).

To generate the samples conditioned on label *y*, the standard GAN has been extended to Conditional Generative Adversarial Network (C-GAN), which allows generating samples based on auxiliary condition *y* [131]. C-GAN also consists of two modules, generator $G(z|y)$ and discriminator $D(x|y)$, but this time conditioned on label y. Conditioning is performed by

feeding both modules to an additional layer y. The vector of prior input noise $p_z(z)$ is combined with the label y, which is then fed as an input to the generator. Then, the discriminator tries to correctly classify if the samples are from the real dataset or synthesized by the generator module. Generator and Discriminator compete with each other, therefore, forming the following minimax objective function:

$$\min_G \max_D V(D,G) = E_{x\sim p_{data}(x)}[\log D(x|y)] + E_{z\sim p_z(z)}[\log(1 - D(G(z|y)))] \quad (4.7)$$

where $z\sim p_z(z)$ is the noise variable vector and $x\sim p_{data}(x)$ is the training set of real samples. The overall schematics of C-GAN is presented in Figure 4-2. The ultimate goal of this study is to generate six-bar linkage dimensions and coordinates of the fixed joint that satisfy the desired coupler curves set out by the user.

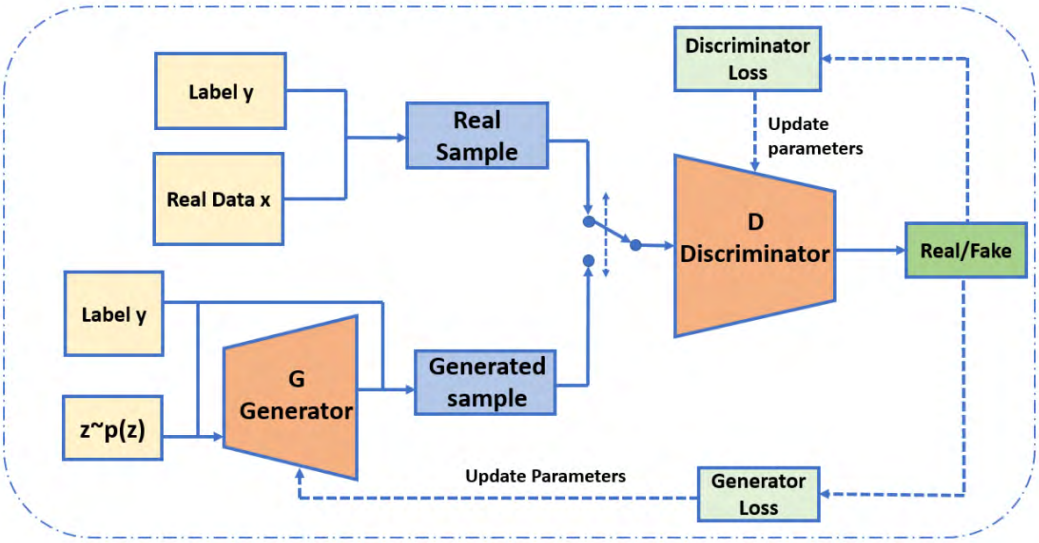


Figure 4-2. Conditional GAN architecture.

The GAN algorithm is usually applied for image, video, or voice generation problems. Such problems do not have explicit evaluation metrics to assess the quality of generated samples, therefore, adversarial learning is applied, which promotes continuous improvement of the generator and discriminator modules, as they compete with each other until an equilibrium is achieved where the discriminator is unable to distinguish between the real and the synthesized samples. The evaluation metric in our task is explicit since we are targeting specific coupler curves or trajectories, which will be specified by the user. Therefore, we introduce some modifications to the standard learning objective of the C-GAN model such that our discriminator does not require any training and is rather pre-defined by the Kinematic Solver (cf. Equations

(4.1-4.5)). The kinematic solver provides the requisite relations between the joints and the links of the mechanism together with its geometric properties. Therefore, it is possible to state that the discriminator part is already at its maximum performance and can fully discriminate the samples coming from the generator if the samples do not meet specific design requirements or criteria. The detailed structure of the deep learning framework used is described in the next section.

## 4.3 Conditional Deep Generative Neural Network Design

### 4.3.1 Overall Model Description

The mechanism has two coupler curves generated at joints $E$ and $K$. The coupler curves are set as label *C* for the mechanisms; therefore, we attempt to generate linkage parameters conditioned on coupler curves *C*. The locations of fixed joints *A* and *G* are constant and not varied in this work. Since $G$ represents the hip joint and $A$ is where the motor is placed. GIM® software was used to heuristically initialize the location of the fixed joints [123].

Since two coupler curves set for joints $E$ and $K$ are presented as a set of 100 points for each curve with corresponding *x* and *y* coordinate positions on a Cartesian coordinate plane, the size of the vector containing the points for both curves is $C \in \mathbb{R}^{100\times4}$. The following pseudo-code provides the step-by-step implementation of the conditional deep generative neural network used to generate the linkage dimensions.

---

**Pseudo Code 1** for the Conditional Deep Generative Neural Network

---

**Data:** *N* linkage curve pairs, *K* number of iterations (steps), *Cn* number of input curves, *z* sample noise, *L* linkage lengths ($L_i$), *POS* x,y coordinate position of fixed joint B, *C* curves generated from random samples *LL* using kinematic Equations (4.1-4.5).

Every sample contains:

- *Linkage dimensions* ($L_i$),
- *x,y coordinate position of fixed joint B*
- *True trajectory curves for joints E and K derived from kinematic equations*

**Result:** Trained Generator G

**for** k in range (1 to K):

**Generator part:**

---

1 Generate random samples LL

2 Calculate curves C using kinematic Eq. (4.3-4.7)

3 Generate random noise z

4 Generate predicted LL deltas, given C and z

5 Predicted LL = Base LL + predicted LL deltas

**Kinematic Solver part:**

Check predicted LL validity.

**if** LL is valid (kinematic equations produced curves):

1 Calculate Predicted C from predicted LL using kinematic equations.

2 Calculate G loss between Target C and Predicted C.

**else**:

1 Calculate G loss between Target LL and Predicted LL*10 from Eq. (4.8)

**2** Update G using gradient-based optimizer (Adam)

**end**

The multiplication factor of 10, by which the predicted linkage length (LL) is multiplied, was chosen empirically. So, the penalty is ten times more severe for predictions that result in invalid lengths' prediction. The overall schematics of the proposed conditional generative deep learning neural network is presented in Figure 4-3.

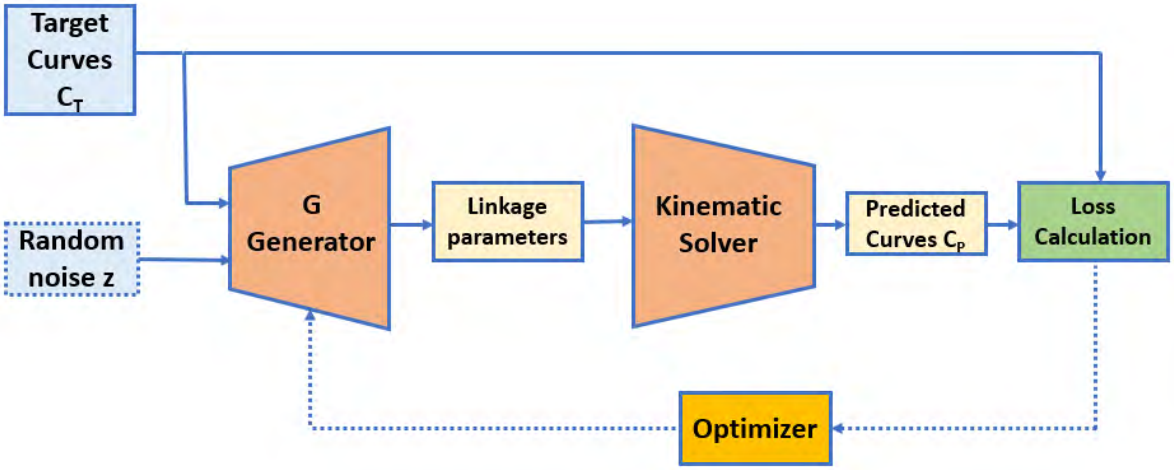


Figure 4-3. Overall schematics of the proposed conditional deep generative neural network framework.

In order to create completely new instances of data, the noise variable vector *z*, sampled usually from a unit Gaussian distribution, should be fed as input to the generator module, which is then transformed into meaningful output. By introducing the noise variable to the generator

module, it is possible to generate a large variety of data. The noise variable vector used in our problem has been sampled from a random uniform distribution and has the size of 100×1.

The generator module accepts as input the target coupler curves *C* and noise vector *z*, which are concatenated and transformed to the size of 5×100. At the output, the generator produces possible dimensions for 9 links ($L1, L2, L3, L4, L5, L6, L7, L8$ and $L9$) and x, y coordinate position for fixed joint $B$. The predicted parameters are then analyzed via kinematics Equations (5-9), implemented for calculating the corresponding coupler curves $C_P$. In the next step, we calculate the Mean Squared Error (MSE) loss between the target coupler curve $C_T$ and coupler curve $C_P$ calculated from generated dimensions using the following equation for *n* points:

$$MSE = \frac{1}{n}\sum_{i=1}^{n}(C_T - C_P)^2 \tag{4.8}$$

After the loss computation, generator parameters are updated using the Adam gradient-based optimizer [132]. Adam optimization algorithm iteratively updates the network weights in training data. Specifically, the exponential moving average of the gradient and squared gradient are computed. As it was mentioned previously, the synthesis of the six-bar linkage problem is considered to be a non-convex optimization problem [108]. The Adam gradient-based optimizer is considered to have various attractive benefits when applied to non-convex optimization problems. It is computationally efficient, invariant to the gradients' diagonal rescaling, and demands fewer memory requirements. Moreover, due to its intuitive interpretation, it doesn't require much hyperparameters tuning.

## 4.4 Conditional Generator

The generator allows us to generate 9 linkage dimensions and the x, y coordinate position of fixed joint $B$ given an input of the noise vector *z* and target coupler curves $C_T$, which are used as an input to a recurrent neural network Long Short-Term Memory (LSTM) block. The overall schematic of the generator is shown in Figure 4-4.

We chose LSTMs due to their excellent sequence modelling capabilities. They have further been shown to perform well in generative modelling [133, 134]. To satisfy the needs of the LSTM input structure size, the target coupler curve and noise vector have been concatenated and transposed to the size of 5×100. The target coupler curves are produced from linkages with randomly generated dimensions of ± 30% of the initially empirically chosen dimensions. The $x$ and $y$ positions of joint B are produced within the square region with area of 25cm$^2$ where

the center is initially an empirically chosen position. Details of the LSTM parameters used in the model are given in Table 4-1.

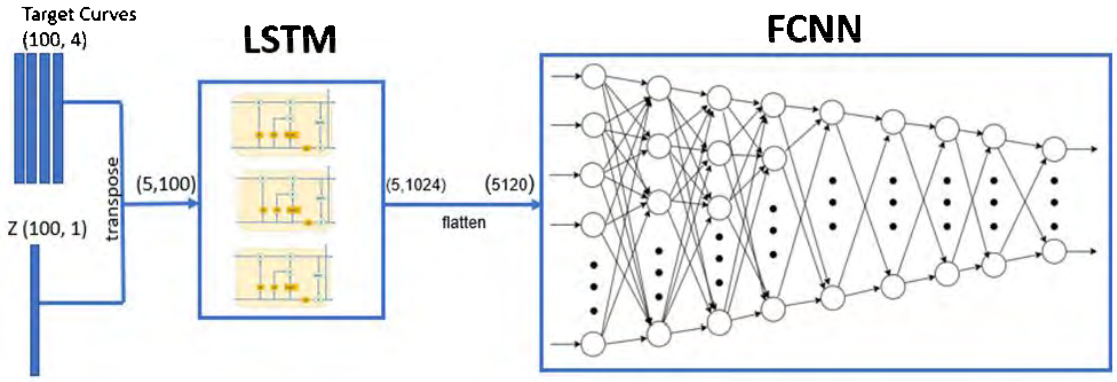


Figure 4-4. Generator architecture. Our proposed Generator comprises a Long Short-Term Memory (LSTM) Network followed by a multi-layered Fully Connected Neural Network (FCNN).

Table 4-1. LSTM parameters chosen for the generator module.

| | |
|---|---|
| **Hidden size** | 1024 |
| **Number of LSTM layers** | 2 |
| **Input size** | 100 |

The size of the output produced by the LSTM block is 5×1024. In the next step, the vector is flattened to form a column vector of size 5120. We feed that column vector into the fully connected neural network (FCNN), the parameters of which are presented in Table 4-2.

Table 4-2. FCNN parameters used in the generator module.

| | |
|---|---|
| **Number of layers** | 9 |
| **Activation function** | Leaky ReLU |
| **Input size** | 5120 |
| **Output size** | 11 |

The activation function used for each neuron in the FCNN is the Leaky rectified linear (ReLU) activation function, which is given by the following equation.

$$f(x) = \begin{cases} x, & if\ x \geq 0 \\ negative\_slope \times x, & otherwise \end{cases} \tag{4.9}$$

Regarding the output, FCNN outputs a vector of size 11, where 9 of them correspond to the dimensions of links, and the other 2 correspond to the x and y coordinates of the fixed joint $G$

in our mechanism. The overall construction of a six-bar type linkage imposes some additional constraints. One of the fundamental constraints in similar linkage-based mechanisms is called the Grashof criterion, which states that the shortest and longest links should be smaller than the sum of the other ternary links in a given four-bar linkage. To ensure continuous closed-loop circular motion at the crank (link $\overline{AD}$), the length of the links should satisfy the inequality as in Equation (3.17). If the generated linkage dimensions do not satisfy the Grashof criterion, the kinematic Equations (4.1-4.5) will not be able to compute the $E$ and $K$ without the complex part in it. Therefore, invalid dimensions are ignored in the kinematic solver part. The algorithm has been coded using the machine learning (ML) framework PyTorch 1.12 and CUDA 11.7 toolkit.

## 4.5 Results and Discussion

In this section, we demonstrate the effectiveness of the proposed algorithm described in the previous section by feeding various human-like gait coupler curves with different shapes into the model and provide a detailed analysis of a single real human gait trajectory. The overall efficacy of the algorithm and its ability to generate proper linkage dimensions, which can trace similar shape coupler curves, is evaluated by computing the Mean Squared Error (MSE) loss over the number of iterations as shown in Figure 4-5. The loss is presented in Figure 4-5(a) and also shown using the logarithmic scale in Figure 4-5(b) to demonstrate its convergence with clarity. It can be noticed from the graph that the loss converged close to zero after around 40,000 steps, where each step corresponds to the batch of 100 different variations of mechanisms, making the training set size to be more than 4 million unique mechanisms with corresponding 2 target curves. The learning rate scheduler from Pytorch ReduceLROnPlateau was utilized for improving the model learning once it stagnates [135]. The progression of the learning rate over the training steps is shown in Figure 4-6.

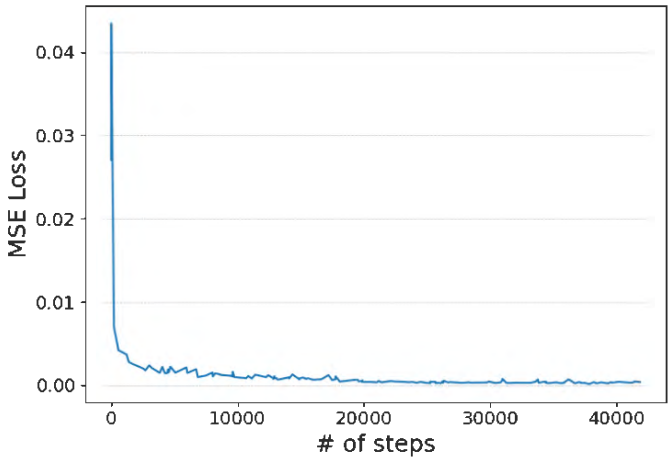


(a)

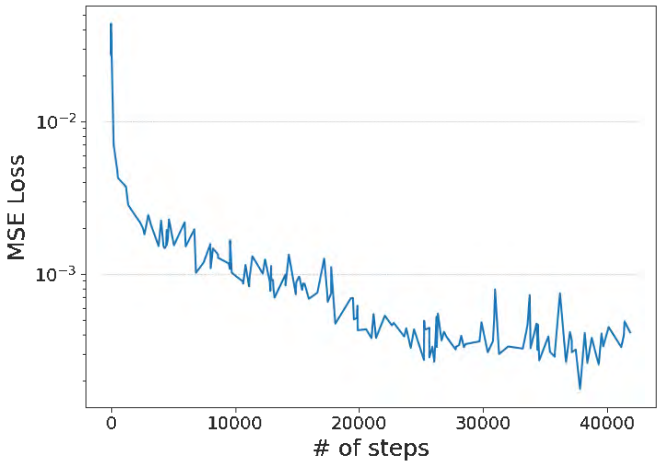


(b)

Figure 4-5. MSE loss presented on usual (a) and logarithmic (b) scales over the number of steps.

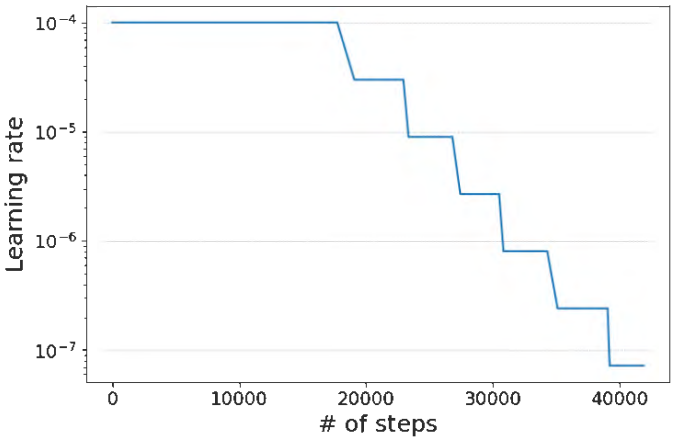


Figure 4-6. Learning rate scheduler.

The parameters applied to the learning rate scheduler are listed in Table 4-3.

Table 4-3. Parameters used for ReduceLROnPlateau Scheduler

| | |
|---|---|
| **Factor** | 0.3 |
| **Patience** | 12 |
| **Cooldown** | 5 |

That means if for consecutive 12 steps, MSE loss is not decreased, then the learning rate is reduced by 70% by multiplying by the factor of 0.3 after that cooldown period starts when the model does not observe the loss for the consecutive 5 steps, and then checking of the loss for the next 12 steps is performed again. Based on the learning rate scheduler, it is possible to note that the learning rate was constant until around 18,000 steps, which means the model was learning faster in less than 12 steps. Overall, the scheduler was used to dynamically adjust the learning rate in real time based on the performance of the model. The MSE loss eventually dropped down to a value close to zero, which means the model has been successfully trained and learned the relation between the linkage dimensions, position of fixed joint $B$, and targeting coupler curves. In total, it took 541 minutes for the model to be trained. Once the model is trained, there is no need to retrain it to generate optimal linkage dimensions and the position of the fixed joint for the given gait trajectories.

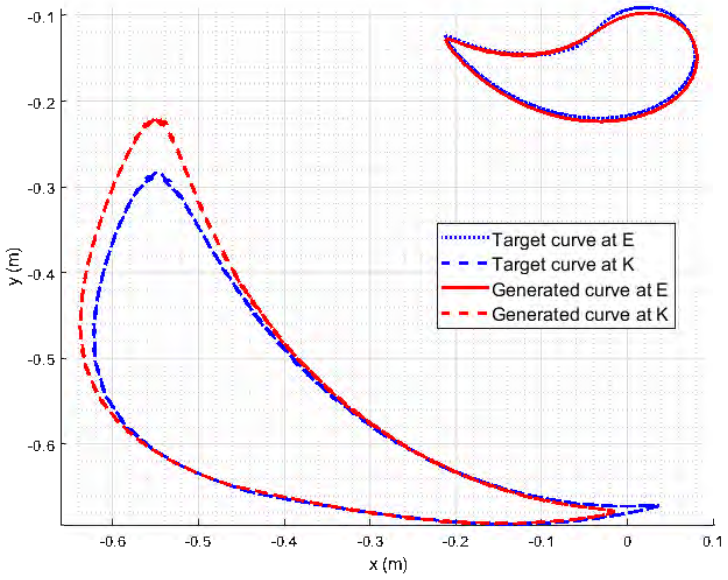


Figure 4-7. The target and predicted coupler curves from generated dimensions for a real human subject.

Since the objective of this research is to generate the linkage parameters, which can simultaneously follow desired coupler curves that correspond to knee and ankle joints, we also feed a

set of real biomechanical trajectories of a human walking lower limb [136] into the model. As can be seen from Figure 4-7, the generated curves from the predicted dimensions of the linkage closely follow the subject's target curves. The average error between the target and predicted curves for a real human subject at joints $E$ and $K$ are $5.812*10^{-5}$ m and 0.0021 m, respectively. Since, the errors are small, the trajectories can be considered closely aligned. The corresponding generated dimensions of each link for the proposed orthosis and the coordinate position of fixed joint B are specified in Table 4-4.

Table 4-4. Generated linkage dimensions for the human lower limb walking trajectories.

| **Parameter** | **Value (m)** |
|---|---|
| L1 | 0.371 |
| L2 | 0.529 |
| L3 | 0.580 |
| L4 | 0.092 |
| L5 | 0.087 |
| L6 | 0.277 |
| L7 | 0.150 |
| L8 | 0.169 |
| L9 | 0.077 |
| B(x,y) | (-0.133, 0.0506) |

The initially chosen coordinates for fixed joint A, G are (0, 0) and (-0.171, 0.203) in meters, respectively. The fixed joint G corresponds to the hip joint, therefore it has not been varied. The target and generated knee joint trajectories displacement along the x and y axes over a given period of time are presented in Figure 4-8.

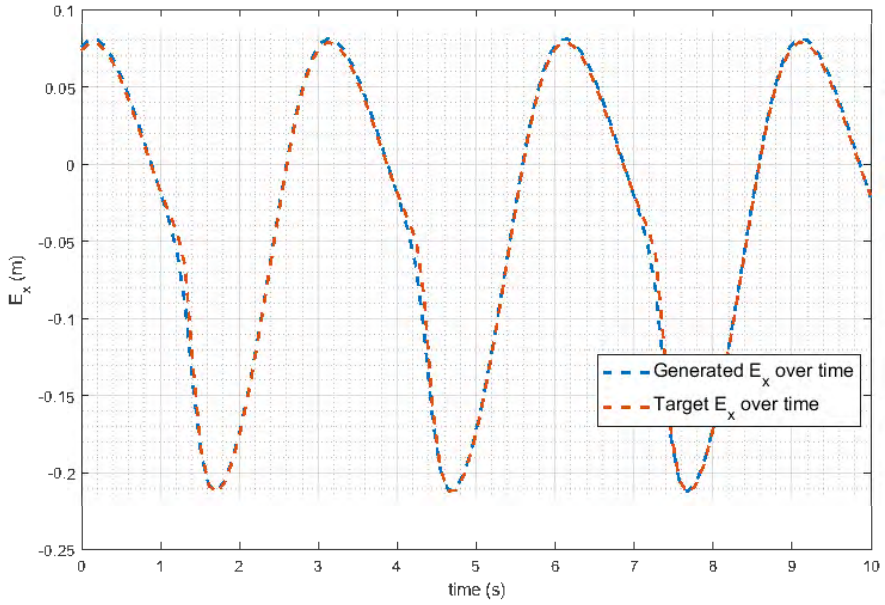


(a)

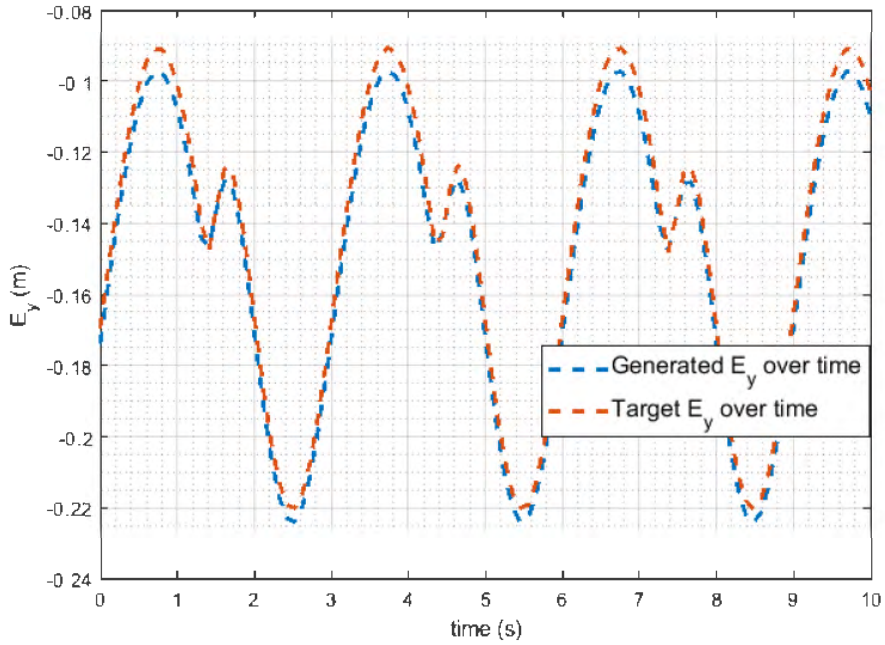


(b)

Figure 4-8. Target and predicted knee joint trajectories over time (a) along the x-axis (b) along the y-axis.

As it can be seen from the graphs the generated trajectories closely replicate the target ones. A similar trend appears in Figure 4-9 where the target and generated ankle joint displacement along x and y axes are plotted over 10 s. Given the constant input of 2.1 rad/s at the crank, the resultant velocity of the knee and ankle joints from the generated and target trajectories are shown in Figure 4-10. The peak error between velocities from the target and generated trajectories of knee and ankle joints is 0.15 m/s and 0.26 m/s, respectively.

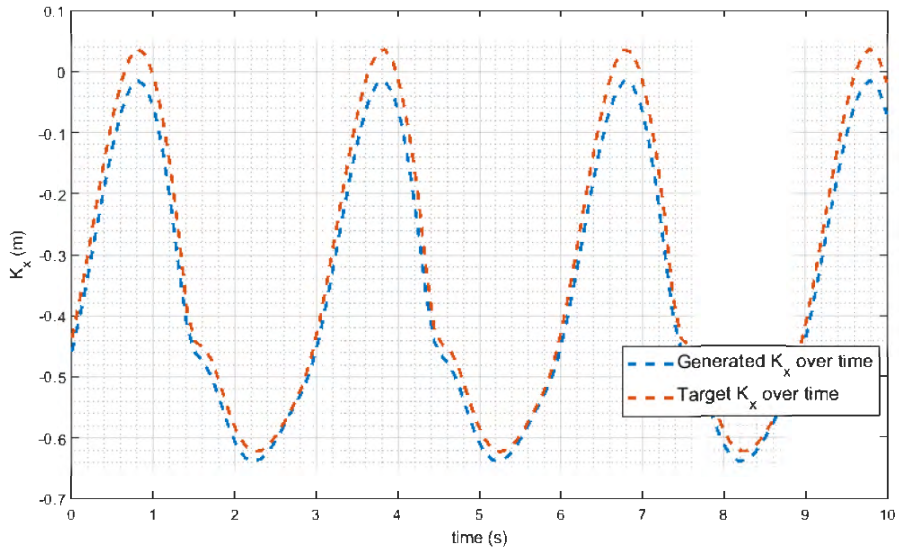


(a)

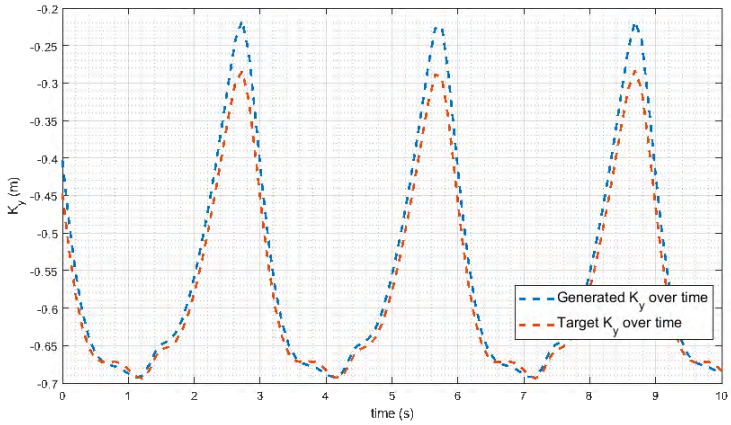


(b)

Figure 4-9. Target and predicted ankle joint trajectories over time (a) along the x-axis (b) along the y-axis

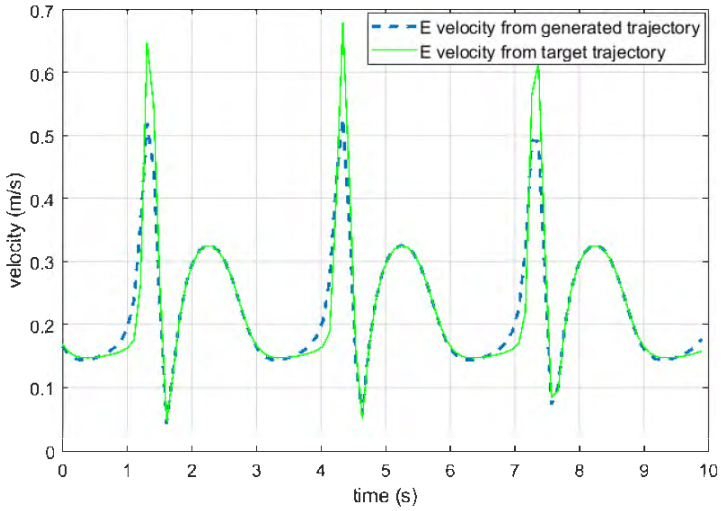


(a)

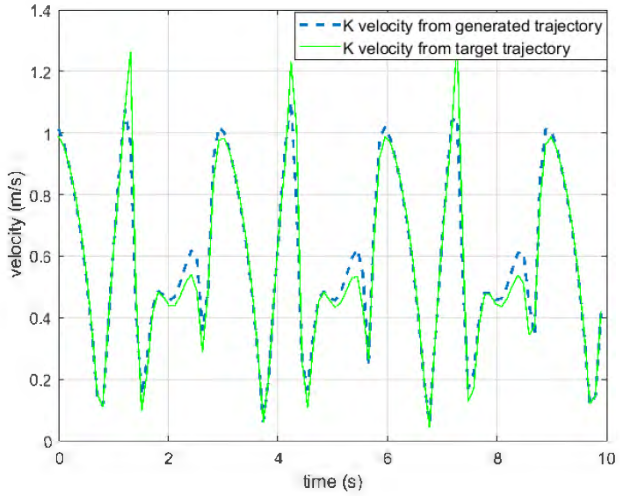


(b)

Figure 4-10. Velocity from target and predicted trajectories for (a) joint E (b) joint K.

To further provide clarity to the reader and visualize on how the orthosis will be used on a human, a 3D model of the rehabilitation system has been further constructed and attached to the human model as shown in Figure 4-11. In general, the person will be also attached to a body-weight support system to unload the person's weight, which has not been added in a 3D model for the sake of visual simplicity. The system uses only a single motor on each side of the leg, which will be rotating at a constant speed.

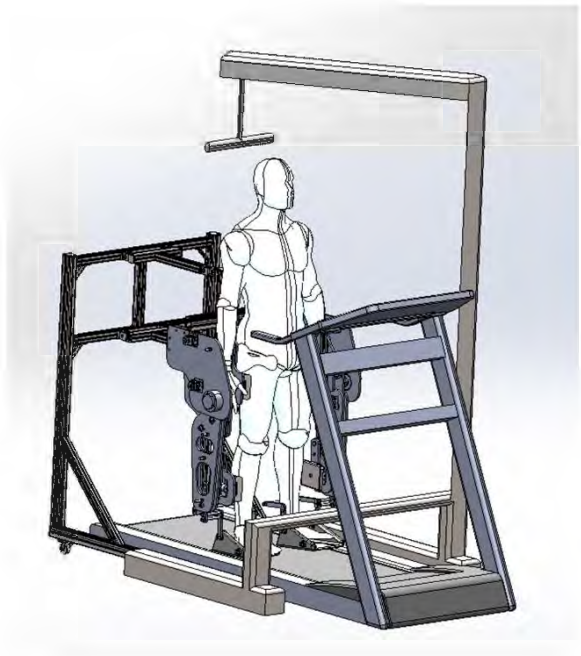

Figure 4-11. 3D model of the six-bar linkage-based rehabilitation system.

The developed deep generative model uses a similar foundation as the C-GAN model except for the Discriminator part, which is fixed and pre-defined in terms of the Kinematic Solver (see

Equations (4.1-4.5)). Since the problem of generating linkage dimensions has explicit evaluation criteria because it is exactly known what kind of target coupler curves the mechanism should produce, we do not need to learn a discriminator module. This is because kinematics equations provide the full geometrical description of the proposed linkage and can serve to reliably quantify the quality of the generated samples.

To illustrate further the overall model efficiency, we have tried to supply some examples of various human-like gait shapes of coupler curves for joints *E* and K into the model and visually observed the generated trajectories from the mechanism shown in Figure 4-12. It was found from the simulations that the generated linkage dimensions can replicate the target trajectories with very small errors, as quantified in MSE loss graphs. The MSE between the target and generated trajectories are presented for each case. The MSE here indicates on how closely the predicted trajectories follow the target human trajectories, therefore indication of small errors leads to the conclusion that both trajectories are closely aligned. Considering that anthropometric parameters and gait patterns differ among individuals with different knee and ankle trajectories, the proposed model will be able to reproduce similar target trajectories with small errors. In addition, the proposed gait rehabilitation orthosis, which is based on Stephenson III six-bar linkage has benefits because it provides naturalistic lower limb movements, is lightweight, has a simple control architecture, and requires only a single motor to actuate the mechanism.

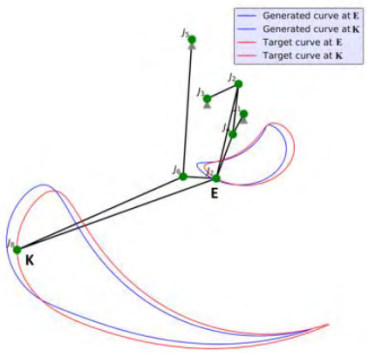


1) MSE Loss $6.768*10^{-5}$ m

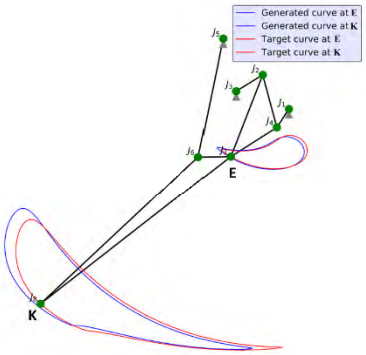


2) MSE Loss $5.863*10^{-6}$ m

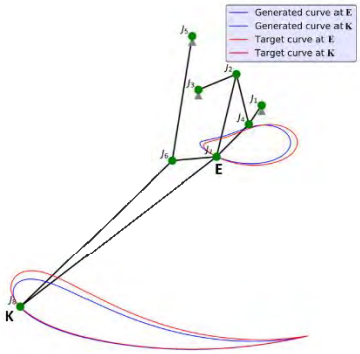


3) MSE Loss $4.915*10^{-6}$ m

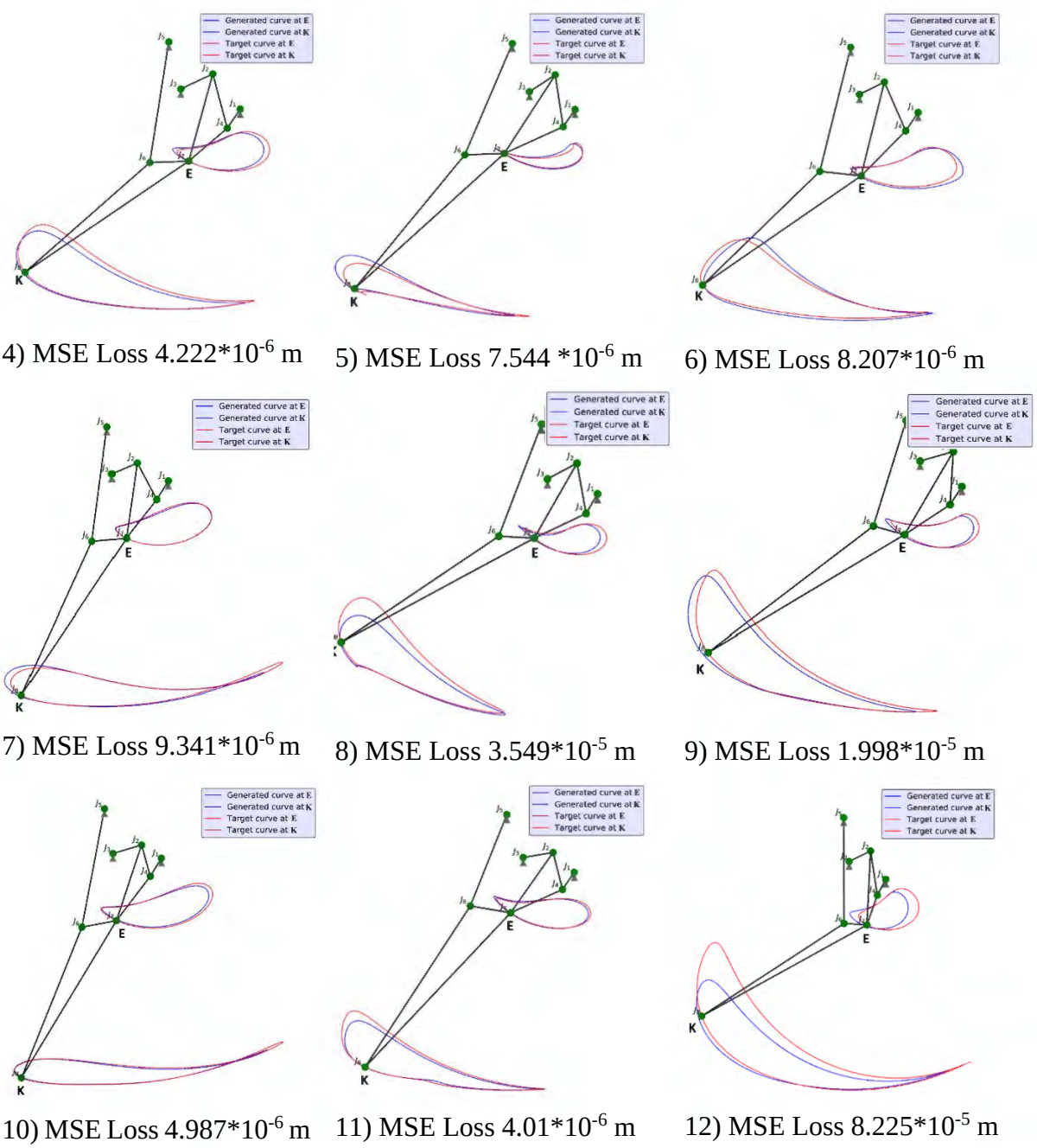


4) MSE Loss $4.222*10^{-6}$ m 5) MSE Loss $7.544*10^{-6}$ m 6) MSE Loss $8.207*10^{-6}$ m

7) MSE Loss $9.341*10^{-6}$ m 8) MSE Loss $3.549*10^{-5}$ m 9) MSE Loss $1.998*10^{-5}$ m

10) MSE Loss $4.987*10^{-6}$ m 11) MSE Loss $4.01*10^{-6}$ m 12) MSE Loss $8.225*10^{-5}$ m

Figure 4-12. Various target coupler curve shapes and their corresponding predicted mechanisms with the coupler curves produced.

## 4.6 Chapter Summary

Synthesis of linkage-based dimensions is the inverse kinematics problem, where traditional synthesis methods typically require solving higher-order nonlinear equations. Which are analytically complex and may result in zero, one, or infinitely many solutions. Such an approach is computationally prohibitive on regular computing machines, in addition, it will not necessarily be able to compute the desired linkage parameters given the complexity of the

problem, where two coupler curves have to be followed with small errors by the single linkage mechanism.

In this chapter, a novel approach for the synthesis of a Stephenson III six-bar linkage to generate two trajectories corresponding to ankle and knee joint trajectories for the purpose of gait rehabilitation was presented. We have introduced and connected methods from computational kinematics and machine learning tools to solve the complex synthesis problem. Deep learning tools demonstrated their effectiveness in determining the relationship between the desired coupler curves and linkage parameters. Deep generative neural network model presented here was inspired from GAN approach, which turned to be efficient approach for synthesis problem. The training of the model that has covered more than 4 million variations of the mechanism dimensions allowed to extensively learn and discover the link between the linkage parameters and the corresponding generated curves, because the proposed model has demonstrated high accuracy in replicating the target curves.

Subsequently, a 3D model of the synthesized orthosis has been constructed, which is actuated using only a single motor at each leg. The implemented deep learning framework has successfully generated linkage samples given various target trajectories. Moreover, the coupler curve trajectories generated by linkages are close to the desired paths.

Deep learning models are effective when dealing with modelling high-dimensional data distributions, thus providing a solution based on the statistics of the training dataset. The proposed deep learning framework's loss function has converged to a very small value, indicating that the generated linkage dimensions can follow target curves with a very low error. Moreover, computing the linkage dimensions with a trained neural network can be done efficiently in real-time, unlike computationally demanding conventional analytical methods. The training time took around 9 hours. Once the model is trained, there is no need to retrain it to obtain new linkage dimensions for the given new target trajectories. Designers of linkage-based mechanisms will benefit from the proposed model when solving for optimized linkage dimensions. The constraints and various parameters can be tuned according to an individual's needs.

The proposed method makes a considerable contribution to the field of computational kinematics with machine learning. This approach paves the way for chapter 5, where the theory is put into practice. Specifically, the concept of a gait rehabilitation system is realized, and the

focus shifts to controlling the robot to ensure its effectiveness in real-world applications. The learnings from chapter 4 set a strong foundation upon which the advancements in chapter 5 are built.

# Chapter 5. Design of an Underactuated Gait Rehabilitation System and its Velocity Regulation Using Deep Reinforcement Learning

## 5.1 Introduction

Previous theoretical works have proposed closed-loop linkage single DOF mechanisms, stating that a constant speed crank rotation would suffice to control the system [89, 104, 108, 110, 117]. However, in practice the reaction torque resulting from external disturbances, the inertia of unbalanced mechanisms, and forces (human subjects in the case of gait rehabilitation) can cause fluctuations in the crank's angular speed, thereby affecting the overall performance [137, 138]. The continuous variation in angular velocity makes the system highly nonlinear, leading to undesired behaviour and complications in controlling such mechanisms. Due to the nonlinear dynamics of a six-bar linkage-based mechanism, advanced nonlinear control algorithms are necessary to achieve desired motion. Classical control approaches require a comprehensive understanding of the system dynamics, which can be challenging in real-life dynamical systems. Adaptive control methods, capable of adapting in real-time to system uncertainties, have been utilized for many years in process control in various industries. However, accurately modelling adaptive control schemes in rehabilitation applications is difficult due to the nonlinearity of human-robot interaction [139].

Recently, Reinforcement Learning (RL) based control, with ties to adaptive and optimal control techniques, has been used to enhance the performance of adaptive controllers [140]. RL iteratively tunes control parameters to maximize the reward [141]. However, conventional RL control still requires a system dynamics formulation and can only learn in discrete observation states, resulting in discrete actions [142, 143]. On the other hand, Deep Reinforcement Learning (DRL) based control is a promising approach to regulate the velocity of the proposed underactuated robotic orthosis. Such control does not require a system dynamics model and can learn the parameters of the robotic mechanism through iterative interaction with the physical environment [144]. Velocity regulation by utilizing DRL-based control can be achieved by providing continuous action, such as the required joint torque at the crank.

In this chapter, we present further physical development of the underactuated gait rehabilitation robot, an upgraded version of the proof-of-concept prototype presented in chapter 3 based on the linkage dimensions and the overall gait rehabilitation system presented in chapter 4. The prototype was redesigned to make it applicable to the proper clinical gait rehabilitation

environment. Additional features, such as passive dorsiflexion using springs and different leg length adjustability, were incorporated during prototyping. Furthermore, a control system based on DRL was developed and tested with healthy subjects, regulating and maintaining the required velocity at the input joint. To the best knowledge of the authors, no previous studies have explored the application of DRL-based control implementation for velocity regulation of any linkage mechanisms, particularly an underactuated gait rehabilitation robot.

## 5.2 Description of the Fully Functional Gait Rehabilitation System

The design was further improved, and a fully working prototype was constructed using aluminum for both legs. The complete system comprises two robot orthoses for both legs, a BWS system to unload the human weight, a rehabilitation treadmill, and a frame holding robots above the treadmill, as shown in Figure 5-1. The robot is fixed to the legs at the thigh and shank regions using braces. To ensure proper and ergonomic alignment with human legs, braces have translational and rotational movement features to adjust accordingly during walking. Muscle spasticity at the foot and ankle joint is commonly observed among stroke survivors [145]; therefore, a footplate with springs was designed to enable passive assistive motion, facilitating dorsiflexion, and mitigating the challenges caused by the plantarflexed position of the foot. High-precision industrial potentiometers were installed at each revolute joint to monitor the robot's position. The tension/compression load cells are installed at the thigh and shank regions to monitor the interaction force between the human and the robot, as shown in Figure 5-1 (c), creating a patient cooperative control strategy in the next step. A brushless DC servo motor with a 64:1 gearbox ratio and a 14-bit encoder drives the robot, controlled using a real-time control system consisting of Simulink Realtime, Matlab® R2022B, and a dSPACE MicroLabBox.

The robot's weight is approximately 15 kg, which also includes the weight of the main plate to which the motor and fixed joints are attached. The main plate is hung on the frame holding the orthosis and remains still while walking, having no effect on human. Therefore, the actual weight of the links interacting with the lower limb is around 10 kg. In general, the heavy weight of the robot can significantly affect the cadence during walking. For example the commercially available treadmill-based gait rehabilitation robot Lokomat weighs approximately 1000 kg (2204 lb.) according to the manufacturer's website [52]. Heavy weights can lead to unnecessary deviation in cadence during walking, cause high energy expenditure in humans, and adversely affect the outcomes of the gait training therapy.

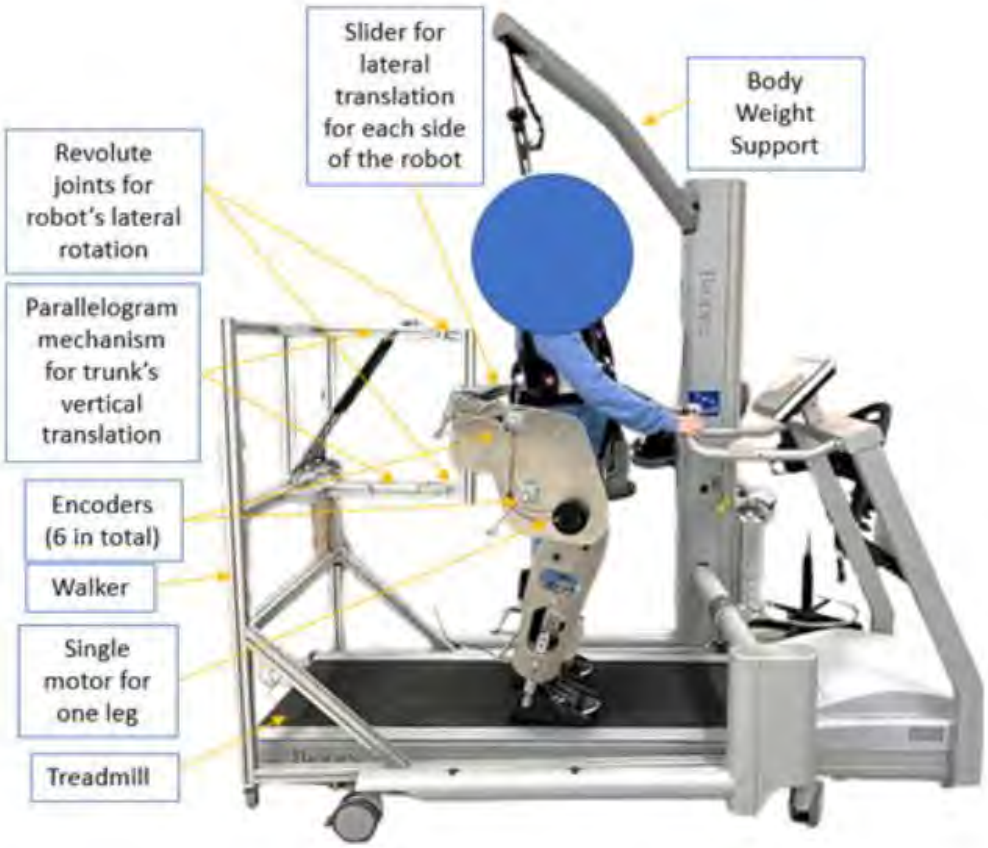
Slider for lateral translation for each side of the robot
Body Weight Support
Revolute joints for robot's lateral rotation
Parallelogram mechanism for trunk's vertical translation
Encoders (6 in total)
Walker
Single motor for one leg
Treadmill

(a)

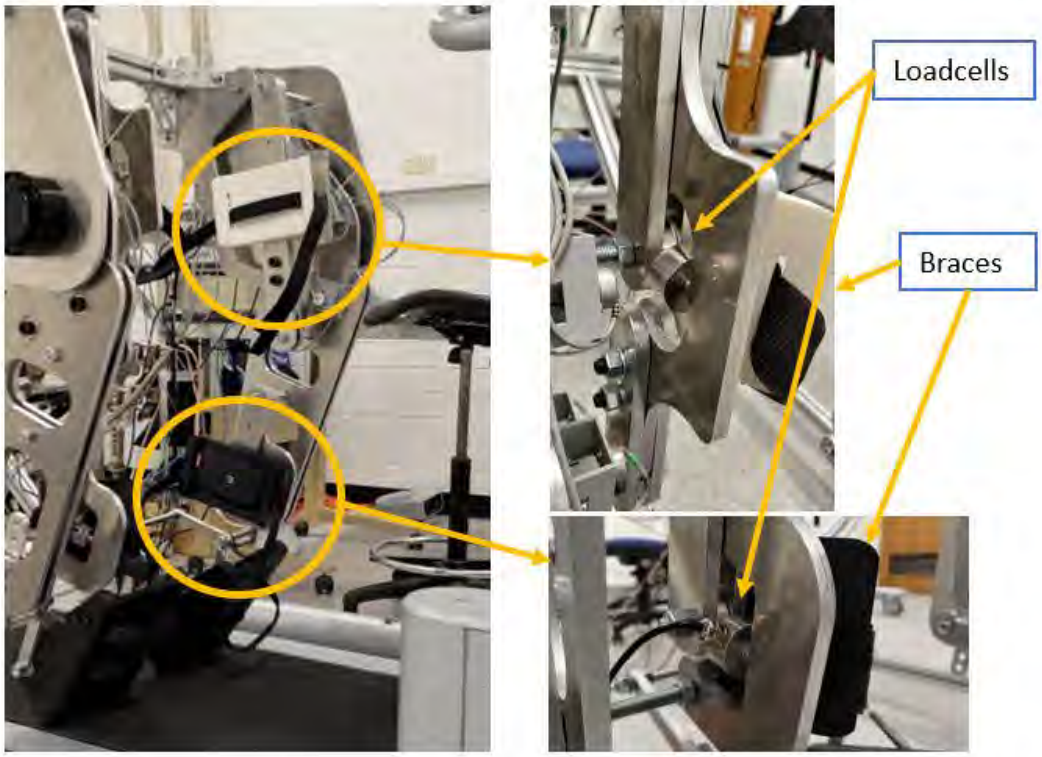
Loadcells
Braces

(b)

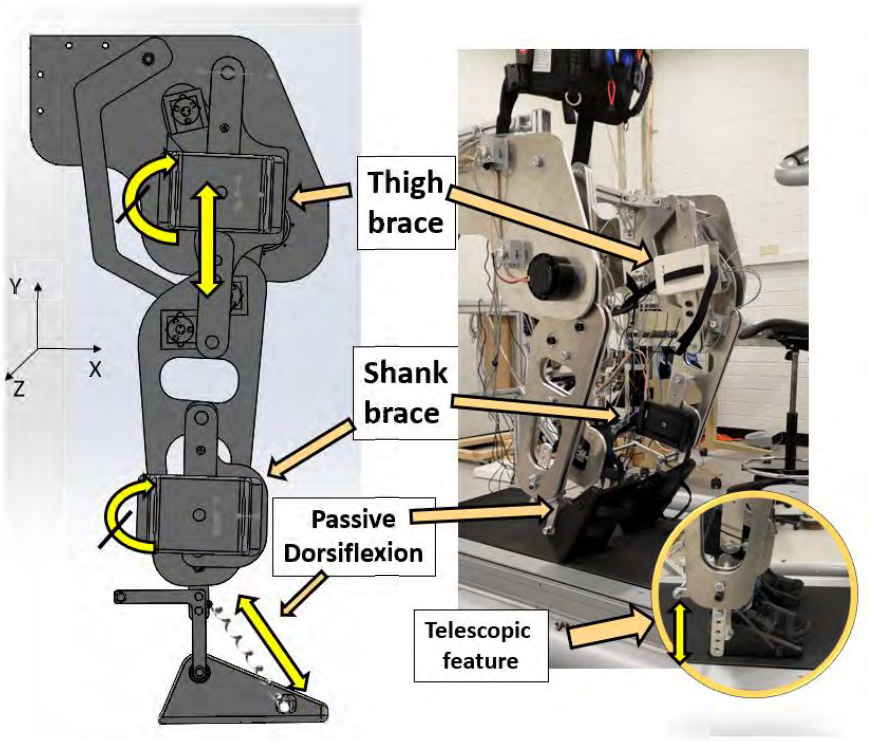


(c)

Figure 5-1. (a) An overall gait rehabilitation system and its major components with passive DOFs labelled, (b) Loadcell placement principle behind the brace for capturing the human/robot interaction force. (c) An internal description of the gait rehabilitation robot.

The developed prototype can adjust to individuals with different leg lengths by varying the telescopic feature incorporated in links L2 and L3. The change in the length of L2 and L3 occurs simultaneously, allowing the footplate to be positioned further or closer depending on individual needs.

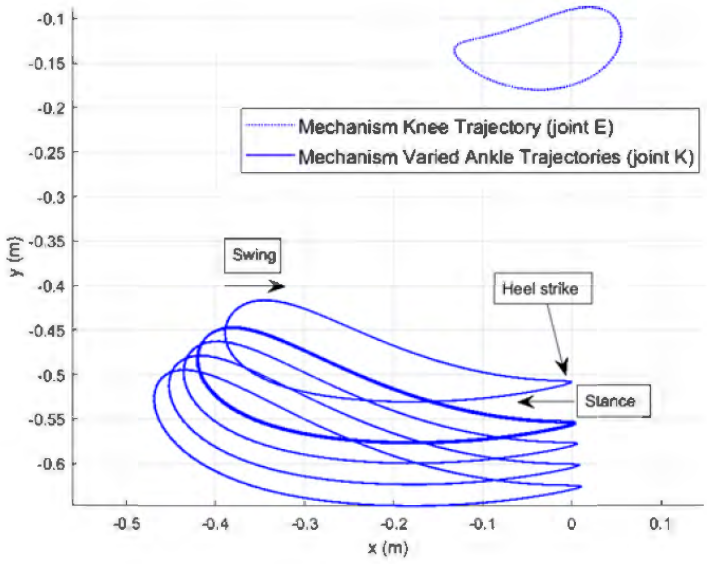


Figure 5-2. Change of ankle trajectories by extending the link attached to link $\overline{EA}$ and $\overline{KA}$.

Keeping the length difference proportion between two links does not significantly change the shape of the produced ankle joint trajectory. The links can be extended to accommodate people with height in the range from 160 to 180 cm. The ankle joint trajectories resulting from the telescopic feature are shown in Figure 5-2.

During manual gait training, therapists guide patients' legs along the trajectory that forms the closed loop. The trajectory traced by the patients' legs is not planar due to movements in the trunk and abduction/adduction motion in the hip joint. However, successful results from treatment with Lokomat have indicated that planar motion in the sagittal plane is sufficient to treat the walking capability. Moreover, the motion constraints imposed by the mechanism kinematics prevent the legs from going beyond the predefined trajectory, making the training process safe and reliable when compared to orthosis mechanisms that employ open loop chains. The proposed robot orthosis is designed for stroke survivors, including those who are paraplegic or hemiplegic and are unable to maintain their balance while walking. During the initial stage of rehabilitation, it is advised to provide constrained motion to the subjects in the sagittal plane. However, during the later stages, when patients regain their lost strength and are able to maintain balance, motions in other planes can be allowed.

## 5.3 PID Based Control

The Proportional, Integral and Derivative (PID) control scheme is a widely used controller for biomedical and industrial applications. Velocity feedback PID control has been applied to the mechanism at the initial control stage to understand the dynamics and behaviour of the mechanism. Moreover, it can be used as a good reference point to compare and evaluate other types of controls. The following velocity feedback controller input was used:

$$u = K_p e + K_t \int_0^t e(t)dt + K_d \frac{d}{dt} e(t) \tag{5.1}$$

$$e(t) = \dot{\theta}_{des}(\mathrm{t}) - \dot{\theta}_{curr}(t) \tag{5.2}$$

where coefficients $K_P$, $K_I$ and $K_D$ represent the errors of the proportional, integral and derivative terms, respectively, and error $e(t)$ at a given time *t* is represented by the difference between the desired angular velocity of the crank. The proportional part is based on the present error, while the integral and derivative parts depend on the accumulation of past errors and future errors, respectively. The PID controller considers disturbance rejection through the proportional term. To obtain perfect gain values, the coefficients of the PID block need to be properly tuned. The

parameters have been tuned using Matlab's built-in PID tuner app, which automatically adjusts the gains based on the step response of the system.

## 5.4 Deep Reinforcement Learning based Control

Deep reinforcement learning uses a deep neural network with a reinforcement learning framework to learn the continuous high-dimensional observation vector and the continuous action space, mapping states to actions [146]. DRL outperforms standard reinforcement learning and can accurately determine actions without acquiring a predefined or learned dynamic model [147]. In this paper, a Deep Deterministic Policy Gradient (DDPG) [146] algorithm was used to regulate the crank velocity. The overall architecture of the implemented control is presented in Figure 5-3.

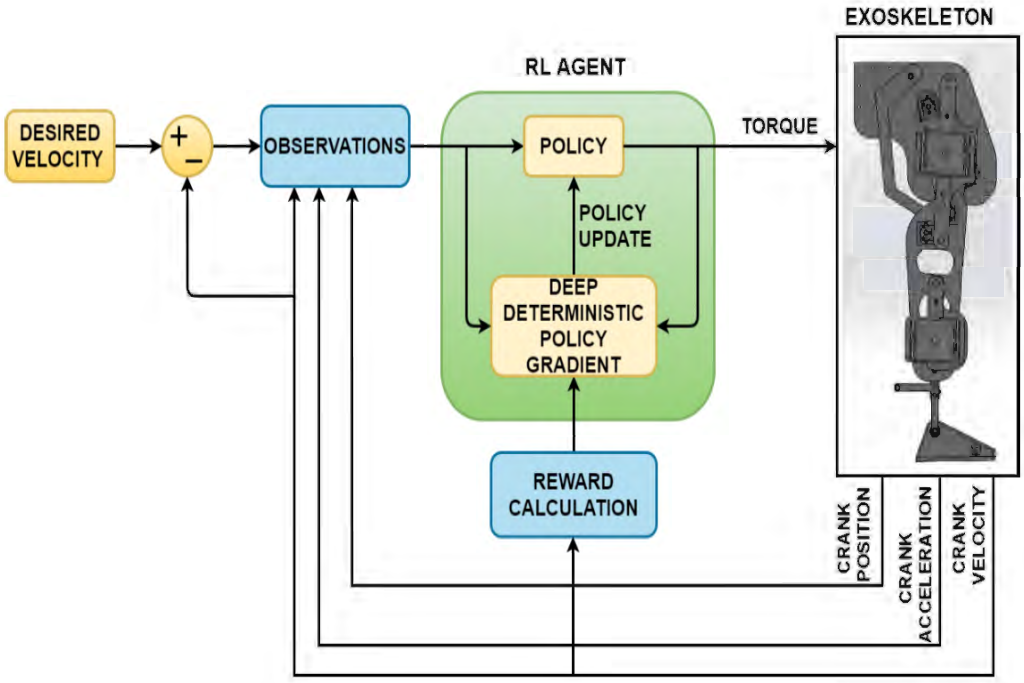


Figure 5-3. Overall block diagram of Deep Reinforcement Learning based control.

The DDPG agent comprises Actor and Critic neural network components, representing policy and value parts, respectively [146]. Depending on the current policy and collected observations from the environment, the actor generates actions, which are further evaluated by the critic based on observations and rewards. The simulation environment consists of the orthosis model implemented in Matlab® 2022a Simulink using the Simscape Multibody framework. To reduce the gap between simulation and real-life prototype behaviour, the stiffness and damping coefficient of revolute joints for each link were added, along with additional loads of 10 kg attached to brace parts to resemble the human leg. The model is trained

through continuous interaction with the environment. The details of the implemented approach are presented further.

### 5.4.1 Deep Deterministic Policy Gradient (DDPG)

DDPG is a model-free actor-critic algorithm that operates in a continuous space [146]. At each time step the learning agent receive a reward $r_t$, environment observations $o_t$, creates an action $a_t$ while trying to maximize the total reward $R$ in (5.3).

$$R = \sum_{i=t}^{T} \gamma^{(i)} r_i(o_i, a_i) \tag{5.3}$$

where $\gamma \epsilon$ [0,1] is the discount factor. The DDPG agent uses a policy gradient to learn. The addition of exploration noise to the actions helps in exploring the environment.

The DDPG agent is trained to regulate the velocity of the crank at the input joint, which has fluctuations due to external disturbances and moments of inertia. The observations vector is $[\int e\, dt,\ e,\ \dot{\theta}_{act}, \theta_0, \ddot{\theta}\ ]$. The single episode reward is calculated as follows:

$$r_{ep} = 10 \cdot (|\ e\ | < 0.1) - 1 \cdot (|\ e\ | \geq 0.1) - 100 \cdot (\dot{\varphi}_{act} \leq 0\ ||\ \dot{\varphi}_{act} \geq 20) \tag{5.4}$$

If the difference error between the target and output crank velocity is less than 0.1 rad/s, then the model is rewarded by 10 units, or penalized by 1 unit if the error is equal or larger than 0.1 rad/s. If the output velocity is less or equal to 0 and larger or equal to 20 rad/s, then the model is penalized by 100 units. The velocity range has been set to keep the model running the environment within that range. Additionally, a custom reset function was introduced to initiate each training episode, where the orthosis model starts to actuate from a random position, velocity and acceleration every time. This helps the model to learn and explore more of the solution space while successfully actuating the environment. The training simulation was set to terminate once the goal of the required velocity was reached, i.e., where the velocity continuously maintains in the range of 0 to 10 rad/s over 20 consecutive episodes. The simulation time of a single episode is 5.0 seconds. The sampling time is set to 0.01 seconds. The configuration of the critic network is shown in Figure 5-4.

## 5.5 Safety

To ensure the safety of individuals engaged in experimental activities, the robotic system has been equipped with essential safety provisions. Emergency stop buttons, integrated into an

independent circuit, are incorporated within the system, accessible to both the researcher and the participant during the experiment. These buttons serve the purpose of promptly deactivating the power source in the event of an emergency or when the subject experiences discomfort.

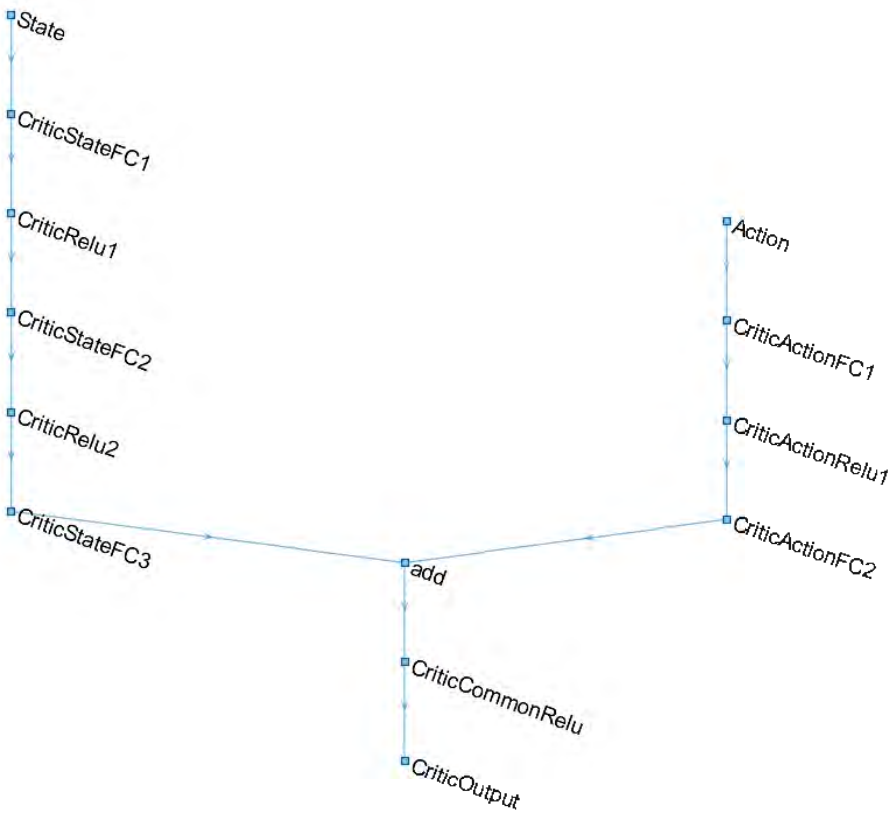


Figure 5-4. Critic network architecture.

While the developed mechanism is designed to follow predetermined trajectories, supplementary mechanical stops have been installed as an additional safety measure at the rocker links to avoid going beyond the range of motion. These mechanical stops serve to restrict the robot from surpassing physiological ranges of motion, particularly in unforeseen circumstances. They can withstand the peak torque delivered by the motor, thereby safeguarding against potential hazards.

## 5.6 Experimental Protocol

Five healthy individuals with no prior history of neurological disorders nor injuries in the lower limb that might affect walking were recruited to the study to check the applicability of the developed gait rehabilitation system with the implemented velocity regulation. All participants have provided written consent. The research protocol has been approved by Human

Research Ethics Committee at the University of Canberra. The legs of the participants were attached using Velcro straps on the braces of the orthosis at mid-thigh and mid-shank. Subjects were also attached to the BWS system to ensure the stability of the walking mechanism in the first trial. During the first stage, participants were asked to remain passive and allow the mechanism to move their limbs. The robot was actuated during this time to check the capability of a single motor to lift and move the legs in a predefined trajectory. The treadmill speed and the crank velocity were synchronized, and the walking speed during all experiments was set in the range between 0.2- 0.6 m/s. Data for 60 gait cycles were recorded for further analysis. A snapshot of a human wearing the robot during the experimental trial is shown in Figure 5-5.

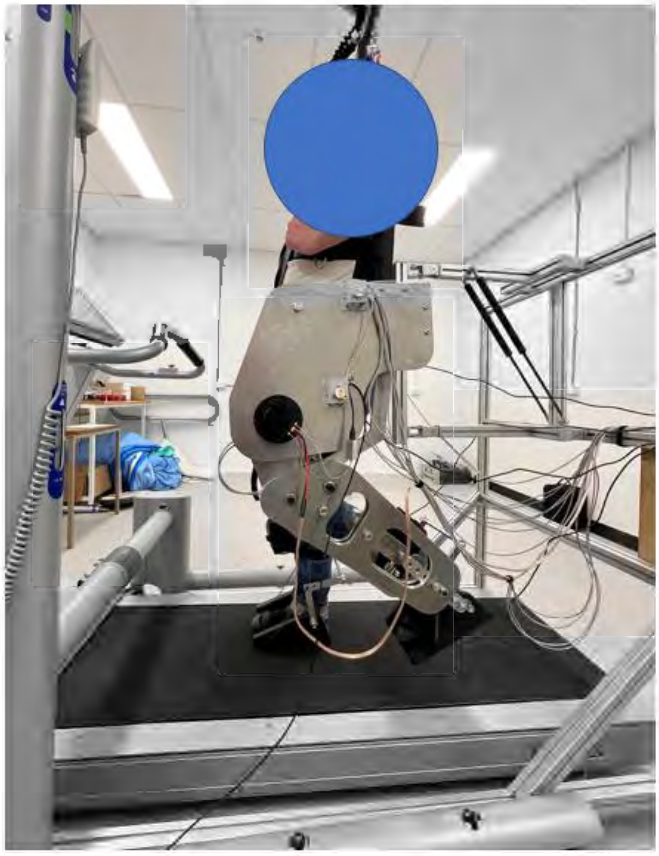

Figure 5-5.Experimental trial with human subjects.

## 5.7 Simulation and Experimental Results

Since the mechanism has external disturbances and the links possess a moment of inertia, simple PID control has been applied initially at the first step. However, as can be seen from Figure 5-6, the output of the crank velocity regulation through PID control is not smooth due to nonlinearity in the system and the external disturbances in terms of leg weight and inertia. It

exhibits high overshoot during some periods, reaching up to almost 7 rad/s for short periods, which is not the best scenario during a gait training process.

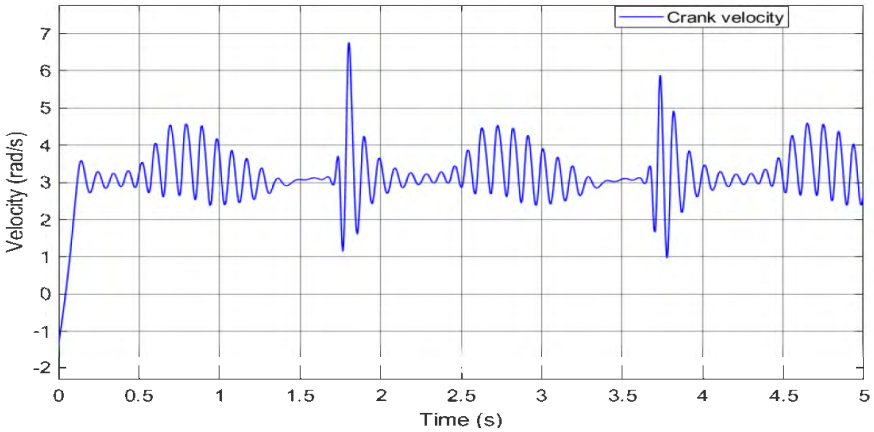


Figure 5-6 Output crank velocity using PID control in response to disturbance applied externally and 3 rad/s target velocity.

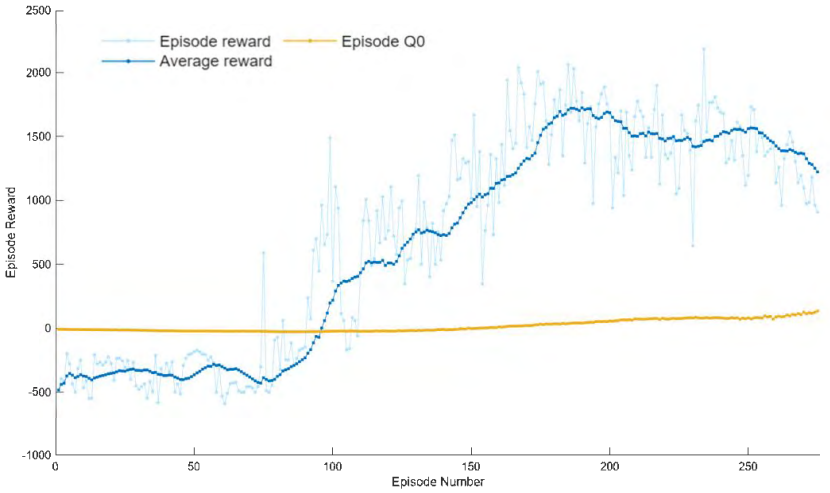


Figure 5-7. Reinforcement Learning training curve.

Moreover, the crank for a short instance of time has a negative velocity leading to undesired scenarios during the start of the walk. To improve the regulation of the crank velocity in response to external disturbance, a DRL-based control model was implemented. The model was trained on an Intel Core i7-9700 CPU for approximately 500 episodes. After around 275 episodes, the average reward reached its target of maintaining above 1275 units for more than 100 episodes, terminating the training process as shown in Figure 5-7. Single gait cycle snapshots, as presented in Figure 5-8, recorded during the experiments demonstrate that the prototype can provide complex lower limb motion trajectories during walking. The trained DRL model was further tested on the actual prototype, and the experimental results of three different angular

velocities of the crank of the mechanism with attached legs are presented in Figure 5-9. The actual speed of the crank fluctuates close to the target speed, and although there is a slightly longer rise time to reach the target speed, it does not have a negative impact on patients during rehabilitation training, as the actual speed doesn't go beyond the target range.

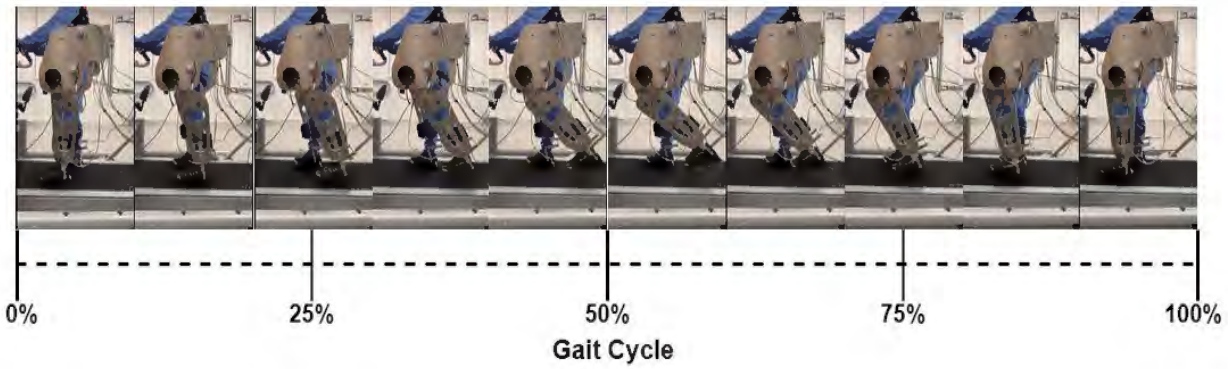


Figure 5-8. Snapshots taken during one gait cycle.

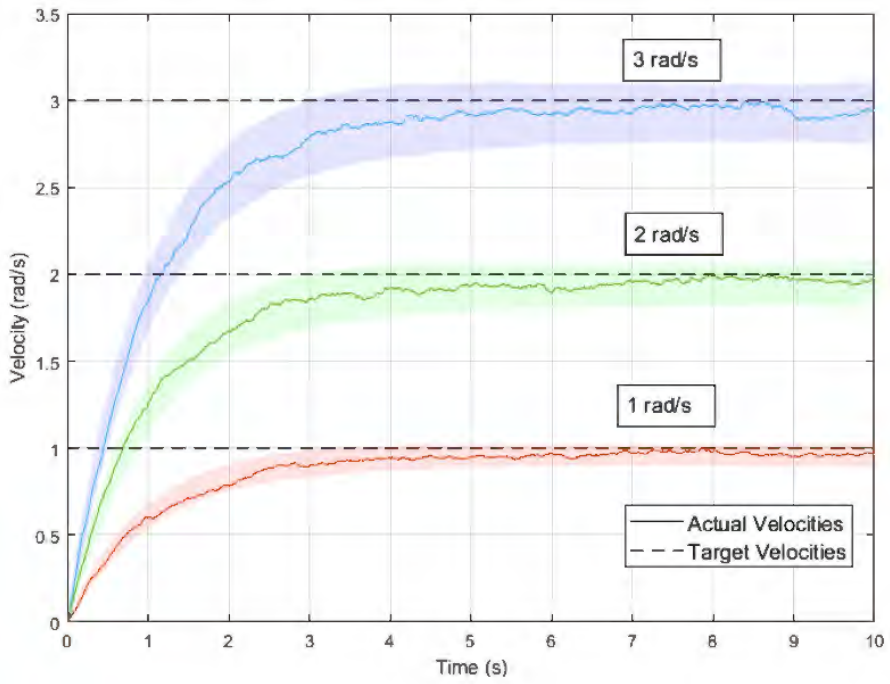


Figure 5-9. Average velocity of the crank for 5 healthy subjects using trained DRL model with 95% confidence interval.

## 5.8 Chapter Summary

This chapter presents the design of a novel underactuated robotic gait rehabilitation orthosis with a velocity control scheme. The core mechanism of the orthosis is based on a Stephenson III six-bar linkage, which is the most optimal candidate among closed-loop linkage mechanisms

for robotic gait rehabilitation applications. This mechanism can operate without compromising the accuracy of lower limb trajectories and at the same time avoiding bulkiness in the frame.

The proposed robotic orthosis, based on the Stephenson III six-bar linkage, is actuated by rotating the mechanism's crank. Previously proposed theoretical single DOF mechanisms state that the angular velocity of the crank is constant; however, in reality, due to external disturbances and inertia of the links, the angular speed of the crank fluctuates. In this work, we have first applied and tested the performance of a standard PID controller. The outcome demonstrated that PID control is sensitive to nonlinearities and therefore may not be sufficient to stabilize the velocity of the crank. Therefore, we have designed and applied a model-free DRL-based velocity control scheme on the robotic orthosis. The controller is designed to regulate the speed fluctuations in the crank of a gait rehabilitation robot based on a six-bar linkage mechanism driven by a servo motor.

According to the authors' best knowledge, this is the first work where an underactuated robotic gait rehabilitation orthosis was regulated through a DRL-based controller for stabilizing the angular velocity of the crank, and evaluations with human subjects were conducted and revealed promising results. Considering the human subject's input and movement during gait training process is crucial. Patient-cooperative control strategies can promote active patient engagement in the training process, which can help expedite recovery from lost muscular capabilities. Thus, the upcoming chapter explores the potential application of such control on the robot. This approach aims to facilitate a more natural and comfortable experience for the patient while promoting optimal recovery.

# Chapter 6. Patient Cooperative Control via Impedance Learning

## 6.1 Introduction

The control of previously developed single DOF mechanisms is assumed to be done by only constant speed control. While this approach may offer benefits for stroke patients with a less severe disability, it is crucial to consider the interaction force between the human and the robot in more severe disability scenarios. In such scenarios, it becomes necessary to adjust and vary the torque supplied by the robot at different stages of the gait cycle. In addition, active human participation during gait training can significantly enhance the effectiveness and speed of recovery [148, 149]. Therefore, establishing an active interaction between the human and the robot is an important aspect of gait rehabilitation robots. Following the velocity regulation control development introduced in Chapter 5, this chapter further elaborates and expands on the critical aspect of human-robot interaction.

In this context, impedance control emerges as a valuable approach to facilitating effective and personalized gait rehabilitation. The concept of impedance control, pioneered by Hogan [150], allows for the precise adjustment of robot impedance, enabling the robot to exhibit either stiffness or compliance. By tailoring the robot's impedance to match the severity of the patient's condition, personalized assistance can be provided. For patients with mild impairments, a compliant robot accommodates natural movement patterns, while for individuals unable to move their legs, a stiffer robot offers the necessary stability and support. Impedance learning control has been applied to soft exosuits, which assisted in improving human walking over different terrains [151]. This control approach has also demonstrated satisfactory results in assisting sit-to-stand motions [152]. It is commonly accepted that control of human joints can be imitated using an impedance control approach [153]. Thus, in this chapter implementation of impedance control on the Stephenson III six-bar linkage-based gait rehabilitation robot to provide assist-as-needed training is presented.

The organization of the chapter is as follows. Section 6.2 describes dynamical modelling using Lagrangian approach, impedance control scheme, and human torque estimation using an Artificial Neural Network (ANN). Section 6.3 presents the experimental protocol and the results from the impedance control scheme. Section 6.4 provides the discussion and summary of the chapter.

The contributions of this chapter involve the development of an impedance control strategy

for a Stephenson III six-bar linkage actuated by a single motor. According to the authors' best knowledge, no prior work has investigated or implemented a human interactive control strategy on single DOF mechanisms designed for gait rehabilitation purposes. Thus, the novelty of this work is in demonstrating the applicability of impedance learning control technique on linkage-based mechanisms. This work will also serve as a foundation for building patient-cooperative control strategies for single DOF linkage-based rehabilitation robots.

## 6.2 Methodology

### 6.2.1 Dynamic Formulation of the Mechanism

The overall motion of the mechanism can be described using the Lagrange modelling methodology [154]. The notations and configurations defined for solving the dynamics of the mechanism are presented in Figure 3-3. The masses of links $\overline{GH}, \overline{HEK}, \overline{BC}, \overline{CDE}$ and $\overline{AD}$ are defined as $m_1, m_2, m_5, m_6$ and $m_9$, respectively, and $I_i$ is the mass moment of inertia for the corresponding link. $V_i$ is the velocity at the mass center of the corresponding link. The distance from the joint to the center of mass of the ternary link is defined by $R_i$. Some derivations of the Lagrangian partial derivatives are provided at the end of the manuscript in Appendix A section. The whole system's Lagrangian is defined as the difference between the total kinetic energy and the total potential energy.

$$\mathcal{L} = K - P \tag{6.1}$$

The definition of kinetic energy $K$ of the mechanism can be expressed as follows:

$$K = \frac{1}{2}\left[\left(m_1 V_1^2 + I_1 \dot{\theta}^2{}_1\right) + \left(m_2 V_2^2 + I_2 \dot{\theta}^2{}_3\right) + \left(m_5 V_5^2 + I_5 \dot{\theta}^2{}_5\right) + \left(m_6 V_6^2 + I_6 \dot{\theta}^2{}_6\right) + \left(m_9 V_9^2 + I_9 \dot{\theta}^2\right)\right] \tag{6.2}$$

where

$$\theta_1 = \alpha_2 + \beta_2$$

$$\theta_5 = \beta - \gamma$$

$$\theta_3 = \alpha_3 + \beta_3$$

$$\theta_6 = \alpha_1 + \beta_1$$

$$V_1^2 = \frac{L_1^2}{4} \dot{\theta}^2{}_1$$

$$V_2^2 = L_1^2 \dot{\theta}^2{}_1 + R_2^2 \dot{\gamma}_2^2 + 2 L_1 R_2 \dot{\theta}_1 \dot{\gamma}_2 \cos(\theta_1 - \gamma_2)$$

$$V_5^2 = \frac{L_5^2}{4}\dot{\theta}^2{}_5$$

$$V_6^2 = L_9^2\dot{\theta}^2 + R_6^2\dot{\gamma}^2{}_6 + 2L_9R_6\dot{\theta}\dot{\gamma}_6\cos(\theta - \gamma_6)$$

$$V_9^2 = \frac{L_9^2}{4}\dot{\theta}^2$$

Then, the potential energy $P$ is determined as:

$$P = m_1 g\frac{L_1}{2}\sin\theta_1 + m_2 g(L_1\sin\theta_1 + R_2\sin\gamma_2) + m_6 g(L_9\sin\theta + R_6\sin\theta_6) + m_5 g\frac{L_5}{2}\sin\theta_5 + m_9 g\frac{L_9}{2}\sin\theta \quad (6.3)$$

where $g$ is the gravitational acceleration. After reconfiguring (6.3), the final expression for the Lagrangian of the mechanism has the following form:

$$\mathcal{L} = J_1\dot{\theta}^2{}_1 + J_3\dot{\theta}^2{}_3 + J_5\dot{\theta}^2{}_5 + J_6\dot{\theta}^2{}_6 + J_0\dot{\theta}^2 + M_1\dot{\gamma_2^2} + M_2\dot{\gamma}^2{}_6 + P_1C_1(\theta_1,\gamma_2)\dot{\theta}_1\dot{\gamma}_2 + P_6C_6(\theta,\gamma_6)\dot{\theta}\dot{\gamma}_6 + G(\theta_1,\theta_5,\theta_6,\theta,\gamma_2) \quad (6.4)$$

where

$$J_1 = \frac{1}{2}\left[m_1\frac{L_1^2}{4} + I_1 + m_2L_1^2\right]$$

$$J_3 = \frac{1}{2}[I_2]$$

$$J_5 = \frac{1}{2}\left[m_5\frac{L_5^2}{4} + I_5\right]$$

$$J_6 = \frac{1}{2}\left[m_6L_9^2 + m_9\frac{L_9^2}{4} + I_6\right]$$

$$J_0 = \frac{1}{2}[I_9]$$

$$M_1 = \frac{1}{2}[m_2R_2^2]$$

$$M_2 = \frac{1}{2}[m_6R_6^2]$$

$$P_1 = \frac{1}{2}[m_2 2L_1R_2]$$

$$C_1(\theta_1,\gamma_2) = \cos(\theta_1 - \gamma_2)$$

$$P_6 = \frac{1}{2}[m_6 2L_9R_6]$$

$$C_6(\theta,\gamma_6) = \cos(\theta - \gamma_6)$$

$$G(\theta_1, \theta_5, \theta_6, \theta, \gamma_2) = m_1 g \frac{L_1}{2} \sin\theta_1 + m_2 g(L_1 \sin\theta_1 + R_2 \sin[\![\gamma_2)]\!] + m_6 g(L_9 \sin\theta + R_6 \sin\theta_6) + m_5 g \frac{L_5}{2} \sin\theta_5 + m_9 g \frac{L_9}{2} \sin\theta$$

By introducing function $S$ which is the derivative of the assumed angles $\dot{\gamma}_2, \dot{\gamma}_6, \dot{\theta}_1, \dot{\theta}_3, \dot{\theta}_5, \dot{\theta}_6$ with respect to $\dot{\theta}$ we could replace these velocity terms and present Lagrangian in the terms of $\theta$:

$$\mathcal{L} = \big(J_0 + J_1 S_1^2(\theta, \alpha_2, \beta_2) + J_3 S_3^2(\theta, \alpha_3, \beta_3) + J_5 S_5^2(\theta, \beta, \gamma) + J_6 S_6^2(\theta, \alpha_1, \beta_1) + M_1 S_2^2(\theta, \gamma) + M_2 S_7^2(\theta, \gamma) + P_1 C_1(\theta_1, \gamma_2) S_8(\theta, \alpha_2, \beta_2, \alpha_3) + P_6 C_6(\theta, \gamma_6) S_9(\theta, \alpha_1)\big)\dot{\theta}^2 + G(\theta_1, \theta_5, \theta_6, \theta, \gamma_2) \quad (6.5)$$

The expression for the Lagrangian contains parameters that are also functions of $\theta$. Next, we need to identify the equation of motion by:

$$\frac{d}{dt}\left(\frac{\partial \mathcal{L}}{\partial \dot{\theta}}\right) - \frac{\partial \mathcal{L}}{\partial \theta} = T_{rob} \quad (6.6)$$

$T_{rob}$ is the torque supplied by the robot, $\dot{\theta}$ is the angular velocity of the crank $\overline{AD}$. Since the damping in the mechanism is small, the dissipative energy can be ignored and is not considered in this work. To finalize the equation of motion, first determine the following:

$$\frac{\partial \mathcal{L}}{\partial \dot{\theta}} = 2(J_0 + J_1 S_1^2(\theta, \alpha_2, \beta_2) + J_3 S_3^2(\theta, \alpha_3, \beta_3) + J_5 S_5^2(\theta, \beta, \gamma) + J_6 S_6^2(\theta, \alpha_1, \beta_1) + M_1 S_2^2(\theta, \gamma) + M_2 S_7^2(\theta, \gamma) + P_1 C_1(\theta_1, \gamma_2) S_8(\theta, \alpha_2, \beta_2, \alpha_3) + P_6 C_6(\theta, \gamma_6) S_9(\theta, \alpha_1))\dot{\theta} \quad (6.7)$$

Next, the derivations for $\frac{d}{dt}\left(\frac{\partial \mathcal{L}}{\partial \dot{\theta}}\right)$ and $\frac{\partial \mathcal{L}}{\partial \theta}$ can be found in (A.1) and (A.2), respectively, in the Appendix A. The overall dynamic equation of motion for the system can be described using the following expression:

$$2(J_0 + J_1 S_1^2 + J_3 S_3^2 + J_5 S_5^2 + J_6 S_6^2 + M_1 S_2^2 + M_2 S_7^2 + P_1 C_1 S_8 + P_6 C_6 S_9)\ddot{\theta} + \Bigg[2J_1 S_1 \left(\frac{\partial S_1}{\partial \theta} + \frac{\partial S_1}{\partial \alpha_2}\frac{\partial \alpha_2}{\partial \theta} + \frac{\partial S_1}{\partial \beta_2}\frac{\partial \beta_2}{\partial \theta}\right) + 2J_3 S_3 \left(\frac{\partial S_3}{\partial \theta} + \frac{\partial S_3}{\partial \alpha_3}\frac{\partial \alpha_3}{\partial \theta} + \frac{\partial S_3}{\partial \beta_3}\frac{\partial \beta_3}{\partial \theta}\right) + 2J_5 S_5 \left(\frac{\partial S_5}{\partial \theta} + \frac{\partial S_5}{\partial \beta}\frac{\partial \beta}{\partial \theta} + \frac{\partial S_5}{\partial \gamma}\frac{\partial \gamma}{\partial \theta}\right) + 2J_6 S_6 \left(\frac{\partial S_6}{\partial \theta} + \frac{\partial S_6}{\partial \alpha_1}\frac{\partial \alpha_1}{\partial \theta} + \frac{\partial S_6}{\partial \beta_1}\frac{\partial \beta_1}{\partial \theta}\right) + 2M_1 S_2 \left(\frac{\partial S_2}{\partial \theta} + \frac{\partial S_2}{\partial \gamma}\frac{\partial \gamma}{\partial \theta}\right) + 2M_2 S_7 \left(\frac{\partial S_7}{\partial \theta} + \frac{\partial S_7}{\partial \gamma}\frac{\partial \gamma}{\partial \theta}\right) +$$

$$P_1\left(C_1\left(\frac{\partial S_8}{\partial\theta}+\frac{\partial S_8}{\partial\alpha_2}\frac{\partial\alpha_2}{\partial\theta}+\frac{\partial S_8}{\partial\beta_2}\frac{\partial\beta_2}{\partial\theta}+\frac{\partial S_8}{\partial\alpha_3}\frac{\partial\alpha_3}{\partial\theta}\right)+S_8\left(\frac{\partial C_1}{\partial\theta_1}\frac{\partial\theta_1}{\partial\theta}+\frac{\partial C_1}{\partial\gamma_2}\frac{\partial\gamma_2}{\partial\theta}\right)\right)+P_6\left(C_6\left(\frac{\partial S_9}{\partial\theta}+\right.\right.$$

$$\left.\left.\frac{\partial S_9}{\partial\alpha_1}\frac{\partial\alpha_1}{\partial\theta}\right)+S_9\left(\frac{\partial C_6}{\partial\theta}+\frac{\partial C_6}{\partial\gamma_6}\frac{\partial\gamma_6}{\partial\theta}\right)\right)\Bigg]\dot{\theta}^2-\frac{\partial G}{\partial\theta}+\frac{\partial G}{\partial\theta_1}\frac{\partial\theta_1}{\partial\theta}+\frac{\partial G}{\partial\theta_5}\frac{\partial\theta_5}{\partial\theta}+\frac{\partial G}{\partial\theta_6}\frac{\partial\theta_6}{\partial\theta}+\frac{\partial G}{\partial\gamma_2}\frac{\partial\gamma_2}{\partial\theta}=T_{rob} \quad (6.8)$$

## 6.3 Impedance Control Architecture

The impedance control technique is a widely used technique in the field of rehabilitation robotics, which helps regulate the human-robot interaction forces [150]. Depending on the level of lesion, the disability in the lower limbs among stroke patients may vary substantially. Impedance control can adjust and provide the necessary assistive motion to the subject based on his/her needs. The assistance from the robot is modified by considering the human joint torques supplied by the subject. When the subject does not move, the robot is set to the high impedance mode (low compliance), which means the robot increases the assistance to guide the subject along the physiological gait trajectories. On the other hand, if the subject makes an effort to walk, the robot acts in a low impedance mode (high compliance). This mode keeps the interaction force between the human and the robot within a specified range, allowing some deviation from the required trajectory. This deviation can be determined and set depending on the patient's ability to move their lower limbs. In case, if the deviation increases beyond a predefined threshold, the robot adjusts the moment to return the leg to the permissible range. This approach is effective in patients requiring gait training, as it encourages active participation from them, which facilitates the recovery process of impaired gait capabilities.

The architecture of the implemented impedance controller is illustrated in Figure 6-1, which was used to control the six-bar linkage-based gait rehabilitation robot. The angular position of the robot's joints is measured using the rotary encoders. The gait rehabilitation robot provides naturalistic ankle and knee joint trajectories relative to the hip joint, and it is assumed to be in alignment with the human joints. The load cells are installed on the thigh and shank regions to track the interaction force between the human and the robot during walking. The human-robot interaction forces occurring at the shank $F_{sh}$ and thigh regions $F_{th}$, measured crank position $\theta$, and its angular velocity $\dot{\theta}$ serve as essential inputs for the overall control scheme. The inputs are further processed through the control framework, which involves the dynamic model of the robot and the ANN-based human torque estimation blocks. The dynamic model from (6.8) determines the robot's torque based on the inputs of crank angle $\theta$ and its angular velocity $\dot{\theta}$, providing a more accurate understanding of how the robot behaves.

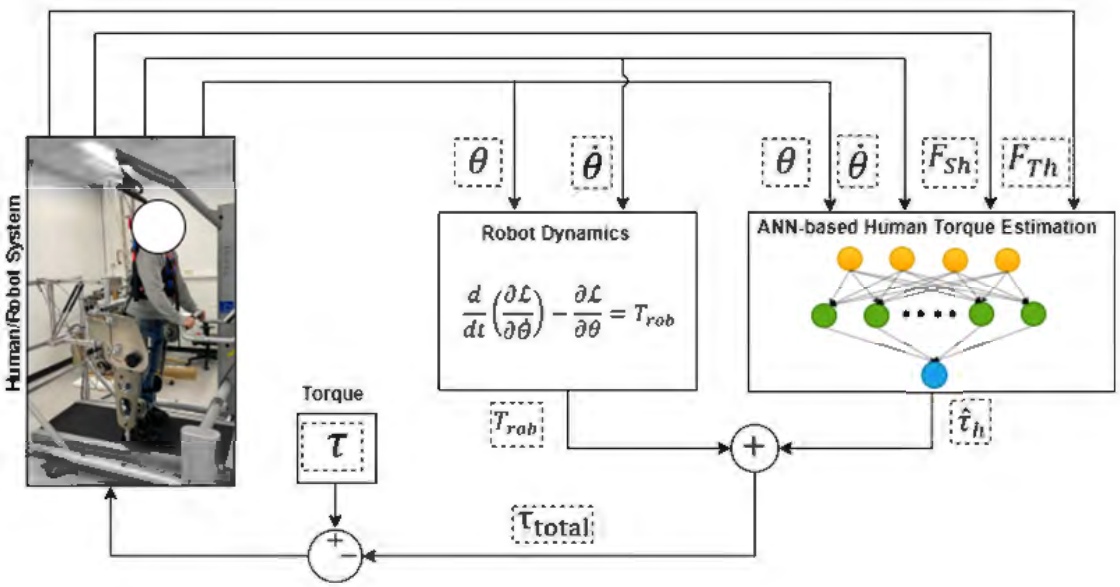


Figure 6-1. Impedance learning control scheme for the gait rehabilitation. The robot outputs the crank position, crank angular velocity, and interaction forces at shank and thigh regions. The robot dynamics block calculates the robot's torque, while an ANN block estimates the human's torque. These torques are added, subtracted from the initial robot torque, resulting in an updated torque. This scheme enables dynamic adjustment of the robot's assistance based on the human's input.

The ANN module, denoted as $h(\cdot)$, accepts four measured inputs from the human-robot system and produces a single output of predicted human torque exerted on the system as follows:

$$h\left(F_{sh}, F_{th}, \theta, \dot{\theta}\right) \approx \hat{\tau}_h \tag{6.9}$$

where $\hat{\tau}_h$ is the predicted human torque obtained from the ANN model. Further, the robot's torque $T_{rob}$ and the predicted human torque $\hat{\tau}_h$ are added together producing the total human-robot torque. The combined torques from the dynamics and ANN modules provide a comprehensive understanding of the torque acting on the system. Which allows to refine and modify the supplied torque from the robot to align the subject's intended motion, managing all the deviations or disturbances that occur during walking. The proposed impedance control scheme with neural network-based human torque prediction can improve and optimize the interaction between the human subject and the gait rehabilitation robot. Provision of required and adaptable assistive motion depending on human subjects' needs, can facilitate the individual's functional recovery, and improve the quality of life.

## 6.4 Artificial Neural Network for Human Torque Estimation

In this section, a description of a neural network-based system identification approach to estimate the torque exerted by the human joints during gait rehabilitation is provided. Employing existing machine learning techniques in the control schemes of robotic systems has many benefits, such as managing uncertainties, including additional evaluation criteria of the system's performance and does not require strict knowledge of the system's model [155]. Specifically, due to the simplicity of design and implementation, ANNs have proven themselves to be a powerful tool for nonlinear function approximation. It is a feedforward network architecture with a single hidden layer containing 32 neurons. The input layer is represented by the vector $x = [F_{sh}, F_{th}, \theta, \dot{\theta}]$, where $F_{sh}$ and $F_{th}$ stand for human-robot interaction force values from loadcells installed at the shank and thigh regions, respectively. $\theta$ and $\dot{\theta}$ are position and its derivative of the crank, respectively. The output of the network is a single value, the predicted human torque. Various hyperparameters, such as, number of hidden layers, number of nodes/neurons per layer, learning rate, momentum, etc. were chosen heuristically using grid search [156]. ReLU is used as the activation function here to avoid the vanishing gradients problem and save the computational time. The network is trained using the Adam (Adaptive Movement Estimation algorithm) gradient-based optimizer [157] with a learning rate of 0.001. The architecture of the ANN used can be written as follows:

$$h(x) = W_2 \cdot ReLU(W_1 \cdot x + b_1) + b_2 \tag{6.10}$$

where ReLU is the Rectified Linear Unit activation function [158], represented by

$$ReLU(x) = \begin{cases} x, & if\ x \geq 0 \\ negative\_slope \times x, & otherwise \end{cases} \tag{6.11}$$

$W_1 \in \mathbb{R}^{32\times4}, W_2 \in \mathbb{R}^{1\times32}$ are weight matrices, and $b_1 \in \mathbb{R}^{32\times1}$, $b_2 \in \mathbb{R}$ are bias vectors. $\boldsymbol{\psi} = (W_1, W_2, b_1, b_2)$ are learnable parameters of the ANN model and are optimized using an objective function. The diagram of the ANN model employed in this work is shown in Figure 6-2. The training objective is to minimize the Mean Squared Error (MSE) loss between the network's predictions and the actual torque values and a regularizer to balance variance-bias trade-off. Here, the actual torque values refer to the measured torque from the motor driving the human/robot system and the torque required to drive empty robot without human subject, which provides the ground truth against which the network's performance is evaluated. The MSE loss is defined as follows:

$$\mathcal{L}_{MSE} = \frac{1}{N}\sum_{j=1}^{N}\sum_{i=1}^{Ns}\left(\hat{\tau}_{h_{(i,j)}} - (\tau_{motor_{(i,j)}} - \tau_{r_{(i,j)}})\right)^2 + \lambda\boldsymbol{\psi} \quad (6.12)$$

Where $N$ is the number of samples, $T$ is the number of instances recorded in a single gait cycle, $\hat{\tau}_h$ is the predicted value of the human torque, $\tau_{motor}$ is the actual torque motor provided to drive the human/robot system and $\tau_r$ is the torque supplied to drive the robot without a human subject.

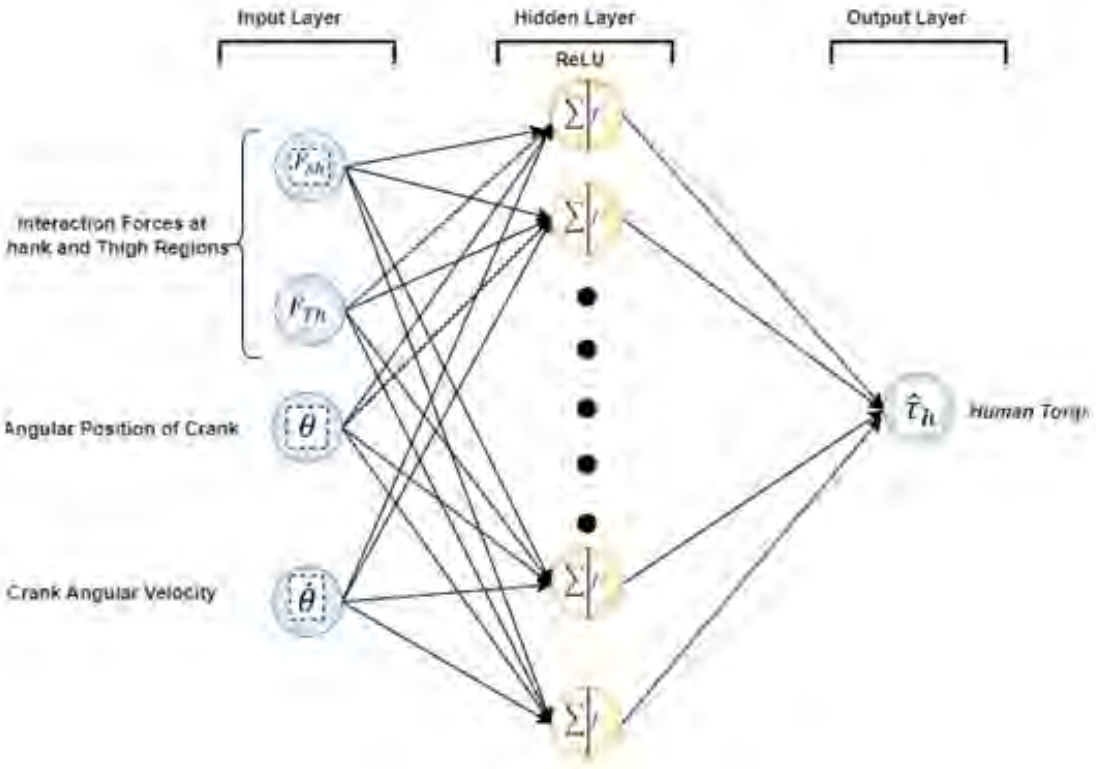


Figure 6-2. Artificial Neural Network architecture.

In (6.12), the subscripts $(i, j)$ correspond to two different aspects of the data. The '$i$' index refers to the specific sample within the batch and can take on any value within the total number of samples, N. On the other hand, the $'j'$ index refers to the specific instance within a single gait cycle torque trajectory, with '$j$' being any value within the total instances, $T$. $\lambda$ is a regularization parameter used to reduce the risk of overfitting. Prior to feeding the data into the model, it was pre-processed to remove outliers and scaled accordingly, ensuring that all features are on the same scale. The dataset consists of 330,397 points, recorded at a sampling rate of 100 Hz from the loadcells and encoders. The processed data was then split into a training set (60%), validation set (20%), and testing set (20%) to assess the model's performance. The dataset is obtained from eight participants (7m, 1f) who were asked to stay passive while wearing the

robot and allowing it to move their legs in a predefined motion and walk concurrently while wearing the robot, to ensure capturing both end extremities in the interaction forces' values.

## 6.5 Experimental Evaluation

### 6.5.1 Experimental Protocol

Prior to the start of the experiments, corresponding ethics approval to experiment on eight neurologically intact subjects (7m, 1f) (age 22-45 years) was granted by the Human Research Ethics Committee at the University of Canberra. The subjects reported no history of having neurologic disorders. During the experiments, participants' legs were fixed to the robot legs with the braces located in the thigh and shank segments using Velcro straps. Subjects' feet were attached to the footplate. The BWS system was used to balance the weight of human subjects against gravity, thus allowing them to keep their legs passive during the first stage of the experiment. During this stage, the robot moved subjects' legs on a predefined trajectory at constant speed. In passive mode, participants were asked to stay relaxed without moving their legs and allowing the robot to direct the lower limbs along the predefined trajectory. During the active mode, participants were asked to perform the usual walking while wearing the robot. The walking speed for the participants was set by the speed of the treadmill.

In our study, we sought to determine if there were significant differences between the interaction forces (at the robot and human interface) observed during passive and active modes. We utilized the Wilcoxon Rank-Sum test [159], a non-parametric method, to perform this analysis as it offers robustness against data not adhering to a normal distribution. Wilcoxon Rank-Sum test was used for both thigh and shank interaction forces and the torque supplied by the robot during active and passive modes.

## 6.6 Results

Initial results of the impedance learning control scheme developed for the proposed mechanism are presented in this section. The control scheme can increase or decrease the support from the robot depending on how much torque the person is exhibiting during the gait training. In case less effort is detected, the robot will supply more torque to keep the legs along the naturalistic lower limb trajectories and vice versa. As it can be seen the torque supplied by the robot during passive mode when the person is not moving the legs is more than the torque supplied

during the active mode. Basically, the torque supplied during active mode is the torque required to keep the robot moving while being aligned to the walking of the person.

The estimation of torques exerted by the human subject is done via the use of the ANN algorithm. As an input, the model receives the values for human-robot interaction forces at thigh and shank regions, the current position (input angle $\theta$) of the robot and tries to predict the torque exerted by the human. The model has been trained using the Pytorch Lightning framework, which has been further converted to the Open Neural Network Exchange (ONNX) format and then imported to Matlab® 2022B. It took the model less than 1 hour to be trained on 2nd Gen Intel(R) Core(TM) i7-1265U. The training and testing loss results are presented in Figure 6-3.

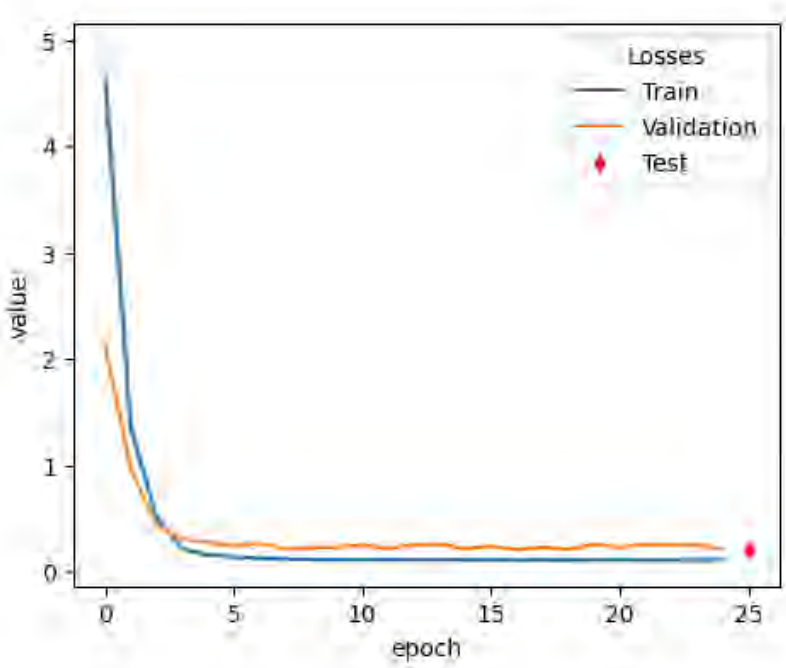


Figure 6-3. Performance of the model: Training Loss, Validation Loss, and Testing results.

The training Mean Squared Error (MSE) is approximately 0.0835 $Nm^2$. The small value for MSE indicates a high level of accuracy in predicting torque values based on the given input features, which include joint angular positions, angular velocity, and interaction forces. The validation set has been introduced to avoid common problems in machine learning such as overfitting. The validation loss has been constantly monitored to make the model learn generalizable patterns instead of memorizing the training data. As such, the selected hyperparameters effectively balanced the need for accuracy, computational efficiency and the model interpretability. Regularization introduced with the cross-validation technique using validation sets enabled to avoid overfitting. Parameters of the network are finetuned using validation set, thus validation set evaluated at every epoch. Once learning curve is stabilized, we stop training the

model and evaluate the model on the test dataset. Figure 6-3 demonstrates that test dataset loss is similar to the validation dataset, and thus indicates that the model is generalized well to unseen data. The test has been done once at the last stage to verify it is the same as validation loss. We fine-tune the parameters of the network using the validation set; thus, the validation set is evaluated at every epoch. Once the learning curve has stabilized, we stop training the model and test the model on the test set. Figure 6-3 demonstrates that the test set loss is similar to validation, thus indicating the model is generalized well to unseen data. The test has been done once at the last stage to verify it is the same as validation loss.

These findings demonstrate the model's ability to generalize well to unseen data and make accurate human torque predictions for robotic applications. The results obtained serve as evidence of the model's strong performance and reliability, further reinforcing its potential practical utility in torque prediction tasks. The model's ability to generate accurate torque predictions with low error suggests that it has the potential to contribute to stable robot control. By accurately estimating the torque values exerted by the robot, the model provides valuable information for control algorithms to make informed decisions and adjust control signals accordingly. This can aid in achieving better control stability by enabling precise torque control and reducing potential control errors.

Further, participants were asked to stay passive for about 20 seconds and not move their legs, while allowing the robot to direct the lower limbs along the trajectory. After that, participants were asked to start moving their legs to perform walking. The torques supplied by the robot ($T_{rob}$) during the two phases of passive and active are demonstrated in Figure 6-4. The values for the torques are the average across eight healthy participants. The torques supplied by the robot during active and passive phases can be observed. During the passive phase, the robot supplied more torque to help a person complete the gait trajectory, and during the active phase when the person started actively walking, so the torque supplied by the robot is decreased. The crank of the robot was rotating at around 3 rad/s, driving a stride frequency of 0.47 Hz. The transition of the change in torque supplied by the robot in response to switching from active to passive and from passive to active modes is shown in Figure 6-5.

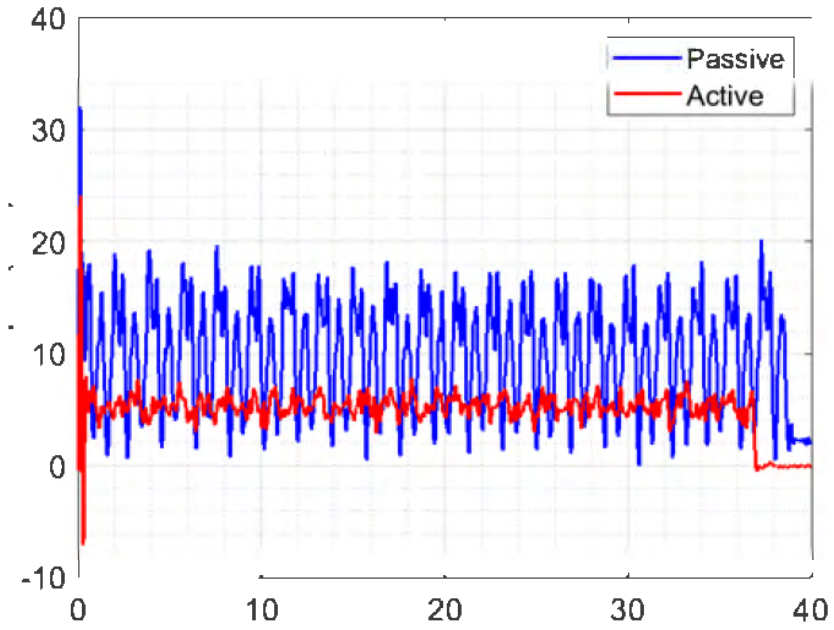


Figure 6-4. The averaged personalized torque provided by the robot during the passive and active phases.

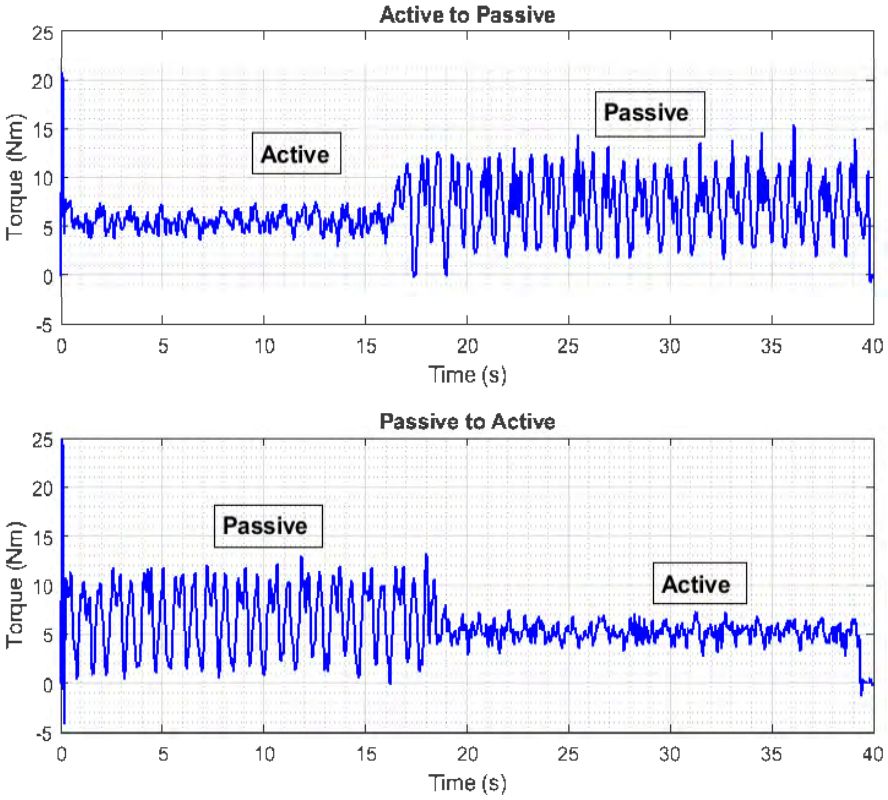


Figure 6-5. The overall torque supplied by the robot during the transition from active to passive and passive to active modes.

Further, the interaction forces that occurred during the active and passive phases are plotted in Figure 6-6.

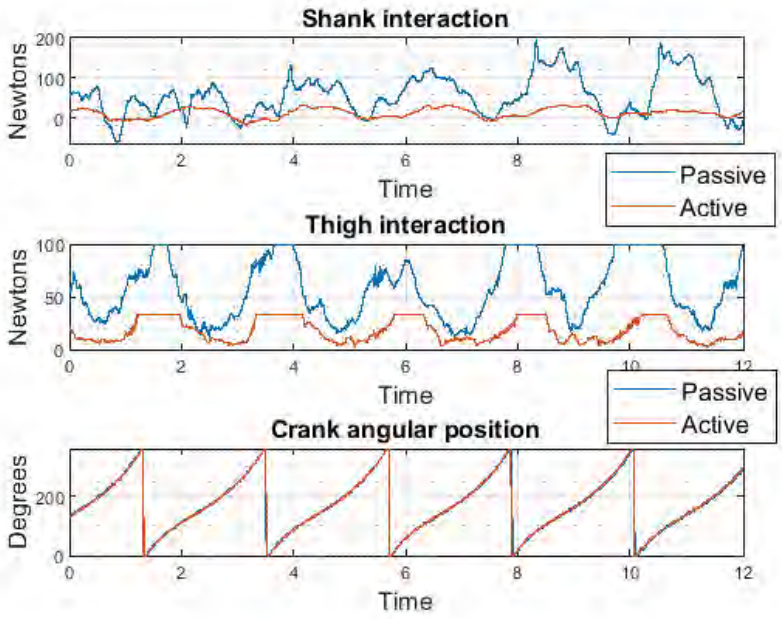


Figure 6-6. The human/robot interaction forces occurring during the passive and active modes.

The interaction forces occurring at the shank and thigh regions of the leg during the passive phase are significantly larger than the interaction forces happening during the active phase. Each spike in the graph representing the crank angular position corresponds to a single gait cycle.

## 6.7 Discussion and Chapter Summary

Gait training therapy using robotic devices is gaining significant attention in the field of rehabilitation engineering as it can help reduce the burden on healthcare systems and replace or complement manual therapy, which requires the constant presence of nurses or physiotherapists. Although due to the high cost of currently available gait rehabilitation robots in the market, many patients may not have access to it and the benefit of saving on labour costs can be diminished. On the other hand, the introduction of simpler designs such as linkage-based mechanisms can drastically reduce the cost of the robots and make it affordable to more patients. Single DOF linkage-based mechanisms can provide the required motion in the sagittal plane for gait rehabilitation using only a single actuator. The gait rehabilitation robots proposed previously based on linkage mechanisms employ only constant speed control. Such control schemes do not consider the interaction force between the human and the robot. Since stroke patients have different levels of disability, directing the legs at a constant speed without any

feedback from the patient's leg may adversely affect the training progress. Therefore, it is critical to consider the force supplied by the patient to the robot to monitor the engagement of the patient in the rehabilitation process. Active engagement of the patient during the training process can enhance and speed up the recovery of the affected lower limb capabilities after stroke [148]. In this work, a patient cooperative control strategy was implemented in the form of impedance learning control applied on a single DOF gait rehabilitation robot which is based on Stephenson III six-bar linkage.

The exploration of the collected data provided an answer to the research question posed in this study: 'Can the robot adapt the assistive torque in active and passive conditions?' Upon analysis, significant differences were noted in the data from both the human-robot interaction forces and the torques supplied by the robot during the active and passive stages. The medians of the interaction forces and torques differed between active and passive modes, with both measures yielding a p-value of less than 0.01. This finding signifies a statistically significant difference in both interaction forces and robot-supplied torques between the two modes.

The maximum absolute values recorded for the interaction forces at shank and thigh regions with standard deviation are presented in Table 6-1.

Table 6-1. Maximum absolute values parameters. Standard Deviations ± are presented for within-subject variability.

| **Parameter** | **Active** | **Passive** | ***p*-Values** |
|---|---|---|---|
| $\boldsymbol{T_{rob}}$ | 21.44 Nm ± 2.86 | 31.96 Nm ± 5.40 | $p < 0.01$ |
| $\boldsymbol{F_{sh}}$ | 38.46 N ± 9.01 | 200.01 N ± 58.21 | $p < 0.01$ |
| $\boldsymbol{F_{th}}$ | 33.33 N ± 9.81 | 100.00 N ± 29.06 | $p < 0.01$ |

The maximum value of $T_{rob}$ provided during active and passive stages of walking is also included in Table 6-1. As can be seen, the motor provides relatively small torque to drive the passive lower limbs of the human along the gait trajectory, which confirms the mechanical advantage of such a type of mechanism. A smaller torque at the input can give the necessary torque at the output. The peak value for the robot's torques is close between the active and passive phases, which indicates the instantaneous torque recorded at the starting point when the robot needs to start the motion from the resting stage. Furthermore, the standard deviation in the active phase is much smaller than in the passive phase.

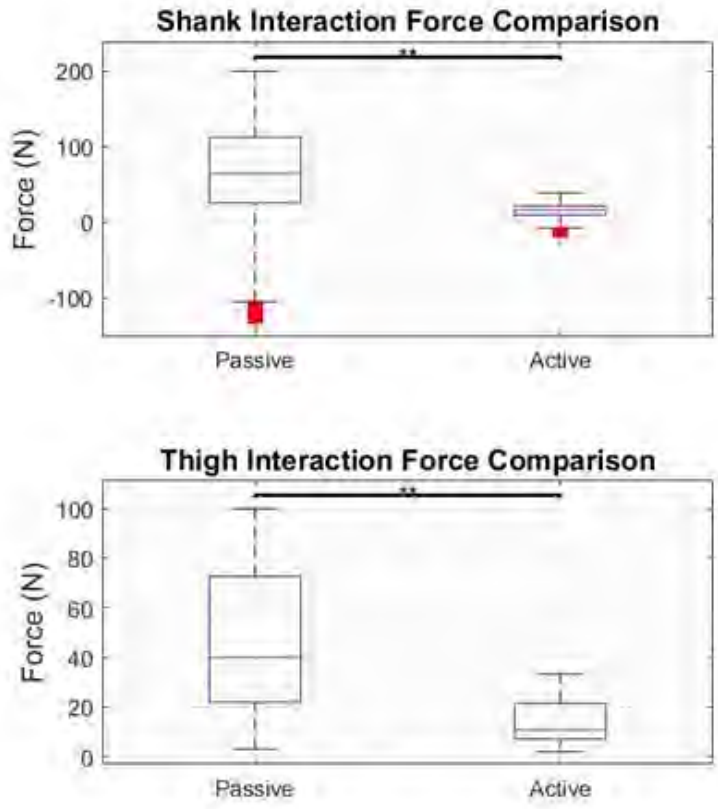


Figure 6-7. Distribution and comparison of human/robot interaction forces occurring at thigh and shank regions during active and passive phases.

Additionally, the boxplots that provide a graphical representation of the shank and thigh parts' interaction forces observed during the passive and active modes have been drawn in Figure 6-7. For the shank interaction forces, the boxplot reveals a distinct difference between the active and passive modes. It can be noticed that the median force in active mode is lower when compared to the passive mode. The interquartile range in active mode appears to be smaller, which means there is a smaller spread of the data. Since, there are few outliers, most of the data are close to the median. Similar trend is observed in boxplot for the thigh interaction forces. However, there is large difference in median forces between the active and passive modes. The active mode has a smaller spread of data, as evidenced by the height of the box. The outliers in this case are few, suggesting that the data is more evenly distributed. This visual representation supports our statistical findings and highlights the significant differences in forces during the two different modes.

In our experiment, two distinct modes of operation were observed - an active mode and a passive mode. We quantified the differences in the mechanical torque generated in these two modes using a set of measurements taken during multiple operational cycles. Our dataset, which

consisted of torque values, was processed using a Butterworth low-pass filter with a cut-off frequency of 100 Hz and a fourth-order response to reduce noise and obtain a smoother signal representation.

The gait rehabilitation robots controlled through impedance control strategies encourages patients to participate actively during the gait training process enabling assist-as-needed training. Active participation and constant effort made by the patient can enhance and increase the recovery speed of the patients. The results demonstrated that the robot could increase or decrease the torque supplied at the crank depending on the torque supplied by the human joints during walking estimated using the machine learning technique. To the authors' best knowledge, no prior work investigated and applied impedance learning control schemes on such types of mechanisms dedicated to gait rehabilitation purposes. Moreover, six-bar linkage-based mechanisms have the mechanical advantage of generating larger torque at the end effector, depending on the length of the crank. The proposed underactuated gait rehabilitation robot with an implemented patient cooperative control strategy does not sacrifice the quality of gait training and could be more affordable for many hospitals and patients around the world than labour-intensive manual therapy.

# Chapter 7. Conclusion

Stroke is a leading cause of disability worldwide [8, 9]. Over half of all stroke survivors experience limb paralysis or hemiplegia, which impairs their locomotion capabilities [15]. Numerous studies have demonstrated that intensive and repetitive gait training therapy can help restore lost lower limb muscular functions [33]. However, conventional manual physical rehabilitation is labour intensive, leading to increased costs for patients. On the other hand, the gait rehabilitation using robotic orthosis offers a promising alternative. This approach can help to restore lost human gait capabilities caused by neurological disorders [40-42]. It can significantly reduce the load on therapists during manual gait training and improve the overall therapeutic process [46-48]. The ability to measure human-robot interaction forces and leg movements during walking with a robotic orthosis introduces a level of objectivity previously missing from manual gait training. This allows for a quantitative assessment of functional motor recovery [23]. Although gait rehabilitation with currently available commercial robotic orthoses has demonstrated its potential to aid in restoring locomotor capabilities, the high cost of these devices renders them unaffordable for many patients worldwide, thus limiting the benefits of robot-based gait rehabilitation. Thus, in this research, a novel and affordable wearable gait rehabilitation orthosis was developed that can provide more naturalistic gait pattern for stroke survivors required for gait rehabilitation. This chapter provides the summary of the primary conclusions drawn from this research and the development of the innovative robot described herein.

## 7.1 Major Outcomes and Contributions

One of the primary outcomes of this research was the conceptualization and realization of a novel wearable bilateral gait rehabilitation orthosis based on the Stephenson III six-bar linkage. The constructed robotic orthosis is lightweight, affordable and can support individualized gait training by providing naturalistic lower limb motions needed for gait rehabilitation. The proposed robotic orthosis due to the use of a smaller number of actuators, is meant to be more affordable without compromising the quality of gait rehabilitation. During the development stage of proof-of-concept prototype several challenges were identified in chapter 3. Determining proper linkage dimensions to satisfy the requirements of two curves simultaneously is a time-consuming process. This process requires solving higher order polynomial equations which sometimes may results in no solution, underscoring the need for application of modern machine learning tools. This challenge was further addressed in chapter

4 by introducing the machine learning framework that is capable of determining optimal linkage dimensions to track two target trajectories. The machine learning framework developed in chapter 4 was used during the linkage dimensional synthesis process led to the naturalistic knee and ankle joint trajectories generation by the robotic orthosis. This proposed framework can also serve as a valuable tool for researchers choosing optimal linkage dimensions during the design stage of linkage-based mechanisms. After finalizing the linkage dimensions, the linkage needed modification to resemble a wearable gait rehabilitation robotic orthosis.

Consequently, the walker was developed to unload the weight of the orthosis from the human subject. A parallelogram mechanism, satisfying the requirements of the trunk's vertical translation during walking, was incorporated into the walker. Additionally, the placement of braces with load cells was designed to measure the human-robot interaction force during the gait training procedure. The passive foot dorsiflexion motion was incorporated using springs at the footplate to ensure smooth foot positioning for stroke patients, addressing the common issue of foot drop among this group [145].

Another challenge revealed was the fluctuating behaviour of the crank's velocity due to the inertia and the possible disturbances that human's leg may have exerted. This issue was addressed in chapter 5 by using machine learning technique. Furthermore, during the gait rehabilitation, it is essential to consider the disability levels of post-stroke patients, as these can differ based on the severity of stroke. Thus, delivering adjusted torque is vital to prevent injuries or damage. A patient-cooperative control strategy, addressing the challenge of robot control to meet patient requirements, was developed, and detailed in chapter 6.

Overall contributions and novelties of the present research work are detailed below:

### 7.1.1 Design of an Underactuated Wearable Gait Rehabilitation Orthosis

1) *Individualized Gait Training*: The optimization of linkage dimensions for individualized gait training that considers both knee and ankle motion generation relative to the hip joint. According to the authors' best knowledge, the knee joint trajectory has not been included previously as the target trajectory during the designing and optimization stage. Integration of additional adjustability of the links' dimensions to match people with different anthropomorphic leg lengths.

2) *Feasibility and Applicability Verification:* A kinematic and dynamic force analysis validated the engineering feasibility of the proposed robotic orthosis. Further validation via a pilot study with a healthy human subject demonstrated its capability to move the legs of a human across the walking trajectory.

3) *Affordability and accessibility:* The proposed robot is convenient to be used owing to its lightweight design. Employing fewer actuators and a simpler control mechanism makes it cost-effective compared to existing commercial orthoses.

### 7.1.2 Mechanism Synthesis Solution for Path Generation

This research makes a significant contribution by creating a novel machine learning framework based on deep generative neural networks. The framework is utilized to synthesize the dimensions of the Stephenson III six-bar linkage to match human walking trajectories. The objective was to identify optimal linkage dimensions that can simultaneously accommodate two distinct lower limb trajectories within a single mechanism - the human knee and ankle joint movements. As a result, the model can produce linkage solutions within acceptable dimension ranges, catering to individuals with different anthropometric parameters and generating their specific gait trajectories. The utilization of a trained neural network for determining linkage dimensions offers real-time efficiency, a marked improvement over traditional methods that consume substantial computational resources. Once the model is trained, there is no need to retrain it to determine new linkage dimensions for different trajectories. This approach benefits designers of linkage-based mechanisms, enabling them to optimize linkage dimensions and adjust parameters to meet individual needs.

### 7.1.3 Velocity Regulation of Stephenson III Six-Bar Linkage Using Deep Reinforcement Learning Control

Our study started with the implementation of a standard PID controller and an assessment of its performance. The results highlighted the PID control's sensitivity to non-linearities and its potential inability to effectively stabilize the crank's velocity. This led to the development of a model-free velocity control scheme using Deep Reinforcement Learning (DRL), which was applied to the robotic orthosis used for gait rehabilitation. The purpose of this controller is to regulate speed fluctuations in the crank of a gait rehabilitation robot, specifically one driven by a servo motor and employing a six-bar linkage mechanism. To the best of the authors' knowledge, this is the first instance of constructing an underactuated robotic gait rehabilitation

orthosis and regulating its velocity using a DRL-based controller. Moreover, the evaluations included interactions with healthy human subjects. As per the experimental results, the actual speed was fluctuating close to the target speed.

### 7.1.4 Patient Cooperative Control based on Impedance Learning to Provide Assist-as-Needed Approach

As mentioned earlier, active human participation is crucial as it can expedite the recovery process of patients and avoid causing an injury to post-stroke patients during the gait rehabilitation. Another significant contribution of the present work is the development of an impedance learning control strategy for a Stephenson III six-bar linkage that operates under the principle of 'assist-as-needed'. This assist-as-needed control is capable of adjusting the assistive torques supplied by the robot in real-time based on the requirements of the patient. Experiments with eight healthy subjects indicated reduced robot torques consequent to an increase in human torque. Results substantiate that customized robotic assistance based on the individual needs of patients can enhance their participation, which is essential to improve the treatment outcomes. This work will also serve as a foundation for building patient-cooperative control strategies for single DOF linkage-based rehabilitation robots. Such control strategies can be useful for stroke patients as the robot's stiffness can be varied meeting the various levels of disability among them.

## 7.2 Work Limitations

One of the limitations of this work is that only one parameter, the location of the motor's placement, is left to be heuristically chosen. This was verified by GIM® software during the dimensional synthesis procedure. However, the designer might choose varying motor's placements instead of joint B during training the model.

Another limitation is that the device has some kinematic constraints as it can only provide assistive motion in the sagittal plane. While this constraint might limit the functional and naturalistic gait training the robot can offer, such constrained movement therapy can be beneficial in the initial stages of rehabilitating paraplegic patients. Nevertheless, in later stages, it's vital to provide motions in other planes.

The treadmill speed remained constant throughout the experiments. There might be a need to adjust the treadmill speed according to the disability level of patients, similar to the method

of automatic treadmill speed adaptation introduced by Zitzewitz et al. [53]. Although the system was tested on a healthy human subject, conducting long-term experiments with stroke patients in a clinical setting is essential to evaluate the robot's effectiveness in post-stroke gait rehabilitation.

And since the aluminum was used to manufacture prototype, it makes the prototype heavier, therefore lighter materials such carbon fiber should be used to reduce the weight of the orthosis.

## 7.3 Suggestions on Future Work

The future work associated with this research includes:

1) Development of Multi DOF Orthosis: To make the prototype more flexible and increase the DOFs to provide assistive movements in multiple planes, which could potentially increase the effectiveness of gait training, and cater to patients with a more diverse range of rehabilitation needs.
2) Lighter material: To reduce the weight of the system even further, lighter materials such as carbon fiber should be used, and topology optimization can be applied to make the exoskeleton lighter and stronger.
3) Extended Training Capabilities: Introducing modifications that enable the robot to be disassembled, allowing for targeted treatment. With such adaptability, the device can train separately the hip, knee or ankle joints, offering a more customized training approach.
4) Clinical Testing with Stroke Patients: After obtaining ethical approval, a larger-scale study will be conducted with stroke patients to evaluate the effectiveness of the orthosis in a clinical setting. This will give us a better understanding of how our orthosis performs in real-world settings.
5) User Engagement: The prototype can be further improved by integrating a graphical user interface (GUI) that includes motivating tasks or games to enhance patient engagement during the therapy process. Active engagement has been shown to be a key factor in effective rehabilitation.
6) Synthesis Method Improvements: The deep generative neural network models can be improved such that different shape of the mechanism can be proposed by the model, which is not constrained with the Stephenson III six-bar linkage mechanism, offering more diverse solutions.

7) Various patient-cooperative control algorithms need to be developed to identify which one will be more optimal for such type of mechanisms during gait rehabilitation process of stroke patients.

## Appendix A. Dynamics Analysis Derivation using Lagrange Modelling.

$$\begin{aligned}\frac{d}{dt}\left(\frac{\partial L}{\partial \dot{\theta}}\right) = 2\big(&J_0 + J_1 S_1^2(\theta,\alpha_2,\beta_2) + J_3 S_3^2(\theta,\alpha_3,\beta_3) + J_5 S_5^2(\theta,\beta,\gamma) + J_6 S_6^2(\theta,\alpha_1,\beta_1)\\ &+ M_1 S_2^2(\theta,\gamma) + M_2 S_7^2(\theta,\gamma) + P_1 C_1(\theta_1,\gamma_2) S_8(\theta,\alpha_2,\beta_2,\alpha_3)\\ &+ P_6 C_6(\theta,\gamma_6) S_9(\theta,\alpha_1)\big)\ddot{\theta}\\ &+ 2\Bigg[2J_1 S_1(\theta,\alpha_2,\beta_2)\left(\frac{\partial S_1(\theta,\alpha_2,\beta_2)}{\partial\theta} + \frac{\partial S_1(\theta,\alpha_2,\beta_2)}{\partial\alpha_2}\frac{\partial\alpha_2}{\partial\theta}\right.\\ &\left. + \frac{\partial S_1(\theta,\alpha_2,\beta_2)}{\partial\beta_2}\frac{\partial\beta_2}{\partial\theta}\right)\\ &+ 2J_3 S_3(\theta,\alpha_3,\beta_3)\left(\frac{\partial S_3(\theta,\alpha_3,\beta_3)}{\partial\theta} + \frac{\partial S_3(\theta,\alpha_3,\beta_3)}{\partial\alpha_3}\frac{\partial\alpha_3}{\partial\theta}\right.\\ &\left. + \frac{\partial S_3(\theta,\alpha_3,\beta_3)}{\partial\beta_3}\frac{\partial\beta_3}{\partial\theta}\right)\\ &+ 2J_5 S_5(\theta,\beta,\gamma)\left(\frac{\partial S_5(\theta,\beta,\gamma)}{\partial\theta} + \frac{\partial S_5(\theta,\beta,\gamma)}{\partial\,\beta}\frac{\partial\,\beta}{\partial\theta} + \frac{\partial S_5(\theta,\beta,\gamma)}{\partial\gamma}\frac{\partial\gamma}{\partial\theta}\right)\\ &+ 2J_6 S_6(\theta,\alpha_1,\beta_1)\left(\frac{\partial S_6(\theta,\alpha_1,\beta_1)}{\partial\theta} + \frac{\partial S_6(\theta,\alpha_1,\beta_1)}{\partial\alpha_1}\frac{\partial\alpha_1}{\partial\theta} + \frac{\partial S_6(\theta,\alpha_1,\beta_1)}{\partial\beta_1}\frac{\partial\beta_1}{\partial\theta}\right)\\ &+ 2M_1 S_2(\theta,\gamma)\left(\frac{\partial S_2(\theta,\gamma)}{\partial\theta} + \frac{\partial S_2(\theta,\gamma)}{\partial\gamma}\frac{\partial\gamma}{\partial\theta}\right)\\ &+ 2M_2 S_7(\theta,\gamma)\left(\frac{\partial S_7(\theta,\gamma)}{\partial\theta} + \frac{\partial S_7(\theta,\gamma)}{\partial\gamma}\frac{\partial\gamma}{\partial\theta}\right)\\ &+ P_1\Bigg(C_1(\theta_1,\gamma_2)\left(\frac{\partial S_8(\theta,\alpha_2,\beta_2,\alpha_3)}{\partial\theta} + \frac{\partial S_8(\theta,\alpha_2,\beta_2,\alpha_3)}{\partial\alpha_2}\frac{\partial\alpha_2}{\partial\theta}\right.\\ &\left. + \frac{\partial S_8(\theta,\alpha_2,\beta_2,\alpha_3)}{\partial\beta_2}\frac{\partial\beta_2}{\partial\theta} + \frac{\partial S_8(\theta,\alpha_2,\beta_2,\alpha_3)}{\partial\alpha_3}\frac{\partial\alpha_3}{\partial\theta}\right)\\ &+ S_8(\theta,\alpha_2,\beta_2,\alpha_3)\left(\frac{\partial C_1(\theta_1,\gamma_2)}{\partial\theta_1}\frac{\partial\theta_1}{\partial\theta} + \frac{\partial C_1(\theta_1,\gamma_2)}{\partial\gamma_2}\frac{\partial\gamma_2}{\partial\theta}\right)\Bigg)\\ &+ P_6\Bigg(C_6(\theta,\gamma_6)\left(\frac{\partial S_9(\theta,\alpha_1)}{\partial\theta} + \frac{\partial S_9(\theta,\alpha_1)}{\partial\alpha_1}\frac{\partial\alpha_1}{\partial\theta}\right)\\ &+ S_9(\theta,\alpha_1)\left(\frac{\partial C_6(\theta,\gamma_6)}{\partial\theta} + \frac{\partial C_6(\theta,\gamma_6)}{\partial\gamma_6}\frac{\partial\gamma_6}{\partial\theta}\right)\Bigg)\Bigg]\dot{\theta}^2\end{aligned} \tag{A.1}$$

Appendix A. Dynamics Analysis Derivation using Lagrange Modelling.

$$\frac{\partial L}{\partial \theta} = \Bigg[ 2J_1 S_1(\theta,\alpha_2,\beta_2)\left(\frac{\partial S_1(\theta,\alpha_2,\beta_2)}{\partial \theta} + \frac{\partial S_1(\theta,\alpha_2,\beta_2)}{\partial \alpha_2}\frac{\partial \alpha_2}{\partial \theta} + \frac{\partial S_1(\theta,\alpha_2,\beta_2)}{\partial \beta_2}\frac{\partial \beta_2}{\partial \theta}\right)$$
$$+ 2J_3 S_3(\theta,\alpha_3,\beta_3)\left(\frac{\partial S_3(\theta,\alpha_3,\beta_3)}{\partial \theta} + \frac{\partial S_3(\theta,\alpha_3,\beta_3)}{\partial \alpha_3}\frac{\partial \alpha_3}{\partial \theta}\right.$$
$$\left. + \frac{\partial S_3(\theta,\alpha_3,\beta_3)}{\partial \beta_3}\frac{\partial \beta_3}{\partial \theta}\right)$$
$$+ 2J_5 S_5(\theta,\beta,\gamma)\left(\frac{\partial S_5(\theta,\beta,\gamma)}{\partial \theta} + \frac{\partial S_5(\theta,\beta,\gamma)}{\partial\, \beta}\frac{\partial\, \beta}{\partial \theta} + \frac{\partial S_5(\theta,\beta,\gamma)}{\partial \gamma}\frac{\partial \gamma}{\partial \theta}\right)$$
$$+ 2J_6 S_6(\theta,\alpha_1,\beta_1)\left(\frac{\partial S_6(\theta,\alpha_1,\beta_1)}{\partial \theta} + \frac{\partial S_6(\theta,\alpha_1,\beta_1)}{\partial \alpha_1}\frac{\partial \alpha_1}{\partial \theta} + \frac{\partial S_6(\theta,\alpha_1,\beta_1)}{\partial \beta_1}\frac{\partial \beta_1}{\partial \theta}\right)$$
$$+ 2M_1 S_2(\theta,\gamma)\left(\frac{\partial S_2(\theta,\gamma)}{\partial \theta} + \frac{\partial S_2(\theta,\gamma)}{\partial \gamma}\frac{\partial \gamma}{\partial \theta}\right)$$
$$+ 2M_2 S_7(\theta,\gamma)\left(\frac{\partial S_7(\theta,\gamma)}{\partial \theta} + \frac{\partial S_7(\theta,\gamma)}{\partial \gamma}\frac{\partial \gamma}{\partial \theta}\right)$$
$$+ P_1\left(C_1(\theta_1,\gamma_2)\left(\frac{\partial S_8(\theta,\alpha_2,\beta_2,\alpha_3)}{\partial \theta} + \frac{\partial S_8(\theta,\alpha_2,\beta_2,\alpha_3)}{\partial \alpha_2}\frac{\partial \alpha_2}{\partial \theta}\right.\right.$$
$$\left. + \frac{\partial S_8(\theta,\alpha_2,\beta_2,\alpha_3)}{\partial \beta_2}\frac{\partial \beta_2}{\partial \theta} + \frac{\partial S_8(\theta,\alpha_2,\beta_2,\alpha_3)}{\partial \alpha_3}\frac{\partial \alpha_3}{\partial \theta}\right)$$
$$\left. + S_8(\theta,\alpha_2,\beta_2,\alpha_3)\left(\frac{\partial C_1(\theta_1,\gamma_2)}{\partial \theta_1}\frac{\partial \theta_1}{\partial \theta} + \frac{\partial C_1(\theta_1,\gamma_2)}{\partial \gamma_2}\frac{\partial \gamma_2}{\partial \theta}\right)\right)$$
$$+ P_6\left(C_6(\theta,\gamma_6)\left(\frac{\partial S_9(\theta,\alpha_1)}{\partial \theta} + \frac{\partial S_9(\theta,\alpha_1)}{\partial \alpha_1}\frac{\partial \alpha_1}{\partial \theta}\right)\right.$$
$$\left. + S_9(\theta,\alpha_1)\left(\frac{\partial C_6(\theta,\gamma_6)}{\partial \theta} + \frac{\partial C_6(\theta,\gamma_6)}{\partial \gamma_6}\frac{\partial \gamma_6}{\partial \theta}\right)\right)\Bigg]\dot{\theta}^2 + \frac{\partial G(\Theta_1,\Theta_5,\Theta_6,\Theta,\gamma_2)}{\partial \theta}$$
$$+ \frac{\partial G(\Theta_1,\Theta_5,\Theta_6,\Theta,\gamma_2)}{\partial \Theta_1}\frac{\partial \theta_1}{\partial \theta} + \frac{\partial G(\Theta_1,\Theta_5,\Theta_6,\Theta,\gamma_2)}{\partial \Theta_5}\frac{\partial \theta_5}{\partial \theta}$$
$$+ \frac{\partial G(\Theta_1,\Theta_5,\Theta_6,\Theta,\gamma_2)}{\partial \Theta_6}\frac{\partial \theta_6}{\partial \theta} + \frac{\partial G(\Theta_1,\Theta_5,\Theta_6,\Theta,\gamma_2)}{\partial \gamma_2}\frac{\partial \gamma_2}{\partial \theta} \tag{A.2}$$

# Appendix B. Participant's Consent Form


Faculty of Science & Technology

University of Canberra

Bruce, ACT – 2617

Australia

**CONSENT FORM**

**(Participants)**

**THIS FORM WILL BE HELD FOR A PERIOD OF 5 YEARS**

Project title: Underactuated Exoskeleton for Walking Rehabilitation

Name(s) of Researchers(s): Akim Kapsalyamov, Assoc Prof. Shahid Hussain, Prof. Nick Brown, Prof. Roland Goecke

I have read the Participant Information Sheet; have understood the nature of the research and why I have been selected. I have had the opportunity to ask questions and have them answered to my satisfaction. I have chosen to participate in this research on a voluntary basis.

- I agree to take part in this research study
- I understand that participation in this research will require physical interaction with a prototype robotic device. My legs will be guided in a walking trajectory by the device, which has been explained to me.
- I understand that there is a slight possibility of injury should the prototype device malfunction, and I accept this risk. I can also press the emergency stop button, which has been shown to me.
- I understand that my identity will not be revealed in publications derived from this research.
- I understand that the information related to the experimental trial in which I am involved will be recorded using sensors on the prototype device and stored electronically with secure access.
- I understand that the data collected will be kept for a period of up to five years as reference for current and possibly future research, but not beyond five years
- I understand that I am free to withdraw my participation at any time.
- I understand that participation in this research study will not affect my grades or my relations with the university (where applicable).
- I agree/do not agree to be video recorded.
- I understand that the data will be kept for five years, after which they will be destroyed.
- I understand that I am only required to attend one 45-minute experimental trial.
- I agree to be informed of any incidental findings that arise from this research.

Name _____

Signature _____ Date _____

# Appendix C. Participant Information Sheet

Faculty of Science & Technology
University of Canberra
Bruce, ACT - 2617

**PARTICIPANT INFORMATION SHEET**
**(Participants)**

Project title: Underactuated Exoskeleton for Walking Rehabilitation
Name(s) of Researchers(s): Akim Kapsalyamov, Assoc Prof. Shahid Hussain, Prof. Nick Brown, Prof. Roland Goecke

**Researcher Introduction**

This research study will be conducted by Akim Kapsalyamov, a Ph.D. student at the Faculty of Science & Technology. The research is supervised by Dr. Shahid Hussain, an Associate Professor in the Faculty of Science & Technology, Dr. Nick Brown, a Professor in the Faculty of Health and Dr. Roland Goecke, a Professor in the Faculty of Science & Technology

**Project Description and Invitation**

This project aims to test a developed underactuated robotic exoskeleton designed to facilitate gait rehabilitation with implemented assist-as-needed control. The exoskeleton is intended for use with patients suffering from musculoskeletal injuries or neurological conditions, which impair lower limb functions. In particular, the part of the research where human participation is required is designed to evaluate the performance of the developed prototype.

You are invited to participate in this research study by carrying out a series of exercises using a prototype of a newly designed gait rehabilitation device. Potential participants in this research study are chosen from colleagues of the researcher who are healthy individuals over the age of 18 years and have no existing neurological impairment, as assessed by general practitioner. You will be shown the experimental setup and briefed about the operation of the prototype before your commitment to participation in this research. Your identity will be kept anonymous from third parties.

**Project Procedures**

You will only be required to take part in one experimental trial. The duration of the trial is expected to span approximately 45 minutes. The experimental trial will be carried out in the Rehabilitation Engineering Research Laboratory at the University of Canberra.

Before the experimental trial begins, the operation of the robotic device will be explained to you, as well as the safety measures put in place to allow the immediate termination of the robot operation should an emergency arise. A brief demonstration of the prototype will also be given. Your age in 5-year age brackets, biological sex and body weight will also be collected so that the results can be normalized with respect to the body weight and related to the corresponding demographic groups.

Prior to the start of the experiment, you will be asked to perform usual walking for about a minute on a treadmill. The researcher will visually assess the walking of participant in terms of balance and coordination of legs to check if you can further participate in this experiment. After the briefing, acquaintance with the whole procedure steps and obtaining informed consent, you will be asked to stand on a treadmill while you will be securely fastened to the Body Weight Support system BIODEX across shoulders and chest to unload your weight. Then, the exoskeleton will be brought and attached on either side of the leg in thigh and tibia regions. Your foot will be strapped to the foot plate of the exoskeleton.

The experimental trial consists of two parts, the first involves the passive movement of the legs by the robotic device. During this part of the trial, you should relax your lower limbs on the robotic device and allow the robot to move the legs passively along a predefined motion path which is similar to normal human walking. During this time, information regarding the position of the foot and the forces exerted by legs on the exoskeleton will be logged and analysed.

In the second part of the trial, you will be asked to move your legs in a direction of usual walking. The robot will provide a small resistance against the motion during this part of the trial. Again, sensor information on the robotic device will be logged and analysed. This part of the trial will allow determination of the active forces applied by the legs to the robot.

You may experience a small level of physical discomfort during a normal trial when the exoskeleton tries to move your legs. However, you can communicate to the researcher about any discomforts you are experiencing at any time of the experiment to reduce them, should the level of discomfort exceed that of the participant’s liking. You can terminate the experimental trial by either indicating to the researcher or by using the emergency stop button provided. The prototype’s range of motions has physical restrictions; therefore, it will not go beyond naturalistic lower limb motions. Moreover, the motor can provide maximum of 60 Nm which is much less than the anatomically applied lower limb forces during walking. Prototype would be tested extensively before the commencement of the experimental trial with dummy legs. In addition to that, the primary researcher will be present to assist and stop the system if required. Along with the researcher, Mr. Jamie Plowman,

the Laboratory engineer will be present during the experiment procedure. He is also a certified first aid officer. To ensure that prompt medical attention is available during emergencies, the trials will be conducted during the operating hours of the University of Canberra Health Clinics from 9 AM to 4 Pm.

**Data Storage/ Retention/ Destruction/ Future Use**

As discussed in the previous section, data collected will be in the form of sensor readings which are used to compute the motion and force/moment observed during the experimental trial. This information will also be used to identify and analyze properties of the participant's lower limb. Additionally, your age, biological sex and body weight will also be recorded. New RedBox research data system of University of Canberra will be used for secure storage and backup of the data, which satisfies the requirements of University of Canberra policy and most research funder requirements. Moreover, the data will be stored in such a way that a third party will not be able to identify the participant through the information stored on the data file, since no personal identifiers in terms of name, ID or others personal details will be stored. The data will be available only to researchers affiliated with this study as shown in the list of researchers above. The information collected will be kept for a period of up to five years as reference for current and possibly future research. The data can be used for future projects but not beyond five years. When no longer required, such data files will be destroyed through permanent deletion. If you are interested, you can also arrange a suitable time with the lead researcher to discuss any information derived from offline analysis of the collected data.

With your permission, a photograph/video of the experimental trial may also be taken using an electronic device. The photograph/video of the trial will also be stored electronically on a RedBox research data system of University of Canberra. The video will record only your lower limbs so that it can't be used to reveal your identity.

**Right to Withdraw from Participation**

You may withdraw from participation at any time. You can also withdraw your data from the research study till 3 months from the date of the experiment.

**Anonymity and Confidentiality**

Your identity will be kept anonymous from all third parties. If the data collected is used in publications, you will be referred to using a generic identifier such as "subject A".

Participation in this research is entirely voluntary and it will not affect either your grades or your relations with the university.

**Incidental Findings**

There is a small chance where anomaly may be found in the data collected regarding the characteristics of your legs. Should this occur, you will be informed and should consult a qualified health professional to verify such findings.

**Funding**

Funding has been obtained for this research study. The Faculty of Science and Technology, University of Canberra has provided the required funding of A$6,000 for this research.

**Contact Details and Approval Wording**

Researcher:
Akim Kapsalyamov
Email: u3211406@uni.canberra.edu.au

Supervisor:
Assoc. Prof. Shahid Hussain
Email: Shahid.Hussain@canberra.edu.au
Phone: +61 2 62068408

Co-supervisor:
Prof. Nick Brown
Email: Nick.Brown@canberra.edu.au
Phone: +61 2 62068415

Co-supervisor:
Prof. Roland Goecke
Email: Roland.Goecke@canberra.edu.au
Phone: +61 2 62012114

# Appendix D. Publications and Submissions

The following journal publications have resulted from the research presented within this thesis:

1) **Akim Kapsalyamov**, Shahid Hussain, Nicholas A.T. Brown, Roland Goecke, Munawar Hayat, Prashant K. Jamwal. "*Synthesis of a six-bar mechanism for generating knee and ankle motion trajectories using deep generative neural network*". Engineering Applications of Artificial Intelligence. Volume 117, Part A. 2023,105500, ISSN 0952-1976, https://doi.org/10.1016/j.engappai.2022.105500.

**The material from this manuscript was used to write chapter 4 and partially chapter 3.**

2) **Akim Kapsalyamov**, Shahid Hussain, Nicholas A.T. Brown, Roland Goecke, Prashant K. Jamwal. "*A Novel Underactuated Robotic Orthosis for Individualized Gait Rehabilitation*," in IEEE Transactions on Medical Robotics and Bionics, doi: 10.1109/TMRB.2023.3328633.

**Chapter 3 is written based on the material from this manuscript.**

3) **Akim Kapsalyamov**, Shahid Hussain, Nicholas A.T. Brown, Roland Goecke, Prashant K. Jamwal. "*Design and Velocity Control of an Underactuated Gait Rehabilitation Robot Using Deep Reinforcement Learning*". IEEE Transactions on Human-Machine Systems. (**Under review after major Revision)**

**Whole chapter 5 is written based on the material from this manuscript.**

4) **Akim Kapsalyamov**, Shahid Hussain, Nicholas A.T. Brown, Roland Goecke, Prashant K. Jamwal and Sunil K. Agrawal. "*Stiffness Tuning-Based Control of a Six-Bar Linkage Gait Rehabilitation Robot: A Step Towards Effective Gait Rehabilitation*". IEEE Transactions on Medical Robotics and Bionics. **(Submitted on October 29, 2023, Under review)**

**Whole chapter 6 is written based on the material from this manuscript**.

# Appendix E. Bill of Materials

| Vendor name | Vendor details | Web | Parts |
|---|---|---|---|
| Ases | Unit 8, 5-7 Wiltshire Street, MINTO, NSW, 2566, Australia | https://www.ases.co/ | Dspace MicroLabBox |
| Element14 | 77 Castlereagh Street, Sydney, NSW 2000, Australia | https://au.element14.com/ | VISHAY, Rotary potentiometer 157S102MX |
| Metromatics Pty Ltd | NSW – 5/21 Kinghorne Street, Nowra NSW 2541 | http://www.metromatics.com.au/ | Futek Load Cell (Miniature/Inline Threaded)/ 50kg, Tension & Compression |
| Alucom | 156-158 Gladstone Street, Fyshwick ACT 2609 | https://www.alucom.com.au/ | Aluminum sheet |
| Biodex | 49Natcon DriveShirley, New York 11967-4704 | Biodex.com | Biodex Rehabilitation Treadmill, body weight support |
| Maytec | 8/175 James Ruse Dr, Rosehill NSW 2142 | https://maytec.net.au/ | Aluminum frame profile |
| MotionDynamics | Unit 12, 6-8 Allen Place, Wetherill Park NSW 2164 | https://www.motiondynamics.com.au/ | Brushless DC motors |
| Bunnings | Australia | https://www.bunnings.com.au/ | Springs, bearings, bolts, resistors, nuts, fasteners, washers, etc. |
| Jaycar | Australia | https://www.jaycar.com.au/ | BNC Connectors, 20m RG174U cable, Veroboard, Motor power cable |
| RS electronics | Australia | https://au.rs-online.com/web | INA126 Instrumentation Amp |
| Element14 | 77 Castlereagh Street, Sydney, NSW 2000, Australia | https://au.element14.com/ | Quick disconnect terminal, 10k trimpot, +/- 12V power supply, M205 1.25A fuse, power switch, etc. |

All the assembly and machining of the parts have been done at the machine shop at the University of Canberra.

# Appendix E. Bill of Materials

## Reference


1. Riener, R., et al., *Patient-Cooperative Strategies for Robot-Aided Treadmill Training: First Experimental Results.* IEEE transactions on neural systems and rehabilitation engineering : a publication of the IEEE Engineering in Medicine and Biology Society, 2005. **13**: p. 380-94.
2. Schaechter, J.D., *Motor rehabilitation and brain plasticity after hemiparetic stroke.* . Progress in neurobiology, 2004. **73**: p. 61-72.
3. D. G. de Sousa, et al., *Interventions involving repetitive practice improve strength after stroke: a systematic review.* J Physiother, 2018. **64**(4): p. 210-221.
4. Veerbeek, J.M., et al., *What is the evidence for physical therapy poststroke? A systematic review and meta-analysis.* PloS one, 2014. **9**(2): p. e87987-e87987.
5. Louie, D.R. and J.J. Eng, *Powered robotic exoskeletons in post-stroke rehabilitation of gait: a scoping review.* Journal of NeuroEngineering and Rehabilitation, 2016. **13**(1): p. 53.
6. *What is Stroke?* The National Heart, Lung, and Blood Institute (NHLBI), www.nhlbi.nih.gov, Retrieved on 18 December 2018.
7. Smith, W.S., et al., *Ischemic Stroke*, in *Harrison's Principles of Internal Medicine, 20e*. 2018, McGraw-Hill Education: New York, NY.
8. Feigin, V.L., B. Norrving, and G.A. Mensah, *Global Burden of Stroke.* Circulation Research, 2017. **120**(3): p. 439-448.
9. He, Q., et al., *Trends in in-hospital mortality among patients with stroke in China.* PLoS One, 2014. **9**(3): p. e92763.
10. *Stroke - Brain Foundation. (2020). Retrieved 18 March 2020, from https://brainfoundation.org.au/disorders/stroke/.*
11. *Deloitte Access Economics – Stroke in Australia – No postcode untouched, 2017.*
12. *Deloitte Access Economics. The economic impact of stroke in Australia, 2013.*
13. Benjamin Ej Fau - Blaha, M.J., et al., *Heart Disease and Stroke Statistics-2017 Update: A Report From the American Heart Association.* (1524-4539 (Electronic)).
14. Duncan Pw Fau - Zorowitz, R., et al., *Management of Adult Stroke Rehabilitation Care: a clinical practice guideline.* (1524-4628 (Electronic)).
15. Johnson, W., et al., *Stroke: a global response is needed.* Bull World Health Organ, 2016. **94**(9): p. 634-634a.
16. Guzik, A., et al., *Validity of the gait variability index for individuals after a stroke in a chronic stage of recovery.* Gait and Posture, 2019. **68**: p. 63-67.
17. Olney, S.J. and C. Richards, *Hemiparetic gait following stroke. Part I: Characteristics.* 1996. **4**(2): p. 136-148.
18. Richards, C.L. and S.J. Olney, *Hemiparetic gait following stroke. Part II: Recovery and physical therapy.* 1996. **4**(2): p. 149-162.
19. Dobkin, B.H., *Clinical practice. Rehabilitation after stroke.* (1533-4406 (Electronic)).
20. Batchelor, F.A., et al., *Falls after stroke.* (1747-4949 (Electronic)).
21. Rodda, J.M., et al., *Sagittal gait patterns in spastic diplegia.* . J Bone Joint Surg, 2004. **86**: p. 251-258.
22. Hussain, S., G. Xie Sq Fau - Liu, and G. Liu, *Robot assisted treadmill training: mechanisms and training strategies.* (1873-4030 (Electronic)).
23. Reinkensmeyer, D.J., S.C. Emken Jl Fau - Cramer, and S.C. Cramer, *Robotics, motor learning, and neurologic recovery.* (1523-9829 (Print)).
24. Paolucci, S., et al., *Quantification of the probability of reaching mobility independence at discharge from a rehabilitation hospital in nonwalking early ischemic stroke patients: a multivariate study.* Cerebrovasc Dis, 2008. **26**(1): p. 16-22.

25. Hebert, D., et al., *Canadian stroke best practice recommendations: Stroke rehabilitation practice guidelines, update 2015.* Int J Stroke, 2016. **11**(4): p. 459-84.
26. *OpenStax, Anatomy & Physiology. OpenStax CNX. 2016* http://cnx.org/contents/14fb4ad7-39a1-4eee-ab6e-3ef2482e3e22@8.24.
27. Richards, J., A. Chohan, and R. Erande, *Biomechanics.* Tidy's Physiotherapy: Fifteenth Edition, 2013: p. 331-368.
28. Behrman, A.L. and S.J. Harkema, *Locomotor training after human spinal cord injury: a series of case studies.* (0031-9023 (Print)).
29. Laufer, Y., et al., *The effect of treadmill training on the ambulation of stroke survivors in the early stages of rehabilitation: a randomized study.* (0748-7711 (Print)).
30. Teixeira da Cunha Filho, I., et al., *A comparison of regular rehabilitation and regular rehabilitation with supported treadmill ambulation training for acute stroke patients.* (0748-7711 (Print)).
31. Murray Mp Fau - Spurr, G.B., et al., *Treadmill vs. floor walking: kinematics, electromyogram, and heart rate.* (8750-7587 (Print)).
32. Hassid, E., et al., *Improved Gait Symmetry in Hemiparetic Stroke Patients Induced During Body Weight-Supported Treadmill Stepping.* Journal of Neurologic Rehabilitation, 1997. **11**(1): p. 21-26.
33. Pohl, M., et al., *Repetitive locomotor training and physiotherapy improve walking and basic activities of daily living after stroke: a single-blind, randomized multicentre trial (DEutsche GAngtrainerStudie, DEGAS).* Clinical Rehabilitation, 2007. **21**(1): p. 17-27.
34. Visintin, M., et al., *A new approach to retrain gait in stroke patients through body weight support and treadmill stimulation.* (0039-2499 (Print)).
35. Hesse, S., et al., *Treadmill training with partial body weight support compared with physiotherapy in nonambulatory hemiparetic patients.* (0039-2499 (Print)).
36. Patterson, S.L., et al., *Effect of treadmill exercise training on spatial and temporal gait parameters in subjects with chronic stroke: a preliminary report.* (1938-1352 (Electronic)).
37. McCain, K.J., et al., *Locomotor treadmill training with partial body-weight support before overground gait in adults with acute stroke: a pilot study.* (1532-821X (Electronic)).
38. Colombo, G., et al., *Treadmill training of paraplegic patients using a robotic orthosis.* (0748-7711 (Print)).
39. Callegaro, A.M., et al., *Robotic Systems for Gait Rehabilitation*. 2014, Springer Netherlands: Dordrecht. p. 265-283.
40. von Schroeder, H.P., et al., *Gait parameters following stroke: a practical assessment.* (0748-7711 (Print)).
41. Dean, C.M., F. Richards Cl Fau - Malouin, and F. Malouin, *Walking speed over 10 metres overestimates locomotor capacity after stroke.* (0269-2155 (Print)).
42. Sanjeevi, N.S.S., Y. Singh, and V. Vashista, *Recent advances in lower-extremity exoskeletons in promoting performance restoration.* 2021. **20**: p. 100338.
43. Alamdari, A. and V. Krovi, *A Review of Computational Musculoskeletal Analysis of Human Lower Extremities*. 2016.
44. Young, A.J. and D.P. Ferris, *State of the Art and Future Directions for Lower Limb Robotic Exoskeletons.* IEEE Transactions on Neural Systems and Rehabilitation Engineering, 2017. **25**(2): p. 171-182.
45. Cao, J., et al., *Control strategies for effective robot assisted gait rehabilitation: The state of art and future prospects.* Medical Engineering & Physics, 2014. **36**(12): p. 1555-1566.

46. Gelderblom, G.J., et al. *Rehabilitation robotics in robotics for healthcare; A roadmap study for the European Commission*. in *2009 IEEE International Conference on Rehabilitation Robotics*. 2009.
47. Van Peppen, R.P., et al., *The impact of physical therapy on functional outcomes after stroke: what's the evidence?* Clin Rehabil, 2004. **18**(8): p. 833-62.
48. Cramer, S.C. and J.D. Riley, *Neuroplasticity and brain repair after stroke.* Curr Opin Neurol, 2008. **21**(1): p. 76-82.
49. Hobbs, B. and P. Artemiadis, *A Review of Robot-Assisted Lower-Limb Stroke Therapy: Unexplored Paths and Future Directions in Gait Rehabilitation.* Frontiers in Neurorobotics, 2020. **14**(19).
50. Riener, R., et al., *Locomotor Training in Subjects with Sensori-Motor Deficits: An Overview of the Robotic Gait Orthosis Lokomat.* Journal of Healthcare Engineering, 2010. **1**: p. 517674.
51. N, M., *Place and Possibilities of the Robotic System Lokomat in the Rehabilitation of Patients After Ischemic Stroke.* Biomedical and Pharmacology Journal, 2019. **11**: p. 131-140.
52. Hocoma. *Lokomat Technical Datasheet*. 2023 [cited 2023 20.07.2023]; Available from: https://www.hocoma.com/solutions/lokomat/techincal-data-sheet/.
53. von Zitzewitz, J., R. Bernhardt M Fau - Riener, and R. Riener, *A novel method for automatic treadmill speed adaptation.* (1534-4320 (Print)).
54. Mantone, J., *Getting a leg up? Rehab patients get an assist from devices such as HealthSouth's AutoAmbulator, but the robots' clinical benefits are still in doubt.* Mod Healthc, 2006. **36**(7): p. 58-60.
55. Freivogel, S., et al., *Gait training with the newly developed 'LokoHelp'-system is feasible for non-ambulatory patients after stroke, spinal cord and brain injury. A feasibility study.* Brain Inj, 2008. **22**(7-8): p. 625-32.
56. Zeilig, G., et al., *Safety and tolerance of the ReWalk™ exoskeleton suit for ambulation by people with complete spinal cord injury: a pilot study.* J Spinal Cord Med, 2012. **35**(2): p. 96-101.
57. Esquenazi, A., et al., *The ReWalk powered exoskeleton to restore ambulatory function to individuals with thoracic-level motor-complete spinal cord injury.* Am J Phys Med Rehabil, 2012. **91**(11): p. 911-21.
58. Fineberg, D.B., et al., *Vertical ground reaction force-based analysis of powered exoskeleton-assisted walking in persons with motor-complete paraplegia.* J Spinal Cord Med, 2013. **36**(4): p. 313-21.
59. Aach, M., et al., *Voluntary driven exoskeleton as a new tool for rehabilitation in chronic spinal cord injury: a pilot study.* Spine J, 2014. **14**(12): p. 2847-53.
60. al., A.M.e., *Exoskeletal Neuro-Rehabilitation in Chronic Paraplegic Patients – Initial Results.* Pons J., Torricelli D., Pajaro M. (eds) Converging Clinical and Engineering Research on Neurorehabilitation. Biosystems & Biorobotics, 2013. **1**.
61. Sczesny-Kaiser, M., et al., *Neurorehabilitation in Chronic Paraplegic Patients with the HAL® Exoskeleton – Preliminary Electrophysiological and fMRI Data of a Pilot Study*. 2013. p. 611-615.
62. Maeshima, S., et al., *Efficacy of a hybrid assistive limb in post-stroke hemiplegic patients: a preliminary report.* BMC Neurology, 2011. **11**(1): p. 116.
63. Nilsson, A., et al., *Gait training early after stroke with a new exoskeleton--the hybrid assistive limb: a study of safety and feasibility.* J Neuroeng Rehabil, 2014. **11**: p. 92.
64. Veneman, J.F., et al., *Design and Evaluation of the LOPES Exoskeleton Robot for Interactive Gait Rehabilitation.* IEEE Transactions on Neural Systems and Rehabilitation Engineering, 2007. **15**(3): p. 379-386.

65. De Rossi, S.M., et al., *Sensing pressure distribution on a lower-limb exoskeleton physical human-machine interface.* (1424-8220 (Electronic)).
66. Meuleman, J., et al., *LOPES II—Design and Evaluation of an Admittance Controlled Gait Training Robot With Shadow-Leg Approach.* IEEE Transactions on Neural Systems and Rehabilitation Engineering, 2016. **24**(3): p. 352-363.
67. Banala, S.K., et al., *Robot Assisted Gait Training With Active Leg Exoskeleton (ALEX).* IEEE Transactions on Neural Systems and Rehabilitation Engineering, 2009. **17**(1): p. 2-8.
68. Guo, Z., H. Yu, and Y.H. Yin, *Developing a Mobile Lower Limb Robotic Exoskeleton for Gait Rehabilitation.* Journal of Medical Devices, 2014. **8**(4).
69. Emken, J.L., et al., *Feasibility of Manual Teach-and-Replay and Continuous Impedance Shaping for Robotic Locomotor Training Following Spinal Cord Injury.* IEEE Transactions on Biomedical Engineering, 2008. **55**(1): p. 322-334.
70. Schmidt, H., et al., *Gait rehabilitation machines based on programmable footplates.* 2007. **4**(1): p. 2.
71. Bruni, M.F., et al., *What does best evidence tell us about robotic gait rehabilitation in stroke patients: A systematic review and meta-analysis.* (1532-2653 (Electronic)).
72. Galli M Fau - Cimolin, V., et al., *Robot-assisted gait training versus treadmill training in patients with Parkinson's disease: a kinematic evaluation with gait profile score.* (1971-3274 (Electronic)).
73. Hesse, S., et al., *Evidence of end-effector based gait machines in gait rehabilitation after CNS lesion.* (1878-6448 (Electronic)).
74. Hesse, S. and C. Werner, *Connecting research to the needs of patients and clinicians.* (1873-2747 (Electronic)).
75. Maranesi, E., et al., *Effectiveness of Intervention Based on End-effector Gait Trainer in Older Patients With Stroke: A Systematic Review.* (1538-9375 (Electronic)).
76. Sale, P., et al., *Use of the robot assisted gait therapy in rehabilitation of patients with stroke and spinal cord injury.* (1973-9095 (Electronic)).
77. Tong, R.K., M.F. Ng, and L.S. Li, *Effectiveness of Gait Training Using an Electromechanical Gait Trainer, With and Without Functional Electric Stimulation, in Subacute Stroke: A Randomized Controlled Trial.* 2006. **87**(10): p. 1298-1304.
78. Hesse, S. and D. Uhlenbrock, *A mechanized gait trainer for restoration of gait.* J Rehabil Res Dev, 2000. **37**(6): p. 701-8.
79. Hesse, S., et al., *An electromechanical gait trainer for restoration of gait in hemiparetic stroke patients: preliminary results.* (1545-9683 (Print)).
80. Singh, R., H. Chaudhary, and A.K. Singh, *A novel gait-based synthesis procedure for the design of 4-bar exoskeleton with natural trajectories. Journal of orthopaedic translation,* 2017. **12**(2214-031X (Print)): p. 6–15.
81. Tsuge, B.Y. and J. Michael McCarthy, *An Adjustable Single Degree-of-Freedom System to Guide Natural Walking Movement for Rehabilitation.* Journal of Medical Devices, 2016. **10**(4).
82. Tsuge, B.Y., M.M. Plecnik, and J. Michael McCarthy, *Homotopy Directed Optimization to Design a Six-Bar Linkage for a Lower Limb With a Natural Ankle Trajectory.* Journal of Mechanisms and Robotics, 2016. **8**(6).
83. Seo, J.A.-O.X. and H.S. Kim, *Biomechanical Analysis in Five Bar Linkage Prototype Machine of Gait Training and Rehabilitation by IMU Sensor and Electromyography. LID - 10.3390/s21051726 [doi] LID - 1726.* (1424-8220 (Electronic)).
84. Shao, Y., et al., *Conceptual design and dimensional synthesis of cam-linkage mechanisms for gait rehabilitation.* 2016. **104**: p. 31-42.

85. Zhou, H., *Dimensional synthesis of adjustable path generation linkages using the optimal slider adjustment.* 2009. **44**(10): p. 1866-1876.
86. Song, W., et al., *Data-Driven Design of a Six-bar Lower-Limb Rehabilitation Mechanism based on Gait Trajectory Prediction.* IEEE Transactions on Neural Systems and Rehabilitation Engineering, 2023. **31**: p. 109-118.
87. Wang, F.C., et al. *Design and control of an active gait trainer*. in *2009 IEEE International Symposium on Industrial Electronics*. 2009.
88. Copilusi, C., M. Ceccarelli, and G. Carbone, *Design and numerical characterization of a new leg exoskeleton for motion assistance.* Robotica, 2015. **33**(5): p. 1147-1162.
89. Yul Shin, S., A.D. Deshpande, and J. Sulzer, *Design of a Single Degree-of-Freedom, Adaptable Electromechanical Gait Trainer for People With Neurological Injury.* Journal of Mechanisms and Robotics, 2018. **10**(4).
90. A. Ravindran, K.M.R., Gintaras V. Reklaitis, *Engineering Optimization: Methods and Applications, 2nd Edition*. 2006: WILEY.
91. Kora, K., J. Stinear, and A. McDaid, *Design, Analysis, and Optimization of an Acute Stroke Gait Rehabilitation Device.* Journal of Medical Devices, 2016. **11**(1).
92. Haghjoo, M.R., et al., *Mech-Walker:A Novel Single-DOF Linkage Device With Movable Frame for Gait Rehabilitation.* IEEE/ASME Transactions on Mechatronics, 2021. **26**(1): p. 13-23.
93. Sabaapour, M.R. and J. Yoon, *A novel method for optimal path synthesis of mechanisms based on tracking control of shadow robot.* 2019. **131**: p. 218-233.
94. Li M Fau - Yan, J., et al., *Mechanically Assisted Neurorehabilitation: A Novel Six-Bar Linkage Mechanism for Gait Rehabilitation. IEEE transactions on neural systems and rehabilitation engineering : a publication of the IEEE Engineering in Medicine and Biology Society*, 2021(1558-0210 (Electronic)): p. 985–992.
95. Muñoz-Reina, J.S., M.G. Villarreal-Cervantes, and L.G. Corona-Ramírez, *Integrated design of a lower limb rehabilitation mechanism using differential evolution.* 2021. **92**: p. 107103.
96. Calva-Yáñez, M.B., et al., *Reconfigurable Mechanical System Design for Tracking an Ankle Trajectory Using an Evolutionary Optimization Algorithm.* IEEE Access, 2017. **5**: p. 5480-5493.
97. Mehrholz, J., et al., *Electromechanical-assisted training for walking after stroke.* Cochrane Database Syst Rev, 2017. **5**(5): p. Cd006185.
98. Nam, K.Y., et al., *Robot-assisted gait training (Lokomat) improves walking function and activity in people with spinal cord injury: a systematic review.* J Neuroeng Rehabil, 2017. **14**(1): p. 24.
99. Akiyama, Y., et al., *Characteristics of Recovery Motion Resulting From Side Contact With a Physical Assistant Robot Worn During Gait.* IEEE Transactions on Human-Machine Systems, 2020. **50**(6): p. 518-528.
100. Chen, C.H., et al., *Transdisciplinary Engineering: A Paradigm Shift: Proceedings of the 24th ISPE Inc. International Conference on Transdisciplinary Engineering*. 2017: Advances in Transdisciplinary Engineering.
101. Lee, J., et al., *Kinematic comparison of single degree-of-freedom robotic gait trainers.* Mechanism and Machine Theory, 2021. **159**: p. 104258.
102. Moubarak, P.M. and P. Ben-Tzvi, *On the Dual-Rod Slider Rocker Mechanism and Its Applications to Tristate Rigid Active Docking.* Journal of Mechanisms and Robotics, 2013. **5**(1).
103. Song, W., et al., *Data-Driven Design of a Six-bar Lower-Limb Rehabilitation Mechanism based on Gait Trajectory Prediction.* IEEE Trans Neural Syst Rehabil Eng, 2022. **Pp**.

104. Ji, Z. and Y. Manna, *Synthesis of a Pattern Generation Mechanism for Gait Rehabilitation.* Journal of Medical Devices, 2008. **2**(3).
105. Alves, P., et al. *Synthesis of a Mechanism for Human Gait Rehabilitation: An Introductory Approach*. in *New Trends in Mechanism and Machine Science*. 2015. Springer International.
106. Hesse, S., et al., *A mechanized gait trainer for restoring gait in nonambulatory subjects.* Arch Phys Med Rehabil, 2000. **81**(9): p. 1158-61.
107. Singh, R., H. Chaudhary, and A.K. Singh, *A novel gait-inspired four-bar lower limb exoskeleton to guide the walking movement.* Journal of Mechanics in Medicine and Biology, 2019. **19**(04): p. 1950020.
108. Tsuge, B., M. Plecnik, and J. McCarthy, *Homotopy Directed Optimization to Design a Six-Bar Linkage for a Lower Limb With a Natural Ankle Trajectory.* Journal of Mechanisms and Robotics, 2016. **8**.
109. Sabaapour, M.R., et al. *Development of a Novel Gait Rehabilitation Device with Hip Interaction and a Single DOF Mechanism*. in *2019 International Conference on Robotics and Automation (ICRA)*. 2019.
110. Tsuge, B.Y. and J.M. McCarthy. *Synthesis of a 10-Bar Linkage to Guide the Gait Cycle of the Human Leg*. in *ASME 2015 International Design Engineering Technical Conferences & Computers and Information in Engineering Conference*. 2015. Boston, Massachusetts, USA: ASME.
111. Chase, T.R. and J.A. Mirth, *Circuits and Branches of Single-Degree-of-Freedom Planar Linkages.* Journal of Mechanical Design, 1993. **115**(2): p. 223-230.
112. Deshpande, S. and A. Purwar, *A Machine Learning Approach to Kinematic Synthesis of Defect-Free Planar Four-Bar Linkages.* Journal of Computing and Information Science in Engineering, 2018. **19**.
113. Kapsalyamov, A., et al., *A Novel Underactuated Robotic Orthosis for Individualized Gait Rehabilitation.* IEEE Transactions on Medical Robotics and Bionics, 2023.
114. Sabaapour, M.R. and J.-R. Yoon, *A novel method for optimal path synthesis of mechanisms based on tracking control of shadow robot.* Mechanism and Machine Theory, 2019.
115. Ghosh, S., N. Robson, and J. McCarthy, *Design of Wearable Lower Leg Orthotic Based on Six-Bar Linkage*. 2017. V05AT08A064.
116. Tsuge, B. and J. McCarthy, *Synthesis of a 10-Bar Linkage to Guide the Gait Cycle of the Human Leg*. 2015. V05BT08A083.
117. Tsuge, B. and J. McCarthy, *An Adjustable Single Degree-of-Freedom System to Guide Natural Walking Movement for Rehabilitation.* Journal of Medical Devices, 2016. **10**.
118. Norton, R.L. and M.P.H. II, *Design of Machinery: An Introduction To The Synthesis and Analysis of Mechanisms and Machines*. 6 ed. 2019: McGraw Hill.
119. Chung, W.Y., *Double configurations of five-link Assur kinematic chain and stationary configurations of Stephenson six-bar.* Mechanism and Machine Theory, 2007. **42**(12): p. 1653-1662.
120. Liu, Y. and S. Yang, *Kinematic solution of spherical Stephenson-III six-bar mechanism.* Chinese Journal of Mechanical Engineering (English Edition), 2013. **26**(5): p. 851-860.
121. Plecnik, M.M. and J.M. McCarthy, *Controlling the movement of a TRR spatial chain with coupled six-bar function generators for biomimetic motion.* Journal of Mechanisms and Robotics, 2016. **8**(5).
122. Winter, D., *Biomechanics and Motor Control of Human Movement, Fourth Edition.* 2009.
123. Petuya, V., et al., *Educational Software Tools for the Kinematic Analysis of Mechanisms.* Computer Applications in Engineering Education, 2014. **22**.

124. Ullah, I., N. Khan, and M. Al-Grafi, *Dimensional synthesis of mechanical linkages using artificial neural networks and Fourier descriptors.* Mechanical Sciences, 2015. **6**: p. 29-34.
125. Zhou, Z., et al., *Individualized Gait Generation for Rehabilitation Robots Based on Recurrent Neural Networks.* IEEE Transactions on Neural Systems and Rehabilitation Engineering, 2021. **29**: p. 273-281.
126. Luu, T.P., et al., *An individual-specific gait pattern prediction model based on generalized regression neural networks.* (1879-2219 (Electronic)).
127. Semwal, V. and G. Nandi, *Generation of Joint Trajectories Using Hybrid Automate-Based Model: A Rocking Block-Based Approach.* 2016. **16**.
128. Semwal, V.B., et al., *Design of Vector Field for Different Subphases of Gait and Regeneration of Gait Pattern.* IEEE Transactions on Automation Science and Engineering, 2018. **15**(1): p. 104-110.
129. Kapsalyamov, A., et al., *Synthesis of a six-bar mechanism for generating knee and ankle motion trajectories using deep generative neural network.* Engineering Applications of Artificial Intelligence, 2023. **117**: p. 105500.
130. Goodfellow, I., et al., *Generative Adversarial Nets.* Proceedings of the International Conference on Neural Information Processing Systems (NIPS 2014), 2014: p. 2672-2680.
131. Mirza, M. and S. Osindero, *Conditional Generative Adversarial Nets.* ArXiv, 2014. **abs/1411.1784**.
132. Kingma, D.P. and J. Ba, *Adam: A Method for Stochastic Optimization.* CoRR, 2015. **abs/1412.6980**.
133. Hochreiter, S. and J. Schmidhuber, *Long Short-term Memory.* Neural computation, 1997. **9**: p. 1735-80.
134. Graves, A., *Generating Sequences With Recurrent Neural Networks.* ArXiv, 2013. **abs/1308.0850**.
135. Zaheer, M., et al., *Adaptive methods for nonconvex optimization*, in *Proceedings of the 32nd International Conference on Neural Information Processing Systems*. 2018, Curran Associates Inc.: Montréal, Canada. p. 9815–9825.
136. Winter, D., *Biomechanics and Motor Control of Human Movement*. 4 ed. 2009.
137. Sadler, J.P., R.W. Mayne, and F.C. Fan, *Generalized study of crank-rocker mechanisms driven by a d.c. motor Part I. Mathematical model.* Mechanism and Machine Theory, 1980. **15**(6): p. 435-445.
138. Mayne, R.W., J.P. Sadler, and K.C. Fan, *Generalized study of crank-rocker mechanisms driven by a d.c. motor Part II. Applications.* Mechanism and Machine Theory, 1980. **15**(6): p. 447-461.
139. Rose, L., M. Bazzocchi, and G. Nejat, *A model-free deep reinforcement learning approach for control of exoskeleton gait patterns.* Robotica, 2021: p. 1-26.
140. Khan, S.G., et al., *Reinforcement learning and optimal adaptive control: An overview and implementation examples.* Annual Reviews in Control, 2012. **36**(1): p. 42-59.
141. Yuan, Y., et al., *DMP-Based Motion Generation for a Walking Exoskeleton Robot Using Reinforcement Learning.* IEEE Transactions on Industrial Electronics, 2020. **67**(5): p. 3830-3839.
142. Pong, V., et al., *Temporal Difference Models: Model-Free Deep RL for Model-Based Control.* ArXiv, 2018.
143. Huang, R., et al., *Learning Physical Human–Robot Interaction With Coupled Cooperative Primitives for a Lower Exoskeleton.* IEEE Transactions on Automation Science and Engineering, 2019. **16**(4): p. 1566-1574.

144. Rajeswaran, A., et al., *Learning Complex Dexterous Manipulation with Deep Reinforcement Learning and Demonstrations*. 2018.
145. Li, S., *Ankle and Foot Spasticity Patterns in Chronic Stroke Survivors with Abnormal Gait.* Toxins, 2020. **12**(10): p. 646.
146. Lillicrap, T., et al., *Continuous control with deep reinforcement learning.* CoRR, 2015.
147. Febbo, D.D., et al. *Does Reinforcement Learning outperform PID in the control of FES-induced elbow flex-extension?* in *2018 IEEE International Symposium on Medical Measurements and Applications (MeMeA)*. 2018.
148. Lotze, M., et al., *Motor learning elicited by voluntary drive.* (0006-8950 (Print)).
149. Kaelin-Lang, A., L.G. Sawaki L Fau - Cohen, and L.G. Cohen, *Role of voluntary drive in encoding an elementary motor memory.* (0022-3077 (Print)).
150. Hogan, N. *Impedance Control: An Approach to Manipulation*. in *1984 American Control Conference*. 1984.
151. Li, Z., et al., *Human-in-the-Loop Control of Soft Exosuits Using Impedance Learning on Different Terrains.* IEEE Transactions on Robotics, 2022. **38**(5): p. 2979-2993.
152. Huo, W., et al., *Impedance Modulation Control of a Lower-Limb Exoskeleton to Assist Sit-to-Stand Movements.* IEEE Transactions on Robotics, 2022. **38**(2): p. 1230-1249.
153. Lachner, J., et al., *Shaping Impedances to Comply With Constrained Task Dynamics.* IEEE Transactions on Robotics, 2022. **38**(5): p. 2750-2767.
154. *Goldstein, H.; Poole, C.; Safko, J. Classical Mechanics ; Pearson Education: London, UK, 2011*.
155. Nguyen, H.T. and C.C. Cheah, *Analytic Deep Neural Network-Based Robot Control.* IEEE/ASME Transactions on Mechatronics, 2022. **27**(4): p. 2176-2184.
156. Jiang, X. and C. Xu, *Deep Learning and Machine Learning with Grid Search to Predict Later Occurrence of Breast Cancer Metastasis Using Clinical Data.* Journal of Clinical Medicine, 2022. **11**(19).
157. Kingma, D. and J. Ba, *Adam: A Method for Stochastic Optimization.* 2014.
158. Nair, V. and G. Hinton, *Rectified Linear Units Improve Restricted Boltzmann Machines Vinod Nair*. 2010. 807-814.
159. Wilcoxon, F., *Individual comparisons of grouped data by ranking methods.* (0022-0493 (Print)).